

Positron annihilation study of equilibrium point defects in GaAs

Dissertation

zur Erlangung des akademischen Grades
Dr. rerum naturalium (Dr. rer. nat.)

vorgelegt der

Mathematisch-Naturwissenschaftlich-Technischen Fakultät
(mathematisch-naturwissenschaftlicher Bereich)
der
Martin-Luther-Universität Halle-Wittenberg

von Herrn

Vladimir Bondarenko

geb. am 15.02.1978 in Sumy, Ukraine

Gutachter:

- (1) Prof. Dr. R. Krause-Rehberg
- (2) Prof. Dr. U. M. Gösele
- (3) Prof. Dr. P. Masher

urn:nbn:de:gbv:3-000006446

[<http://nbn-resolving.de/urn/resolver.pl?urn=nbn%3Ade%3Agbv%3A3-000006446>]

Halle(Saale), November 2003

verteidigt am 30.01.2004

Table of contents

1. Introduction	1
2. Thermodynamics of native point defects in GaAs	3
2.1 GaAs system at melting point	3
2.2 Defects chemistry in GaAs	5
2.3 Tan model and Fermi-level effect	7
2.4 Quantum mechanical calculations	9
2.5 Electrical compensation in n-type GaAs	11
3. Experimental methods	13
3.1 Positron annihilation lifetime spectroscopy	13
3.1.1 Physical background of positron trapping	13
3.1.2 Measurement principle and trapping model	14
3.2 Temperature dependence of positron trapping in semiconductors	16
3.2.1 Theory	16
3.2.2 Model of positron trapping for experimental data fitting	21
3.3 Coincidence Doppler-broadening spectroscopy	24
3.4 Procedure of positron annihilation measurements	26
3.5 Other methods	27
4. Vacancy formation in n-type silicon-doped GaAs	29
4.1 Introduction	29
4.2 Heavily silicon doped GaAs	31
4.2.1 Experimental	31
4.2.2 Defect identification by means of positron annihilation	31
4.2.3 Model of the compensation mechanism	33
4.3 Influence of dislocations on the lateral distribution of $\text{Si}_{\text{Ga}}\text{V}_{\text{Ga}}$ complexes in Si-doped VGF GaAs wafers	35
4.3.1 Experimental details	36
4.3.2 Correlation between photoluminescence and positron annihilation investigations of silicon doped VGF GaAs	37
4.3.3 Lateral variation of the compensation degree in VGF GaAs:Si	41
4.4 Identification of the 0.95 eV luminescence band in VGF GaAs:Si	44
4.4.1 Experimental	44
4.4.2 Cathodoluminescence spectroscopy	45
4.4.3 Defect identification by positron annihilation	47
4.5 Discussion: defects formation in VGF GaAs:Si	49

5. Vacancy formation in semi-insulating and silicon-doped GaAs under equilibrium conditions	51
5.1 Experimental	51
5.2 Defects detected by PALS in annealed GaAs	53
5.2.1 Si-doped GaAs	53
5.2.2 Undoped semi-insulating GaAs	54
5.2.3 Reproducibility of results for annealed SI GaAs	55
5.3 Defect identification in annealed n-type and SI GaAs	59
5.3.1 Identification of vacancies	59
5.3.2 Identification of shallow traps in undoped annealed GaAs	62
5.3.3 Charge state of the V_{As} complex	64
5.3.4 Gibbs free energy of V_{As} formation	66
6. Defects study in intentionally undoped VCz-grown GaAs	67
6.1 Growth method	67
6.2 Carbon controlled growth	69
6.3 Influence of the melt stoichiometry and unintentional doping on vacancy formation	71
6.4 Results of PALS measurements	73
6.4.1 Semi-insulating GaAs	73
6.4.2 p-type GaAs	75
6.4.3 n-type GaAs	77
6.5 Validity of positron annihilation for determination of vacancy concentration	79
6.6 Summary	80
7. On the temperature dependence of positron trapping in GaAs	82
7.1 GaAs:Si vs GaAs:Te	83
7.2 Positron trapping in GaAs doped with Si and Te simultaneously	85
7.2.1 Experimental	85
7.2.2 Results of temperature-dependent PALS measurements	86
7.2.3 Discussion	87
7.3 Systematization of results	89
8. Summary	93
References	95

Eidesstattliche Erklärung

Curriculum Vitae

Acknowledgments

1. Introduction

Gallium arsenide (GaAs) is one of the most frequently used compound semiconductors. Owing to its electronic properties – direct band gap and very high electron mobility – GaAs has founds broad application in production of opto- and microelectronics devices. Microwave devices require high purity quasi-undoped semi-insulating (SI) wafers, whereas optoelectronic devices require semiconducting (SC) n-type (usually Si-doped) substrates. However, despite the attractive properties, GaAs has lost a significant part of the semiconductor market in the last years. The main reasons for this are high operational costs of crystal growth and not high enough quality of GaAs single crystals. These disadvantages are in turn caused by the complexity of the GaAs system, which includes a much larger variety of point defects and defect complexes compared to elemental semiconductors, such as Si. It is known, that point defects may occur in different charge states, interacting with each other via their influence on the position of the Fermi level. However, exact interaction mechanism is still controversial. It was the goal of the present work to contribute to the improvement of this situation.

The choice of material under investigation in this work was dictated by the technological interest. As-grown n-type and semi-insulating GaAs crystals were studied. Positron annihilation lifetime spectroscopy (PALS) was used as the main method of investigation. PALS is a sensitive tool for the detection of vacancy-like defects. However, it would be hardly possible to interpret the results of positron annihilation without application of other experimental methods.

The work has the following structure: in section 2, the theoretical aspects of point defect formation important for further discussion are presented. Section 3 gives a brief review of experimental techniques, which have been used here. Section 4 is devoted to the study of as grown Si-doped GaAs. In section 5, the formation of point defects in n-type and SI GaAs at elevated temperatures is compared. The results of investigations on a variety of GaAs crystals grown by modified LEC-techniques are discussed in section 6. Section 7 deals with the interpretation of temperature-dependent positron annihilation measurements. A summary is given in section 8.

2. Thermodynamics of native point defects in GaAs

The totality of point defects in a crystal comprise those existing in a perfectly chemically pure crystal, so called intrinsic defects, and those associated with some foreign atoms. The latter are termed “dopants” if they are deliberately added or “impurities” if they were introduced unintentionally. There are six principal intrinsic point defects in GaAs: vacancies on both sublattices (V_{Ga} and V_{As}), Ga and As interstitials (Ga_i and As_i) and antisites (Ga_{As} and As_{Ga}). In framework of this work, the term “native defects” is related to the point defects being in thermodynamical equilibrium with a host crystal and not introduced intentionally, e.g. by crystal deformation or irradiation. This definition comprises intrinsic defects, foreign atoms as well as their complexes. The equilibrium concentration of point defects in binary compound semiconductors such as GaAs is a complicated function depending of temperature, Fermi-level position and of the activity of either one of the constituents (gallium or arsenic), i.e. of crystal stoichiometry. In the following sections, some aspects important for this thesis concerning native defect formation are briefly reviewed.

2.1 GaAs system at melting point

Gallium arsenide crystallizes in the zincblendstructure at about 1513 K. The lattice constant is 0.5653 nm at 300 K (Brozel and Stillman 1996). As for any compound, there is a certain thermodynamically allowed region of homogeneity for $\text{Ga}_{1-x}\text{As}_x$. This is shown on

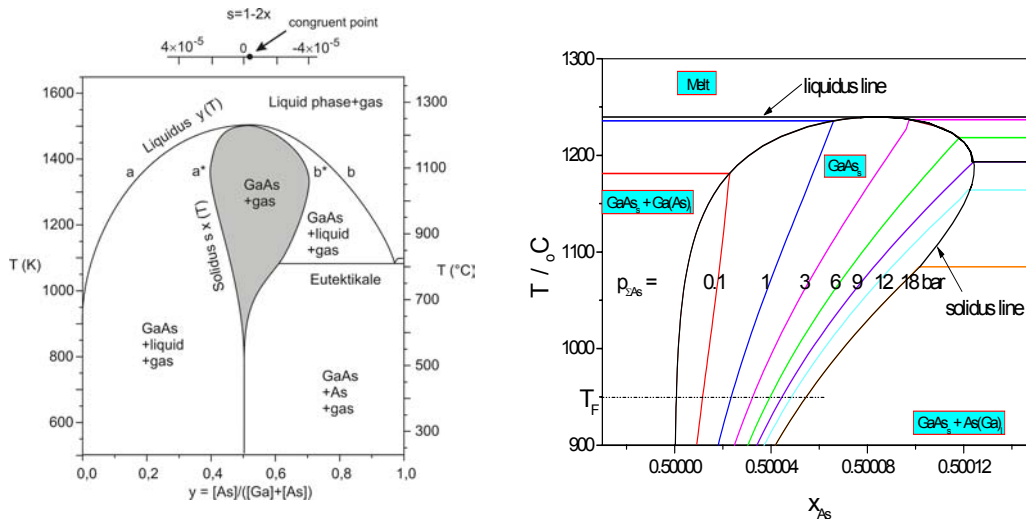


Fig. 2.1: Binary phase diagram of Ga-As-System. Data are taken from Refs. (Wenzl et al. 1991; Wenzl et al. 1994) (left) and (Jurisch and Wenzl 2002) (right)

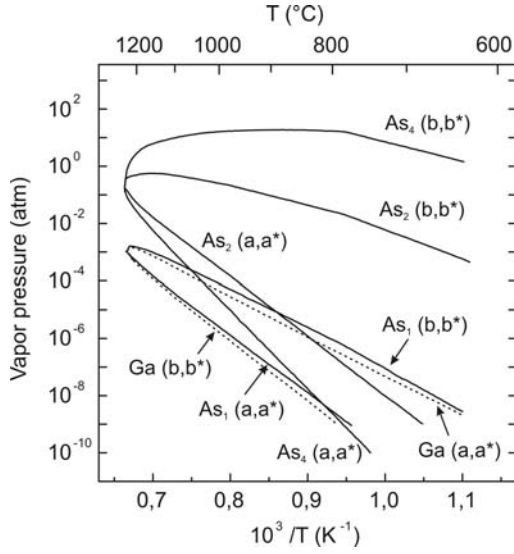


Fig. 2.2: Equilibrium pressures of As , As_2 , As_4 and Ga along the Ga-rich (a,a^*) and As-rich (b,b^*) phase boundary of GaAs. (From Ref. (Arthur 1967))

the binary phase diagram in fig. 2.1. The homogeneity region is represented by the shaded area within the solidus line a^*b^* . If concentration of one of the components (e.g., As) exceeds a value allowed by the solidus line b^* , the GaAs system consists of three phase – GaAs crystal, melt and gas. Inside the homogeneity region, GaAs crystal is in thermal equilibrium with its gas phase. Corresponding vapour pressures determined along the solidus line are shown in fig. 2.2. In case of the arsenic-rich melt, the As_4 -pressure dominates while the vapour pressure of gallium is negligibly small. The resulting pressure is then $\approx p_{As_4}$. On the gallium-rich side, As_2 is the dominating gas component. The Ga pressure becomes important only at low temperatures ($T < 800^\circ C$).

It is important to note that the exact shape of the GaAs phase diagram is unknown at present. This subject is still under investigations. According to the recent thermodynamic calculations of Jurisch and Wenzl, there is no crystallization at all possible on the Ga-rich side [Fig. 2.1 (right)]. This may explain the fact why gallium precipitates were never observed even in the crystals grown from a very Ga-rich melt (Kießling 2003). However, the Wenzl's hypothesis needs stronger experimental evidence. Anyway, it is commonly accepted that the congruent point, where the solidus and liquidus lines osculate, lies on the As-rich side of the phase diagram (Fig. 2.1). Therefore, growth from a stoichiometric melt always yields arsenic-rich material (Wenzl et al. 1991, Hurle 1999).

The deviation from stoichiometry s is realized through the formation of point defects on both sublattices. The deviation can be expressed as $s = 1 - 2x = s_1 - s_2$, where s_1 and s_2 are determined as:

$$\begin{aligned} 2s_1 &= [Ga_i] + [Ga_{As}] - [V_{Ga}] - [As_{Ga}] - [X_{Ga}] \quad \text{and} \\ 2s_2 &= [As_i] + [As_{Ga}] - [V_{As}] - [Ga_{As}] - [X_{As}] \end{aligned} \quad (2.1)$$

where X_{Ga} and X_{As} imply an arbitrary foreign atom on the As or Ga lattice site. The brackets denote defect concentration in atomic units. Thus, by measuring the stoichiome-

try deviation s , type and concentration of the dominating point defects can be determined. There are two direct methods for estimation of s :

- 1) the direct determination of the amounts of Ga and As atoms in a sample by electrochemical titration of one or both of the species;
- 2) the determination of the average mass of the unit cell in a sample by measuring its density (which is the mass per unit volume of crystal) and the cube of its lattice parameter (which is volume of the unit cell). The quotient of these two quantities is, therefore, the mass per unit cell. By subtracting from this the mass of an ideal unit cell (containing one Ga and one As atom), the excess mass per unit cell which is related to the deviation from stoichiometry is obtained.

Application of these two approaches to study GaAs crystals grown from Ga- and As-rich melt showed that deviations on the As sublattice dominate (Hurle 1999). Thus, under As-rich conditions, there are large concentrations of As_i and V_{Ga} grown into the crystals at the melting point. However, deviation from stoichiometry provides information only on dominating defects, which remain in a crystal after its cooling. Investigation of other point defects present at elevated temperatures with the help of these methods is impossible.

There are always some point defects existing in a crystal at thermodynamical equilibrium, which contribute to minimization of the Gibbs free energy. In elemental semiconductor such as Si, the equilibrium concentration of an individual point defect depends on temperature and the position of the Fermi level. For compound semiconductor, the situation is more difficult since the equilibrium concentrations depend additionally on the crystal stoichiometry (Eq. 2.1). This means that defect concentrations, crystal composition and ambient vapour pressure are in thermodynamical equilibrium and thus depend on each other. In addition, many of the point defects may exist in more than one charge state and interact strongly through their influence on the Fermi energy. Thus, dopant solubility can be strongly influenced by charged native point defects grown into the crystal and conversely, doping markedly affects charged native point defect populations.

2.2 Defects chemistry in GaAs

Defect chemistry represents a chemical approach to the problems dealing with imperfections in crystalline solids. This method considers the generation of defects, interaction between them and between defects and ambient as chemical reactions based on the assumption that the crystal is in an equilibrium state (Kröger 1964). Six intrinsic point defects in GaAs can be described by the following six thermodynamic reactions (Hurle 1999):



$$0 = V_{As}^0 + V_{Ga}^0 \quad (2.4)$$

$$Ga_{Ga} = Ga_i^0 + V_{Ga}^0 \quad (2.5)$$

$$As_i^0 + V_{Ga}^0 = As_{Ga}^0 \quad (2.6)$$

$$Ga_i^0 + V_{As}^0 = Ga_{As}^0 \quad (2.7)$$

where the superscript (0) indicates the neutral state. Only one of the reactions involves the external phase (Eq. 2.2). The external phase may be liquid or vapor. To avoid writing different equations for the two cases, the activity of the external phase is expressed in terms of the partial pressure of arsenic dimers which would be in equilibrium either with the vapor or with a liquid which was in equilibrium with that vapor. The arsenic tetramer is chosen, since it is the dominating species in arsenic vapor (Fig. 2.2). Having expressed a condition of equilibrium of one component with the external phase, equilibrium with respect to the other component (Ga) is defined as:

$$p_{Ga} p_{As_4}^{1/4} = \exp(-g^f / kT) \quad (2.8)$$

where p_{Ga} is the partial pressure of gallium monomers and g^f is the free energy of formation of GaAs from gaseous gallium monomer and arsenic tetramers at one atmosphere total pressure and temperature T . Substituting (2.2) into (2.3), one obtains the following reaction for V_{As} formation:

$$As_{As} = V_{As}^0 + 1/4 As_4(\nu) \quad (2.9)$$

From (2.4) and (2.9), a similar reaction for the Ga vacancy may be deduced:

$$1/4 As_4(\nu) = V_{Ga}^0 + As_{As} \quad (2.10)$$

Concentrations of vacancies in their neutral states are determined by mass-action law:

$$[V_{Ga}^0] = K_{V_{Ga}}(T) p_{As_4}^{1/4} \quad (2.11)$$

$$[V_{As}^0] = K_{V_{As}}(T) p_{As_4}^{-1/4} \quad (2.12)$$

where $K_{V_{Ga}}$ and $K_{V_{As}}$ are mass-action constants of formation of gallium and arsenic vacancies, respectively. According to (2.11) and (2.12), the density of V_{Ga} should increase and of V_{As} decrease with increasing arsenic pressure.

In case of charged vacancies, their ionization reactions and corresponding concentrations are given by the following reactions:

Arsenic vacancy

$$V_{As}^0 = V_{As}^+ + e^- \quad (2.13)$$

$$[V_{As}^+] = [V_{As}^0](N_C / n) \exp(-E_{V_{As}} / k_B T) \quad (2.14)$$

$$V_{As}^0 = V_{As}^- + h^+ \quad (2.15)$$

$$[V_{As}^-] = [V_{As}^0](n / N_C) \exp(-E_{V_{As}} / k_B T) \quad (2.16)$$

Gallium vacancy

$$V_{Ga}^0 = V_{Ga}^{q-} + qh^+ \quad (2.17)$$

$$[V_{Ga}^{q-}] = [V_{Ga}^0](n / N_C)^q \exp\left\{\left(qE_g - \sum_q E_{V_{Ga}^{q-}}\right) / k_B T\right\} \quad (2.18)$$

where $q=1,2,3$, $E_g(T)$ is the energy gap. $E_{V_{As}}$ is the ionization energy of the arsenic vacancy and $E_{V_{Ga}^{q-}}$ is the ionization energy of the q charge state of the gallium vacancy. n is the free electron concentration, N_C is the effective density of conduction-band states and k_B is Boltzmann's constant.

2.3 Tan model and Fermi-level effect

The considerations presented in the previous subsection give a qualitative description of vacancy formation. However, they cannot be applied quantitatively if the mass-action constants are unknown. Tan et. al. tried to evaluate the concentrations of equilibrium point defects explicitly (Tan et al. 1993; Tan 1994). According to Tan's model, concentrations of neutral arsenic and gallium vacancies are determined by:

$$[V_{As}^0] = \left(B_{As_4} / p_{As_4}\right)^{1/4} \exp\{-[g^f(V_{As}^0) - \delta g_{As}] / k_B T\} \quad (2.19)$$

$$[V_{Ga}^0] = \left(p_{As_4} / B_{As_4}\right)^{1/4} \exp\{-[g^f(V_{Ga}^0) + \delta g_{As}] / k_B T\} \quad (2.20)$$

$g^f(V_{As}^0)$ and $g^f(V_{Ga}^0)$ are the free energies of formation of neutral arsenic and gallium vacancies, respectively. δg_{As} is the difference:

$$\delta g_{As} = g_{As}(GaAs) - g_{As}(As_4) \quad (2.21)$$

$g_{As}(GaAs)$ is the free energy of bonding of an arsenic atom in the crystal and $g_{As}(As_4)$ is that of bonding of an arsenic atom in the tetramer molecule. $B_{As_4} = (2\pi m_{As_4} / h^2)^{3/2} (kT)^{5/2}$ is the gas constant assuming As_4 can be described as an ideal gas. m_{As_4} is the mass of the As_4 molecule and h – Planck's constant.

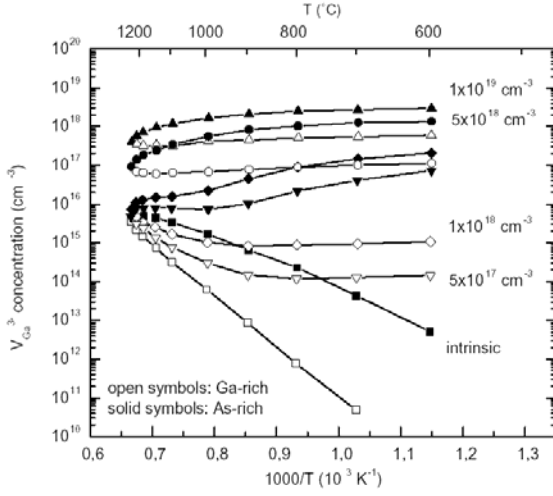


Fig. 2.3: Equilibrium concentrations of V_{Ga}^{3-} in n-type GaAs calculated as a function of temperature for different concentrations of donor atoms, i.e. for different positions of the Fermi level .

Concentrations of the charged defects in Tan's model are determined similarly to the Eq. 2.18

$$[V_{Ga}^{z-}] = [V_{Ga}^0] \exp\left(\left[zE_f - \sum_{m=1}^z E_{am}\right]\right) \quad (2.22)$$

E_F is the Fermi energy, z is the charge and E_{am} are the ionisation energies of the Ga vacancy measured from the valence band. As can be seen from Eq. (2.22), the concentration of the charged vacancies increases with the Fermi-level position moving towards the conduction band edge. The physical reason is the energy difference $E_F - E_a$ gained by a whole system (GaAs crystal) in a process of electron transition to the acceptor level E_a , i.e. formation of an additional acceptor. The dependence of the concentration of a charged point defect in a semiconductor on the charge carrier concentration (i.e. Fermi level position) is called the *Fermi-level effect*.

Assuming V_{Ga} as the only acceptor, Tan et al. calculated the density of gallium vacancies in n-type GaAs (Tan et al. 1991). The As pressures corresponded to those depicted in fig. 2.2. The Gibbs free energies in Eqs. (2.19,2.20) did not include entropy terms, i.e. they were set equal to the corresponding formation enthalpies h^f . The values $h_{V_{Ga}^0}^f = 2.59 eV$ (van Vechten 1975) and $\delta h_{As} = -0.69 eV$ were used. The data for V_{Ga} ionization energies were taken from Ref. (Baraff and Schlüter 1985). The results of the calculations performed for different free electron densities in n-GaAs are presented in fig. 2.3. In intrinsic material, the concentration of Ga vacancies increases with increasing temperature. However, the temperature dependence was found to be dramatically weakened by doping. At high doping level, E_F can be very close to the conduction band at all temperatures. This may result in temperature independence or even a small *negative temperature dependence* of equilibrium concentrations of V_{Ga}^{3-} (Tan 1994). The first experimental evidence of this effect was given by Gebauer et al. in a recent positron annihilation study of Te-doped GaAs (Gebauer et al. 2003). In their analysis, the formation en-

thalpy $h_{V_{Ga}^0}^f$ as well as the formation entropy $s_{V_{Ga}^0}^f$ was considered. The values $h_{V_{Ga}^0}^f = (3.2 \pm 0.5) eV$ and $s_{V_{Ga}^0}^f = (9.6 \pm 1) k_B$ were determined.

2.4 Quantum mechanical calculations

The calculations given in the previous subsection sensitively depend on the knowledge of defect formation and ionization energies. Experimental determination of these properties is usually possible only for a constrained number of defects. The charge state, formation energy E_D and equilibrium concentration C_D of a certain defect may also be obtained with the help of theoretical models based on quantum mechanical calculations. In equilibrium, C_D is given as:

$$C_D = N_s \exp[-E_D(\mu_e, \Delta\mu) / k_B T] \quad (2.23)$$

with $N_s = 2.2 \times 10^{22} \text{ cm}^{-3}$ being the density of lattice sites for one of the sublattices. E_D is a function of μ_e and $\Delta\mu$. μ_e is the electrons chemical potential, i.e. Fermi energy. $\Delta\mu$ is the difference between chemical potentials of Ga(As) in GaAs and in pure Ga(As) elements. In other words, $\Delta\mu$ reflects the stoichiometry deviation. As can be seen from Eq. (2.23), the defect with the lowest binding energy should have the highest equilibrium concentration. Since defect formation energies are usually not exactly known, the accuracy of such kind calculation is often insufficient. Thus, already small numerical uncertainties in the binding energy can affect the calculated defect density by orders of magnitude (Jansen and Sankey 1989). However, a quantum mechanical approach can be used for qualitative predictions of the type of dominating defects.

Fig. 2.4 represents the formation energy of intrinsic point defects in GaAs as a

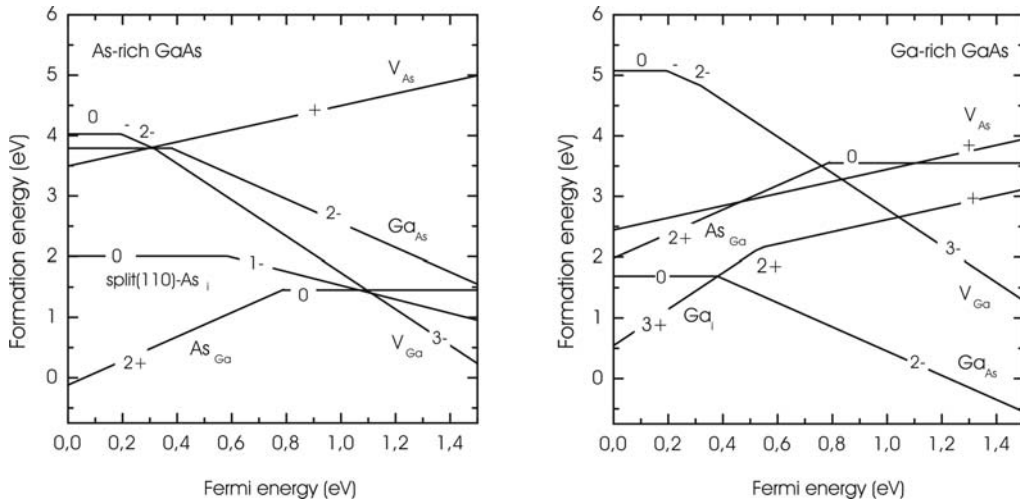


Fig. 2.4: Formation energy of intrinsic defects in As-rich (left) and Ga-rich (right) GaAs as a function of Fermi energy.

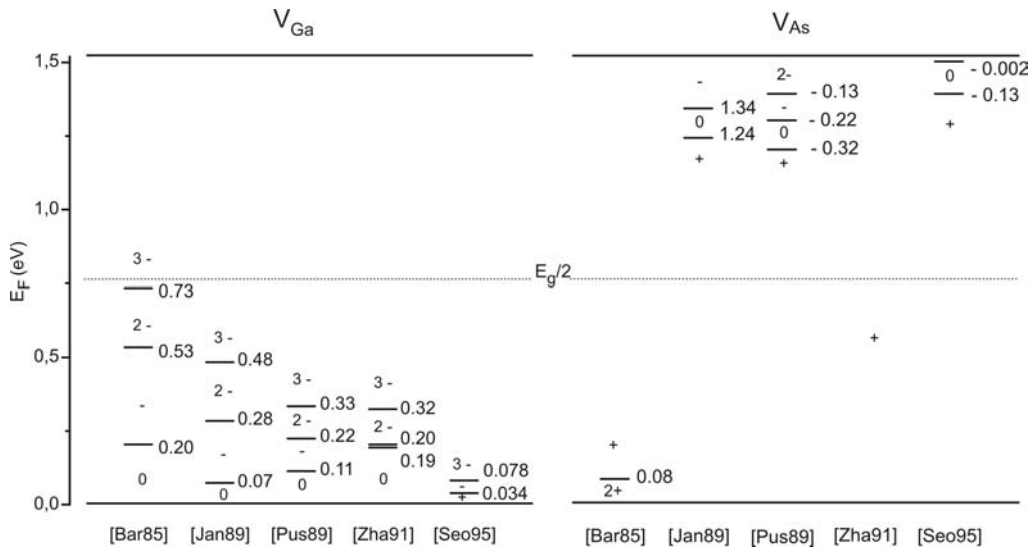


Fig. 2.5: Calculated ionization levels of Ga (left) and As (right) vacancies. Positive numbers designate values measured from the valence band, negative – from conduction band.

function of Fermi energy (from Refs. (Zhang and Northrup 1991; Northrup and Zhang 1993; Landman et al. 1997)). In As-rich, p-type and semi-insulating GaAs, the arsenic antisite As_{Ga} has the smallest formation energy. This is in accordance with the well-known fact that the EL2-centers govern properties of semi-insulating GaAs (Brozel and Stillman 1996). In n-conducting As-rich GaAs, triply negative gallium vacancy has the minimal formation energy. Gallium interstitials Ga_i should dominate in Ga-rich p-type GaAs and gallium antisites Ga_{As} – in SI and n-GaAs. Similar results were obtained in several other theoretical works (Baraff and Schlüter 1985; Jansen and Sankey 1989; Seong and Lewis 1995). According to them, gallium vacancies V_{Ga} should appear in As-rich n-doped GaAs. The formation energy of As-interstitials is according to (Landman et al. 1997) comparable with the formation of V_{Ga} or As_{Ga} in As-rich material. This is in agreement with the results of mass per unit cell measurements, according to which As_i is the dominating defect in As-rich GaAs (Section 2.1).

The arsenic vacancy V_{As} has a formation energy much higher than that of V_{Ga} in n-type Ga- and As-rich GaAs. Consequently, occurrence of V_{As} is rather improbable in n-GaAs. However in p-conducting material, where the Fermi level is positioned in the lower half of the band gap, formation of V_{As} can be energetically more favourable compared to V_{Ga} .

Knowledge about the defect ionisation levels is very important for the interpretation of PALS-results. The positron being a positively charged particle feels the charge of the defects. The direct consequence is that positively charged defects can not be detected by positrons. Unfortunately, ionisation levels of vacancies in GaAs are not well-known experimentally. In principle, they can be determined with the help of quantum mechanical calculations. Fig. 2.5 presents ionisation levels of Ga- and As-vacancy obtained in differ-

ent theoretical works. According to the calculations, the gallium vacancy has ionisation levels in the lower half of the band gap and thus, it is in n-type and SI GaAs triply negative charged. The arsenic vacancy should be positive in p-conducting and semi-insulating material. According to some calculations, V_{As} has ionisation levels near the conduction band (Refs. (Jansen and Sankey 1989; Puska 1989; Seong and Lewis 1995)). Thus, both V_{Ga} and V_{As} must be detectable in n-GaAs. However, calculated ionisation levels demonstrate rather big quantitative differences. Therefore, only qualitative conclusions may be drawn from them, whereas direct comparison with experimental data seems to be questionable.

2.5 Electrical compensation in n-type GaAs

GaAs having electron conductivity type can be produced by means of doping with the atoms of group IV (Si, Ge, Sn) or group VI (S, Se, Te) of the Periodic Table. The elements of the group VI can be incorporated exclusively on the As sublattice forming shallow donors. The atoms of the IV group demonstrate in contrary amphoteric behavior: they behave as shallow donors when incorporated on Ga site and as shallow acceptors – on the As site.

N-doped GaAs is always partially electrically compensated. This means that the free electron density is smaller than the number of introduced dopants. The compensation in GaAs doped with the atoms of the IV group can to some extent be explained by simultaneous formation of donors and acceptors due to the amphoteric dopants incorporation. However, measurements of carrier mobility demonstrated the compensation effect occurring also in S-, Se- or Te- doped material. The degree of compensation N_D/N_A was found to be ~ 0.25 at moderate doping levels regardless of the dopant kind.

Hurle in Ref. (Hurle 1977) supposed that the compensating species was the donor atom complexed with its nearest gallium vacancy to form an acceptor. Positron annihilation studies of Te- and Si-doped GaAs have rather clearly demonstrated the existence of $Te_{As}V_{Ga}$ (Krause-Rehberg et al. 1995; Gebauer et al. 1999) and $Si_{Ga}V_{Ga}$ complexes (Laine et al. 1996; Gebauer et al. 1997). Vacancy-like defects were found also in GaAs doped with S, Ge and Sn atoms (Gebauer 2000). The complexes were found to be negatively charged. However, there is still a lack of knowledge on their exact charge state (e.g., $-1e$ or $-2e$). Nowadays, donor-gallium vacancy complexes are commonly accepted as compensating centers in all kinds of n-GaAs.

Compared to point-like imperfections, influence of large-scale defects on electrical properties of GaAs is much less investigated. Thus, it was found that the distribution of carrier concentration across silicon-doped GaAs wafer showed structures corresponding to the arrangement of dislocations (Börner 2002). This might be due to the decreased concentration of $Si_{Ga}V_{Ga}$ complexes in dislocation-rich regions of a GaAs wafer, as was proposed in the recent photoluminescence study of GaAs:Si (Baeumler et al. 2002).

However, photoluminescence spectroscopy could provide only qualitative information on defect concentrations. In contrary, the method of positron annihilation used in this work is suitable for quantitative analysis of the distribution of $\text{Si}_{\text{Ga}}\text{V}_{\text{Ga}}$ complexes.

3. Experimental methods

3.1 Positron annihilation lifetime spectroscopy

3.1.1 Physical background of positron trapping

The positron (e^+) is the antiparticle of the electron (e^-). Its existence was postulated by P.A.M. Dirac in 1928 as an explanation of negative energy solutions of his quantum theory of electron (Dirac 1928, 1928). In 1932, C.D. Anderson discovered the positron in a cosmic ray event with the help of a Wilson cloud-chamber (Anderson 1932).

Positrons are unstable in matter. After its introduction into a material, the positrons life may be divided into three parts: thermalization, diffusion and annihilation. Thermalization represents a process of the energy loss of the positron via electron and phonon excitation. This process occurs very rapidly, during 3-4 ps (Puska and Nieminen 1994). Thereafter, the positron movement may be described as diffusion. In semiconductors the diffusion constant is about $1.5\text{-}3\text{ cm}^2\text{s}^{-1}$ (Soininen et al. 1992; Shan et al. 1997). In a defect-free material, the positron wave function is a delocalized Bloch wave exhibiting maxima in the interstitial region due to the Coulomb repulsion of the positively charged positron and atom cores (Fig. 3.1). In an imperfect crystal, however, the wave function of the positron may be localized at the sites, where an atom (or group of atoms) is missing, i.e. at the vacancies, vacancy complexes or other open-volume defects [Fig. 3.2 (right)]. The reason is that the absence of the core represents a potential well for the positron [Fig. 3.2 (left)]. Therefore, it is energetically favorable for the positron which has diffused to a vacancy to remain at the vacancy site. This process is called positron trapping.

The positron life is ended by annihilation with an electron. By the annihilation, the energy of the electron-positron pair (e^-e^+) is converted into the annihilation γ -radiation. Mainly, there are two γ -photons emitted, each one having the energy of 511

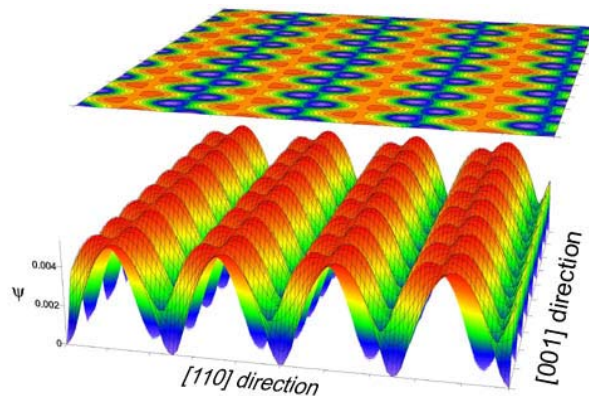


Fig. 3.1: Positron wave function in defect-free GaAs. The calculation was performed using the superimposed-atom (Puska and Nieminen 1983) method for (110) plane.

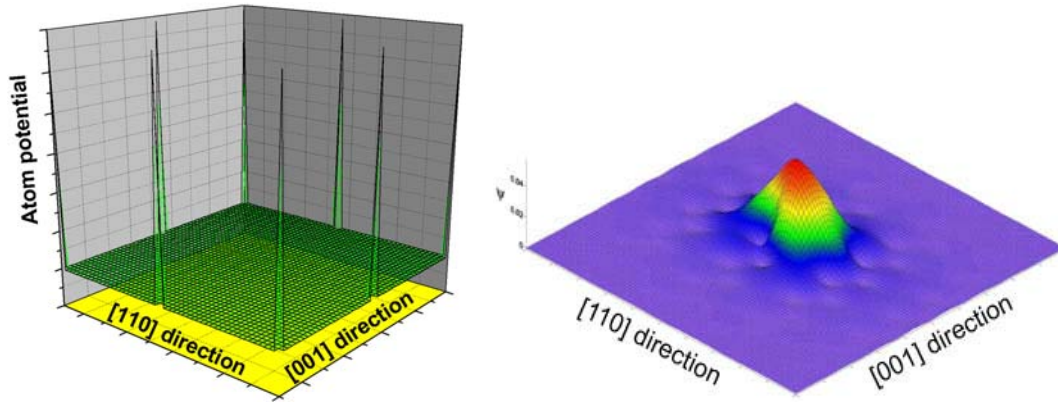


Fig. 3.2: (left) Positive potential of the atom cores around Ga vacancy in (110) plane of GaAs. (right) Corresponding positron wave function for Ga vacancy. Calculations were performed using the superimposed-atom model (Puska and Nieminen 1983)

$keV = m_0c^2$ (m_0 being the electron rest mass, c – speed of light). The positron annihilation rate λ , which is reciprocal of the positron lifetime τ , is determined by the overlap of positron $\psi_+(r)$ and electron $\psi_-(r)$ wave functions:

$$\lambda = 1/\tau = \pi \cdot r_0 \cdot c \int \psi_+(r)\psi_-(r)\gamma dr, \quad (3.1)$$

where r_0 is the classical electron radius and γ is the enhancement factor describing the increase in the electron density at the annihilation site due to electrons-positron Coulomb attraction. The positron lifetime in vacancy-free material is called bulk lifetime, τ_b . In semiconductors, τ_b is in the order of 200 ps (230 ps in GaAs). Compared to a perfect lattice, the electron density in a vacancy defect is decreased. Therefore, the lifetime of a positron trapped at the vacancy is higher than that of positrons annihilating in the defect-free bulk. The method of positron annihilation lifetime spectroscopy (PALS) is based on this effect.

3.1.2 Measurement principle and trapping model

For conventional PALS investigations, positrons are usually obtained by the radioactive decay of the ^{22}Na isotope. The main reason consists in the emission of a γ -photon practically simultaneously with a positron. This photon has the energy of 1.275 MeV and is used to obtain the time of the positron birth (start- γ). Detection of one of the annihilation γ -quanta (stop- γ) denotes the positron death. The time difference between these two events gives the positron lifetime. The necessary condition is that only one positron must be present in a sample at a time.

The positron source is placed between two identical samples in the so-called sandwich geometry. The “sandwich” is positioned between two γ -quanta detectors. One of them serves for the detection of the start- γ and the second of the stop- γ . Each detector

represents a plastic scintillator (Pilot-U) coupled with a photomultiplier tube (Philips XP-2020). Start and stop events are differentiated by their energies (1.275 or 0.511 MeV) with the help of constant fraction discriminators. The time difference between start and stop signals is converted into a time-proportional voltage pulse in a time-to-amplitude converter. This event is saved in a multi-channel analyzer. Further experimental details may be found in e.g. Ref. (Krause-Rehberg and Leipner 1999)

The experimentally obtained spectrum represents a convolution of the spectrometer resolution function and the real lifetime spectrum. The real spectrum is given by the probability $N(t)$ that the positron annihilates at time t (Brandt and Paulin 1972; Frank and Seeger 1974; Krause-Rehberg and Leipner 1999):

$$N(t) = \sum_{i=1}^{N+1} \frac{I_i}{\tau_i} \exp(-t / \tau_i) \quad (3.2)$$

τ_i are called lifetime components with corresponding intensities I_i , whereas $\sum I_i = 1$. The first component τ_1 relates to the time positron spends in the bulk till its annihilation or trapping into a defect; $\tau_2 - \tau_{N+1}$ are lifetimes of the positron trapped by the one of N defects.

In this work, positron capture in a single open-volume defect type was mostly assumed. According to the one-defect trapping model, the lifetime spectrum has two components, τ_1 and τ_2 :

$$\begin{aligned} \tau_1 &= \frac{1}{\lambda_b + k_d}, & \tau_2 &= \frac{1}{\lambda_d}, \\ I_1 &= 1 - I_2, & I_2 &= \frac{k_d}{\lambda_b - \lambda_d + k_d}, \end{aligned} \quad (3.3)$$

where $\lambda_b = 1/\tau_b$ is the positron annihilation rate in a perfect defect-free crystal and $\lambda_d = 1/\tau_d$ is the rate, at which positrons annihilate from a trapped (localized) state. k_d is the positron trapping rate of the defect.

The second lifetime, referred in the following as the defect-related lifetime τ_d , is just the reciprocal of the positron annihilation rate in the defect and does not depend on the defect concentration (Eq. 3.3). According to (3.1), τ_d carries the information about the electron density at the annihilation site and thus can be used as a characteristic value of the open volume of the defect. In semiconductors, the ratio τ_d/τ_b for monovacancy is ~ 1.2 . The defect trapping rate k_d is proportional to the defect concentration.

$$k_d = \mu C = \frac{I_2}{I_1} \left(\frac{1}{\tau_b} - \frac{1}{\tau_d} \right) \quad (3.4)$$

The coefficient of proportionality μ must be determined for every defect type by an independent method explicitly.

Very often, a parameter called *average positron lifetime*, τ_{av} is used in the literature. This parameter is given as:

$$\tau_{av} = \sum_{i=1}^{N+1} I_i \tau_i \quad (3.5)$$

In principle, τ_{av} represents the centre of mass of the lifetime spectrum. Therefore, it is rather insensitive to the numerical fitting procedure applied. If bulk and defect-related lifetime are known, the trapping rate k_d may be determined from the average lifetime as:

$$k_d = \frac{1}{\tau_b} \frac{\tau_{av} - \tau_b}{\tau_d - \tau_{av}} \quad (3.6)$$

3.2 Temperature dependence of positron trapping in semiconductors

In contrast to metals, the trapping coefficient in semiconductors often reveals some temperature dependence, which might be different for different semiconductors or different defect types. A good example is given in section 7, where temperature dependent positron lifetime measurements in silicon- and tellurium-doped GaAs are discussed. Obviously, the temperature behavior of the trapping coefficient is specific for a certain defect and carries important information about defect properties. In order to be able to extract this information, details of positron trapping and reasons of its temperature dependence must be understood. This section gives a short overview of the current state of knowledge of the positron capture mechanisms in semiconductors and their temperature dependence. Firstly, a short description of the theoretical model of positron trapping is given, with an emphasis placed on the calculation of the trapping coefficient as a function of temperature. Secondly, I present the application of the model for fitting of the experimental results.

3.2.1 Theory

Most of the work on the theoretical description of positron trapping in semiconductors was done by a Finnish group (M. Puska, R. Nieminen et al.) in the late 80's. They provided calculations for two kinds of positron traps – vacancies in different charge states and negative ions. The trapping coefficient was obtained with the help of Fermi's golden-rule formula:

$$\nu = 4\pi \sum P_i P_f |M_{i,f}|^2 \delta(E_i - E_f), \quad (3.7)$$

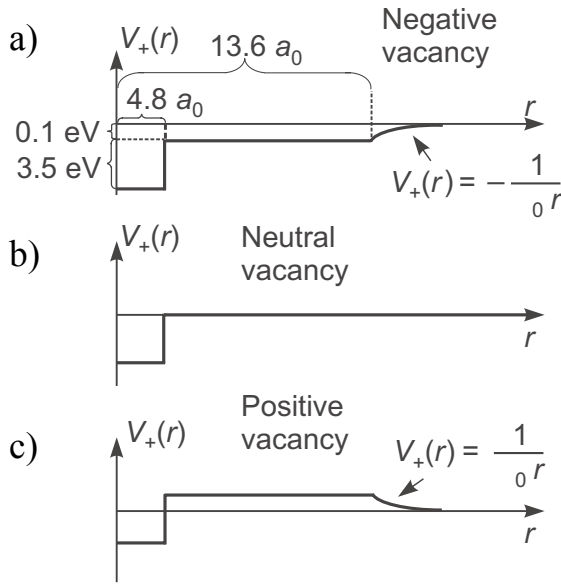


Fig. 3.3: Model of positron potential for (a) negative, (b) neutral and (c) positive vacancy (from Ref. (Puska and Nieminen 1994))

where P_i is the probability that the initial combined positron-host state $|i\rangle$ is occupied and P_f the probability that the final state $|f\rangle$ is allowed. $M_{i,f}$ is the matrix element of the interaction potential, which takes into account the energy transfer during the positron transition from the initial E_i to final E_f state. The summation in (3.7) is taken over all possible states meeting the energy conservation condition. Assuming the Maxwell-Boltzmann form for the initial positron distribution, the trapping coefficient as a function of temperature is given as the average:

$$\nu(T) = \sqrt{\frac{2}{\pi}} \left(\frac{m_+}{k_B T} \right)^{3/2} \int_0^\infty dE \nu(E) e^{-E/k_B T} \sqrt{E}, \quad (3.8)$$

where k_B is the Boltzmann constant and m_+ the positron effective mass.

In order to describe the interaction potential and to define the initial and final positron wave functions, Puska et. al. used the simple model schematically depicted in Fig. 3.3. For the neutral vacancy, the positron states were taken to be solutions for a square-well potential, the depth and width of which were chosen so that the s-like ground state had a binding energy and spatial extension identical to those obtained by first-principles calculations for electron and positron states in semiconductors. Charged vacancies were modeled by adding a $1/\varepsilon(0)r$ tail to the square-well potential, where $\varepsilon(0)$ is the static dielectric constant. The resulting potentials sensed by positrons at the negatively charged vacancy V^- and positively charged vacancy V^+ are shown in fig. 3.3 a) and c). The Coulomb tail has to be cut off when approaching the vacancy from infinity in order to mimic the weak localization of the “extra” electron charge. Therefore, near the vacancy the potential was shifted by the amount of $Q \times 0.1$ eV, where Q is the charge state of the vacancy and 0.1 the value of the Coulomb potential at the cutoff. According to Puska et.

al., this constant potential shift does not change the positron localization in the bound state and the energy value is simply shifted by the same amount as the potential. But the potential shift and the Coulomb tail can have a large effect on the delocalized positron wave functions at thermal energies, as demonstrated in the following.

One of the main model assumptions is that the long-range Coulomb tail introduces several positron Rydbergs states with low binding energies. These states may act as precursor states in the trapping process and thereby enhance the overall trapping coefficient for the defect. Thus, the trapping process of a delocalized positron may be divided into two parts: (i) direct trapping into the ground state at a vacancy and (ii) two-stage trapping – firstly, into a weakly localized Rydberg state from which the positron then makes a transition into a deeper localized state. Corresponding to these two kinds of positron trapping, there are five possible energy-loss mechanisms, in which the energy of a delocalized positron is released:

(i) Direct trapping:

- (a) electron-hole excitation from the valence to the conduction band;
- (b) electron-hole excitation from the localized defect-level to the conduction band;

(ii) Two-stage trapping:

- (c) phonon-assisted capture of a delocalized positron into a Rydberg state;
- (d) phonon-assisted transitions between Rydberg states;
- (e) transition from a Rydberg state to the ground state.

These processes are illustrated in Fig. 3.4.

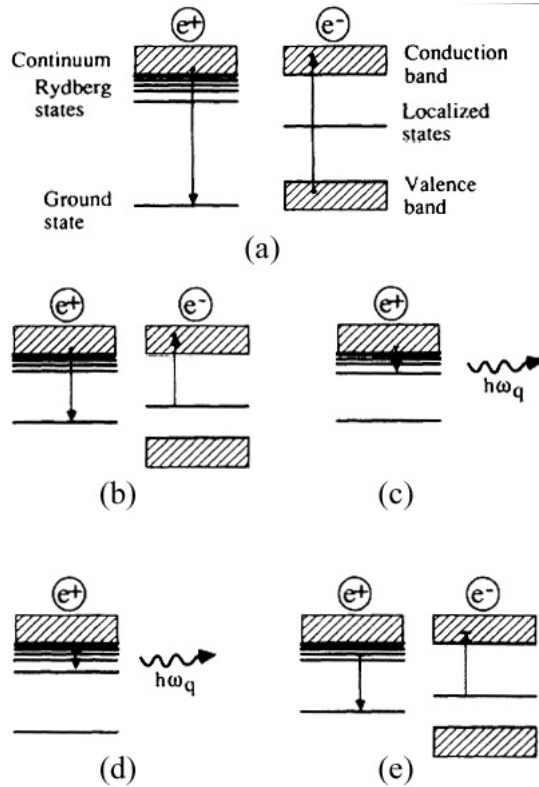


Fig. 3.4: Schematic representation of the positron energy-loss mechanisms: (a) interband electron-hole excitations and (b) exciting of the electron from a defect level to conduction band; (c) trapping into Rydberg states; transition (d) between Rydberg states and (e) between Rydberg and ground states. (From Ref. (Puska and Nieminen 1994))

In fact, only the first three transition mechanisms relate to the capture of a delocalized positron and thus determine the temperature dependence of the trapping coefficient. The process most sensitive to temperature is positron trapping into a Rydberg state of shallow Coulomb potential of a negative vacancy. Since the binding energy of the positron to the trap is low, there is a certain probability of the escape (detrapping) of the positron from the trap back to a delocalized state. When the delocalized and the trapped states are in thermal equilibrium the detrapping rate δ and the trapping rate k at a given temperature are given as (Puska and Nieminen 1994):

$$\frac{\delta}{k} = \frac{1}{c_v} \left[\frac{m_+ k_B T}{2\pi\hbar^2} \right]^{3/2} e^{-E_R/k_B T}, \quad (3.9)$$

where $N_c = [m_+ k_B T / 2\pi\hbar^2]^{3/2}$ is the density of positron states per volume in the positron delocalized states band, C_v is the concentration of negative vacancies and E_R is the positron binding energy of the shallow precursor state.

Using the model of the interaction potential introduced above, Puska et al. calculated temperature dependencies for the three mechanisms of positron trapping. The results are presented in Fig. 3.5. Trapping coefficients for negative vacancies V^- and V^{2-} were obtained using the attractive Coulomb potential tail [Fig. 3.3 (a)]. The initial positron scattering states were then represented by Coulomb waves. Due to the Coulomb tail, the trapping coefficient of the negative vacancy is about one order of magnitude larger than

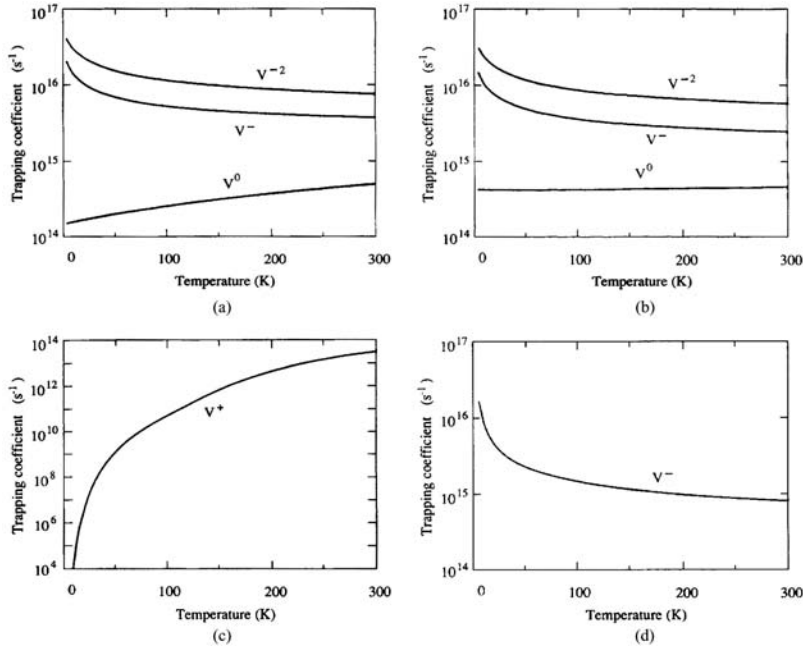


Fig. 3.5: Temperature dependence of the positron trapping coefficient for positive, single and double negative vacancies calculated for different trapping mechanisms: (a) interband electron-hole excitation, (b) and (c) electron excitation from defect level to conduction band, (d) trapping into Rydberg state.

the one of the neutral vacancy [Fig. 3.5 (a, b)]. At 300 K, it amounts to $2\text{-}5 \times 10^{14} \text{ s}^{-1}$ and $2\text{-}4 \times 10^{15} \text{ s}^{-1}$ for the neutral and singly negative vacancy, respectively. These values are in good agreement with the trapping coefficients found experimentally for the negatively charged gallium vacancy in GaAs (Le Berre et al. 1995; Gebauer et al. 1997).

As Fig. 3.5 shows, the temperature coefficient for the neutral vacancy V^0 is either independent of the temperature [Fig. 3.5 (b)] or increases by factor of 3 as temperature rises from 0 to 300 K [Fig. 3.5 (a)]. The increasing behavior is due to p-type scattering resonance for delocalized positron states at energies above the typical thermal energies. If the positron kinetic energy is near the resonance, the initial positron state is strongly enhanced at the vacancy, what increases the overlap of the initial and final states and thus also the positron trapping coefficient. However, the p resonance is significant only for interband electron-hole excitation [Fig. 3.4 (a)], whereas it has a little effect on the trapping coefficient for the trapping process mediated by the excitation of electrons from localized defect levels [Fig. 3.4 (b)]. For a more detailed explanation, the reader is referred to Ref. (Puska et al. 1990).

For the negative vacancy V^- , the trapping coefficient increases towards lower temperatures and diverges at low temperatures being proportional to $T^{-1/2}$. This divergence is a direct consequence of the normalization of the initial positron wave function. The square of the amplitude of the Coulomb wave at the origin, i.e. at the center of the vacancy, is at maximum and behaves as (Mott and Massey 1965):

$$|u_{i,p}(0)|^2 \propto \frac{\alpha}{e^{2\pi\alpha} - 1}, \quad (3.10)$$

where

$$\alpha = \frac{m_+ Q}{\varepsilon p}. \quad (3.11)$$

The ε in Eq. (3.11) is the dielectric constant and p is the positron wave-vector. For a negative charge state Q , the square of the matrix element (3.7) and thus the positron trapping coefficient are inversely proportional to the square root of the positron energy. The integral over energy in Eq. (3.8) becomes then proportional to the temperature, what together with the prefactor of $T^{-3/2}$ gives the trapping coefficient proportional to $T^{-1/2}$. For α close to zero, the amplitude in (3.10) approaches a constant value and the wave function becomes a plane wave. Thus, the trapping coefficient of neutral vacancies does not diverge at low temperatures. For a double negative vacancy V^{2-} , a similar temperature behavior of the trapping coefficient was predicted. According to (3.10), the trapping coefficient is directly proportional to Q and the ratio of the trapping coefficients for V^{2-} and V^- should be a factor of 2 [Fig. 3.5 (a, b)].

The temperature dependence of the trapping coefficient for a positively charged vacancy is plotted in Fig. 3.5 (c). As the calculations show, trapping into positively charged vacancies should be possible at temperatures higher than 200 K ($v \geq 10^{13} \text{ s}^{-1}$).

However, this was never observed experimentally. The probable reason is that the positron does not have enough time to tunnel through the repulsive Coulomb barrier.

The result of the calculations for positron trapping into a Rydberg state of a negative vacancy is shown in Fig. 3.5 (d). The trapping coefficient lies in the same order of magnitude as for the trapping into a ground state. However, it decreases more strongly with increasing temperature, because of detrapping of positrons from the Rydberg state due to the small binding energy (Eq. 3.9).

3.2.2 Model of positron trapping for experimental data fitting

This section describes a model of positron trapping for fitting of $\tau_{av}(T)$ curves obtained experimentally. The average positron lifetime is chosen for fitting, since it is a most stable and thus reliable parameter in the procedure of spectra analysis, which does not depend much on the details of decomposition. At the heart of the model, the theoretical considerations of two-stage positron trapping presented in the previous section are lying. Two cases of positron trapping are considered:

- 1) one-defect model: positron trapping by negative vacancies only;
- 2) two-defect model: positron trapping by negative vacancies and negative ions (shallow traps).

1) One-defect model: negative vacancies.

For positron trapping at a single defect, the trapping rate is given by Eq. 3.6. After a simple algebraic transformation, the average positron lifetime can be expressed as:

$$\tau_{av} = \tau_b \frac{1 + K_d \tau_v}{1 + K_d \tau_b}. \quad (3.12)$$

According to the two-stage trapping model (Fig. 3.6), the global trapping rate K_d is given by the sum of two trapping mechanisms: direct and indirect two-stage trapping. The direct trapping to the ground state of the vacancy occurs at a rate K_v . In the two-stage trapping model, positrons are captured into the Rydberg states of the long-range Coulomb potential at rate K_R and positron detrapping from these states at rate δ_R .

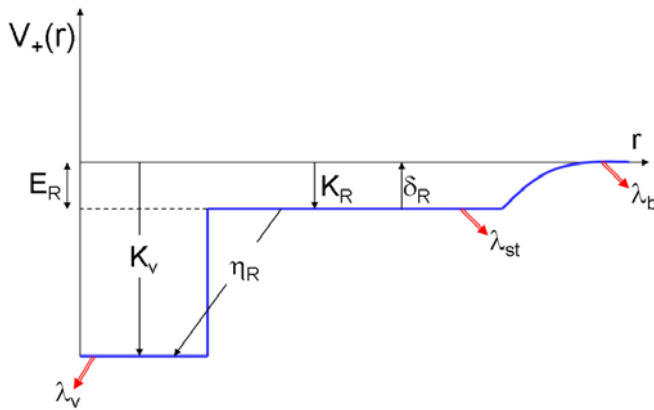


Fig. 3.6: Model of positron trapping into negative vacancy involving positron capture into Rydberg states of the attractive Coulomb potential at rate K_R and positron detrapping from these states at rate δ_R .

Table 3.1 - Fitting parameters for the model of temperature-dependent positron trapping (all parameters correspond to the temperature of 20 K)

Parameter symbol	Parameter definition and its typical values
K_V	Rate of positron trapping directly into the ground state of the vacancy. It is related to vacancy concentration C_V by the relation $K_V = \mu_V C_V$, whereas the trapping coefficient μ_V of a negative vacancy is typically in the order of $1.5-3 \times 10^{16} \text{ cm}^3 \text{ s}^{-1}$ (Le Berre et al. 1995).
K_R	Rate of positron trapping into the Rydberg states of negative Coulomb potential. Typically $K_R/K_V \geq 5$, reflecting the larger overlapping of the delocalized positron wave function with the extended Coulomb potential.
E_R	Positron binding energy to a single effective state approximating the series of Rydberg states. Typical value $70 \pm 30 \text{ meV}$ (Le Berre et al. 1995).
μ_R / η_R	Ratio between the rate of the positron trapping into Rydberg states μ_R and positron transition rate η_R from Rydberg to ground state. Usually $\mu_R / \eta_R \approx 10^4 - 10^5$ is assumed.

potential with a rate K_R . Thereafter, they can either make a transition into the ground state at a rate η or escape from the Rydberg state to a delocalized state at the detrapping rate δ which is given by Eq. (3.9). A net trapping rate of the two-stage trapping is defined as (Puska et al. 1990)

$$K_{indirect} = \frac{K_R \eta_R}{\eta_R + \delta_R}. \quad (3.13)$$

Thus, the K_d can be written as:

$$K_d = K_{direct} + K_{indirect} = K_V + \frac{K_R}{1 + \frac{\mu_R}{N \eta_R} \left[\frac{m_+ k_b T}{2\pi \hbar^2} \right]^{3/2} \exp \left[-\frac{E_R}{k_b T} \right]}, \quad (3.14)$$

where N is the atom concentration per unite volume and μ_R is the trapping coefficient of the positron to Rydberg state, related to K_R through $K_R = \mu_R C_V / N$. Assuming that K_R and K_V vary like $T^{-1/2}$ as predicted by theory in the previous section, K_d may be written as:

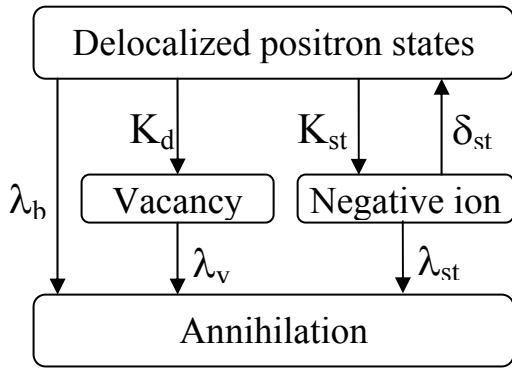


Fig. 3.7: Model of positron trapping into two defects: vacancy and negative ions (shallow positron traps). The model considers positron detrapping from shallow traps.

$$K_d = K_V(20K) \left[\frac{T}{20K} \right]^{-1/2} + \frac{K_R(20K) \left[\frac{T}{20K} \right]^{-1/2}}{1 + \frac{\mu_R}{N\eta_R} \left[\frac{T}{20K} \right]^{-1/2} \left[\frac{m_+ k_b T}{2\pi\hbar^2} \right]^{3/2} \exp \left[-\frac{E_R}{k_b T} \right]}. \quad (3.15)$$

Substituting K_d in Eq. 3.12 by Eq. 3.15, one obtain a $\tau_{av}(T)$ dependent on four independent parameters depicted in Fig. 3.6 and listed in Table 3.1.

2) Two-defect model: negative vacancies and shallow traps

Positron traps are not only restricted to open-volume defects. Also negative ions can capture positrons due to their attractive Coulomb potential (Fig. 3.3, 3.7). The capture mechanism is similar to the process of positron trapping into a Rydberg state of a negative vacancy (Section 3.2.2). Due to the weak positron binding energy, negative ions are often referred to as *shallow positron traps* (Saarinen et al. 1989). Similarly to the positron capture at Rydberg states, positron trapping into shallow traps is efficient only at low temperatures, where positron thermal energies are small. At higher temperatures, detrapping of positrons from shallow traps dominate. The detrapping rate δ_{st} is defined similar to the Eq. (3.9):

$$\frac{\delta_{st}}{K_{st}} = \frac{1}{c_{st}} \left[\frac{m_+ k_b T}{2\pi\hbar^2} \right]^{3/2} e^{-E_{st}/k_b T}, \quad (3.16)$$

with c_{st} and E_{st} being concentration and positron binding energy of a shallow trap defect.

Since there is no open volume associated with a shallow trap, its positron lifetime does not differ from the one in the bulk crystal. Hence, shallow positron traps can not be directly detected by positron lifetime measurements, but only under the condition that some open-volume defects are present in the crystal. In this case, shallow positron traps are clearly seen as a decrease of positron average lifetime at low temperatures¹.

¹ Typical example of a shallow trap defect is a Si_{As} acceptor in silicon doped GaAs (Section 4.2.2)

Thus, when shallow positron traps are present in the crystal, the one-defect trapping model described above is only applicable at temperatures higher than 200 K. At lower temperatures, positrons are trapped into both vacancy and shallow trap defects and thus the two-defect trapping model must be used. The average positron lifetime can be written as (Le Berre et al. 1995):

$$\tau_{av} = \tau_d \frac{(\lambda_d + K_d) \left[\frac{\lambda_{st}}{K_{st}} + \frac{\delta_{st}}{K_{st}} \right] + \lambda_d}{(\lambda_b + K_d) \left[\frac{\lambda_{st}}{K_{st}} + \frac{\delta_{st}}{K_{st}} \right] + \lambda_{st}}, \quad (3.17)$$

where $\lambda_d = 1/\tau_d$ is the annihilation rate at the vacancy defect and $\lambda_{st} = \lambda_b = 1/\tau_b$ are the annihilation rates at the shallow trap defect and in the bulk, respectively. The ratio δ_{st}/K_{st} of the detrapping rate to the trapping rate at the shallow traps is determined by Eq. (1.11). Similar to the K_d , it is assumed that K_{st} varies like $T^{-1/2}$.

At very low temperatures, the positrons thermal detrapping from the shallow traps may be neglected in first approximation. $K_{st}(20K)$ is then calculated using a simple two-defect trapping model:

$$K_{st}(20K) = \lambda_b \frac{\tau_{av}(20K) - \tau_b}{\tau_{st} - \tau_{av}(20K)} - \frac{\tau_{av}(20K) - \tau_d}{\tau_{av}(20K) - \tau_{st}} K_d(20K), \quad (3.18)$$

where τ_{st} is assumed to be equal to τ_b . This formula is useful, if $K_d(300K)$ can be determined from high-temperature measurements using a one-defect model. $K_d(20K)$ can be then calculated from $K_d(300K)$ using the temperature dependence $K(T) \sim T^{-1/2}$ (Le Berre et al. 1995).

3.3 Coincidence Doppler-broadening spectroscopy

The positron and the electron annihilate predominantly by emitting of two γ -quanta. In the center-of-mass frame, the total momentum of the electron-positron pair (e^+e^-) is zero and since the energy and momentum before and after annihilation are conserved the two photons are emitted in opposite directions, each one having an energy equal to 511 keV. In the laboratory frame, the e^+e^- pair carries a total moment \mathbf{p} , which is transferred to the photon pair, as shown in the momentum diagram in fig. 3.8. The longitudinal momentum component p_L results in a Doppler shift ΔE of the annihilation energy of 511 keV:

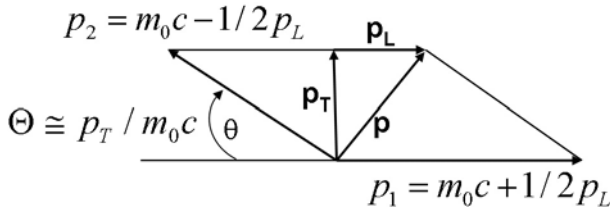


Fig. 3.8: The vector diagram of the momentum conservation in the 2γ -annihilation process. \mathbf{p} denotes the momentum of e^-e^+ pair.

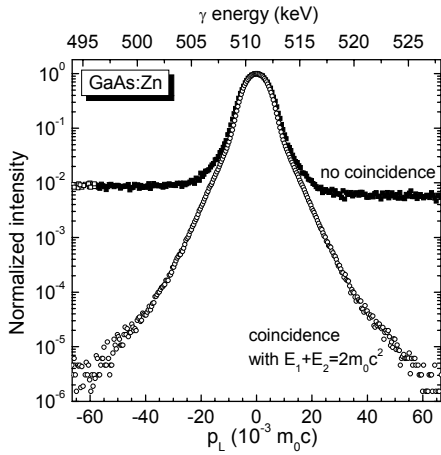


Fig. 3.9: Doppler-broadening spectra obtained in Zn-doped GaAs by the conventional (no coincidence) and coincidence spectroscopy.

$$\Delta E = p_L c / 2 \quad (3.18)$$

The positron is thermalized before annihilation, i.e. it has thermal energy and hence a small momentum. Therefore, p_L corresponds to the momentum of the electron participating in annihilation. Since the directions of \mathbf{p} to and from the detector are equiprobable, both positive and negative ΔE are measured, resulting in the Doppler-broadening of the annihilation line, so called Doppler-broadening spectrum (fig. 3.9). The Doppler spectrum may be considered as the probability of the positron annihilation with the electron having momentum p_L .

The energy of the annihilating γ -quanta is measured by high-resolution Ge- γ -detectors. The γ -photon creates electron-hole pairs in a high-purity Ge crystal, in which a high electric field is applied. The amplitude of the arising electrical pulse is proportional to the energy of the detected γ -quantum. After amplification and digitizing, the energy value is saved in a multi-channel analyzer.

The high energy part of a Doppler-spectrum contains important information on the chemical surrounding of the annihilation site (Alatalo et al. 1995; Alatalo et al. 1996; Alatalo et al. 1998). The large Doppler shift ΔE denotes annihilation with strongly bounded core electrons. The momentum properties of core electrons are not affected by chemical bonds and are specific for a certain atom. The positron localized in a vacancy defect annihilates mainly with the electrons of the nearest neighbor atoms. Thus, in compound semiconductors, analysis of the core-electron annihilation enables the identification of the vacancy sublattices (Alatalo et al. 1995) or impurity-vacancy complexes (Alatalo et al. 1995; Gebauer et al. 1999).

Unfortunately, the high-momentum part of the Doppler spectrum measured with a single γ -detector (conventional Doppler-broadening spectroscopy) is dominated by background and cannot be used for the analysis of core-electron annihilation. The background originates mainly from the Pile-Up-Effects in the detector and Compton scattering of the 1.27 MeV γ -quanta emitted from the source. The background may be dramatically re-

duced by the coincident registrations of both γ -quanta with the help of two detectors (Lynn et al. 1977; MacDonald et al. 1978; Troev et al. 1979). This technique received the name Coincidence Doppler-broadening Spectroscopy (CDBS). Using CDBS, the background may be suppressed by at least two orders of magnitude (fig. 3.9). The detailed description of the procedure to obtain the coincidence spectrum is given in Ref. (Gebauer et al. 1999).

The most important parameter sensitive to the chemical surrounding of the annihilation site is the form of the high-momentum distribution (Myler et al. 1996; Myler and Simpson 1997). In order to make the analysis of the spectrum form easier, so called ratio curves were introduced (Myler et al. 1996; Szpala et al. 1996). The ratio-curves are obtained by dividing the measured spectra by a reference one. As a reference, a spectrum of defect-free samples is usually taken. Often, CDB-measurements are performed in a pure elemental material as a reference in order to obtain a spectrum specific for the chemical element of interest. The characteristic features of the high-momentum part of the spectrum are conserved also in different environments. This provides a possibility to deduce whether the detected vacancy is neighbored by a certain atom (e.g. Cu in GaAs, fig. 5.11).

3.4 Procedure of positron annihilation measurements

The present study is based predominantly on the results of temperature-dependent measurement of positron annihilation lifetime. Three conventional fast-fast coincidence systems with resolution of 225 ps, 240 ps and 250 ps were at the experimentalist's disposal. A small quantity of radioactive Na^{22} -salt covered with 1.5 μm Al-foil was used as a positron source, which was placed in sandwich geometry between two identical samples. Typical source activity amounted to 1-1.5 MBq. The measurement temperature, T_{meas} , could be varied in the 20 K – 600 K range. Usually, the temperature program of lifetime experiments consisted of alternating temperatures. This means that T_{meas} was changed always with a step of $2 \times T_{\text{step}}$ from 300 K (room temperature) to the lowest temperature, then to the highest one and finally back to the room temperature, where T_{step} is a temperature step between two measurement temperatures. So, by T_{step} of 33 K used in this work most often, the temperature program will include following temperatures: 300 K, 234 K, 168 K, 102 K, 36 K, 20 K, 69 K, 135 K, 201 K, 267 K, 333 K, 399 K, 465 K, 498 K, 432, 366 K, 300 K. Such kind of measurement program is used to recognize a temperature-related hysteresis, if such takes place.

In each lifetime spectrum, 3 to 5×10^6 annihilation events were accumulated. The spectra were analyzed with the help of "Lifspecfit" routine (Puska 1978) after source and background correction. A piece of p-type Zn-doped or SI undoped GaAs exhibiting no positron trapping was used as a reference. In the source correction procedure, three lifetime components were assumed corresponding to annihilation inside the NaCl source (τ_{NaCl}) or the covering aluminum foil (τ_{Al}) and to three-photon annihilation from posi-

tronium state (τ_{ps}). The source correction was performed by the analysis of the reference lifetime spectrum. The lifetime intensities and τ_{ps} were used as fitting parameters, whereas τ_{NaC} and τ_{Al} were fixed to 380 ps and 165 ps, respectively (Somieski et al. 1996). The source parameters were considered as determined, when the positron lifetime of 230 ps, the bulk lifetime in GaAs (Gebauer et al. 2000), was obtained. Typically, source contribution did not exceed 15%, where the positronium share was in the order of 1%.

Doppler broadening coincidence spectroscopy was carried out using two Ge- γ -detectors with a channel width of 70.60 eV and an energy resolution of 0.9 keV. In each Doppler spectrum, about 5×10^7 coincident events during 5-6 days were collected. The intensity of the annihilation with high-momentum core electrons was characterized by the W parameter, defined as the relative intensity in the momentum range $(10-20) \times 10^{-3} m_0c$, where m_0c is the electron rest energy. For a qualitative analysis, the CDB curves were always normalized to the data obtained in SI undoped GaAs used as reference.

3.5 Other methods

Except the methods of positron annihilation, several additional methods were applied for the characterization of the GaAs crystals investigated in this work:

Photo- and cathodoluminescence (PL and CL) spectroscopy

Both of these techniques are contactless, nondestructive methods of probing the electronic structure of materials. Their basic principle involves the excitation of electrons from their ground state in the valence band to the conduction band or to some excited state within the band-gap associated with the defect energy level. When these electrons return to their equilibrium states, the excess energy is released and may include the emission of light (a radiative process or luminescence) or may not (a nonradiative process). The excitation is performed either by high-energy photon (photoluminescence) or electrons (cathodoluminescence). The energy of the emitted light is related to the difference in energy levels between the two electron states involved in the transition. Thus, luminescence spectroscopy can provide important information about the energy level of the point defects present in the semiconductor. For further details see e.g. (Yacobi and Holt 1990).

Measurements of the Hall Effect

This is a well-known method for the determination of the type, concentration and mobility of the free charge carriers in semiconductors. By the temperature-dependent Hall-measurements (TDH), it is possible to find out the activation energy of the dominating donor (acceptor) defect (Blakemore 1962).

Secondary Ion and Glow Discharge Mass Spectrometry (SIMS and GDMS)

SIMS and GDMS are destructive techniques for the analysis of the chemical composition of the inorganic solids. In this work, SIMS and GDMS were applied to obtain the concentrations of impurity atoms in the GaAs crystals. The principle of these techniques involves the mass spectrometry analysis of the individual atoms obtained by means of sputtering the sample surface by a primary energetic ion beam (SIMS) by sputtering of the sample in low-pressure DC plasma. For further explanations see e.g. (Feldman and Mayer 1986).

4. Vacancy formation in n-type silicon-doped GaAs

4.1 Introduction

Silicon is a widely used element for doping of gallium arsenide. Like other atoms of group IV, Si can occupy both the anion (arsenic) and cation (gallium) lattice sites exhibiting acceptor and donor properties, respectively. Usually the crystals grown from Ga solution by LPE (liquid phase epitaxy) have a p-type conductivity (Hicks and Greene 1960), whereas the material fabricated by both the Czochralski and Bridgman technique possesses a n-type conductivity. Due to the compensation effect, the concentration of conducting electrons (holes) is lower than the number of silicon dopants. The compensation reduces the doping efficiency and is a subject of great technological interest.

The compensation phenomenon in n-type heavily doped GaAs:Si was especially intensively investigated. In earlier studies, the electrical deactivation of silicon donors (Si_{Ga}^+) was attributed exclusively to silicon acceptors (Si_{As}^-), which were forming due to the amphoteric incorporation of Si atoms into the GaAs crystal lattice (Whelan et al. 1960). This mechanism is known as the “autocompensation”. However, in the late 80s, the analysis of infrared local vibrational mode (LVM) absorption showed that the autocompensation alone could not explain strong electrical deactivation of Si_{Ga} -donors in heavily Si-doped GaAs epitaxial layers (Maguire et al. 1987). Some years later, this was confirmed by near-edge and extended x-ray-absorption fine structure techniques (NEXAFS and EXAFS), see e.g. Refs. (Schuppler et al. 1993, 1995). It was established that only about half of the losses of the electrical activity could be explained by autocompensation and therefore some other compensating center had to be taken into account. A variety of the defects participating in the compensation was proposed: $\text{Si}_{\text{As}}\text{-Si}_{\text{Ga}}$ dimers (Schuppler et al. 1995), Si clusters (Muto et al. 1992) and $\text{Si}_{\text{Ga}}\text{V}_{\text{Ga}}$ (Maguire et al. 1987; McQuaid et al. 1992; Northrup and Zhang 1993; Newman 1994). The last of them, $\text{Si}_{\text{Ga}}\text{V}_{\text{Ga}}$, is of special interest, because the defect complexes of similar configuration were found to be responsible for the compensation in other n-type GaAs crystals, i.e. $\text{Te}_{\text{As}}\text{V}_{\text{Ga}}$ (Williams 1968; Hurlle 1977), $\text{Ge}_{\text{Ga}}\text{V}_{\text{Ga}}$ (Hurlle 1999) and $\text{S}_{\text{As}}\text{V}_{\text{Ga}}$ (Williams 1968; Gutkin et al. 1995) in Te-, Ge- and S-doped GaAs. It was reasonable to suggest that the formation of donor-gallium vacancy complexes is a characteristic reaction of a GaAs crystal on n-type doping.

Although the first observations of $\text{Si}_{\text{Ga}}\text{V}_{\text{Ga}}$ complex formation date back to the 80's, the strongest evidence of their existence have come from relatively recent scanning tunneling microscopy (STM) (Domke et al. 1996) and positron annihilation (PALS) (Laine et al. 1996, Gebauer et al. 1997) studies of highly Si-doped GaAs ($[\text{Si}] \approx 10^{19} \text{ cm}^{-3}$). The combination of these two methods has allowed to determine directly the defect microstructure (STM) and the absolute concentration (PALS). It was shown that the $\text{S}_{\text{Ga}}\text{V}_{\text{Ga}}$ concentration increased dramatically (up to 10^{19} cm^{-3}) vs Si content and that increase was related to strong compensation at high doping levels. Thereafter, some simplified compensation models were developed, in which two types of acceptors, Si_{As} and $\text{Si}_{\text{Ga}}\text{-V}_{\text{Ga}}$, were taken into account (Birkmann et al. 2002). Those models explain satisfactorily the electrical deactivation at high ($>10^{18} \text{ cm}^{-3}$) Si concentrations (see the solid line in Fig. 4.1), whereas the defects formed for lower doping levels are less investigated. Another drawback of those compensation models is the widely used assumption that the compensation degree depends solely on Si content. In other words, the concentration of acceptors responsible for compensation is supposed to be a function of $[\text{Si}]$ only. This may be accepted just as a rough approximation.

The aim of this chapter is to give an overview of defects studies in GaAs crystals doped with silicon, the concentration of which varies over a wide range from 10^{17} cm^{-3} up to 10^{19} cm^{-3} . Some already published results have been complemented with those obtained in this work. The chapter is organized as follows: in Section 4.2 the results of investigations of heavily doped GaAs:Si, in which the compensation due to $\text{Si}_{\text{Ga}}\text{-V}_{\text{Ga}}$ complex dominates, are presented. In Section 4.3, it is shown that the compensation degree in a GaAs:Si wafer may be influenced by local dislocation density distribution. In Section 4.4, the origin of the defect that gives rise to the 1250 nm (0.95 eV) luminescence peak is discussed. It is demonstrated that this defect contributes to the vacancy signal detected by PALS in crystals with the silicon concentration of $[\text{Si}] < 10^{18} \text{ cm}^{-3}$. The defect was not observed in previous studies of heavily doped GaAs:Si since high silicon concentration suppresses its formation.

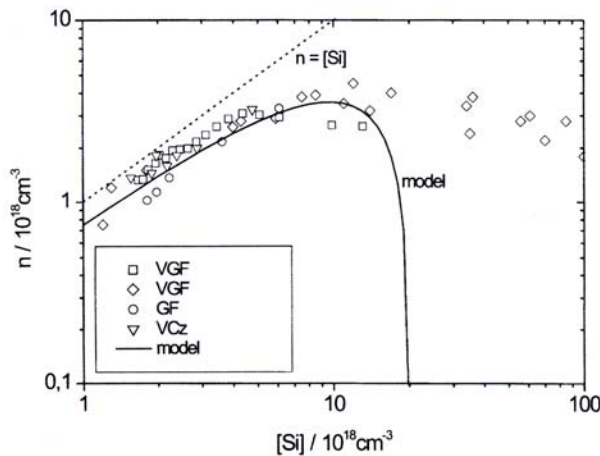


Fig. 4.1 Carrier concentration, n , versus the concentration of silicon dopants, $[\text{Si}]$, in GaAs:Si crystals grown with different techniques. The solid line represents a compensation model from Ref. (Birkmann et al. 2002)

4.2 Heavily silicon doped GaAs

Gallium arsenide doped with silicon in the range of $10^{18} - 10^{19} \text{ cm}^{-3}$ was extensively investigated by various experimental techniques including the positron annihilation. Therefore, the results presented in this section do not really extend the state of knowledge about point defect formation in this material. They were included into this chapter in order to give a complete picture of point defects in GaAs:Si. In addition, investigations of highly doped GaAs:Si represent a starting point for further studies of less doped material providing reference annihilation parameters for the identification of the well-investigated $\text{Si}_{\text{Ga}}\text{V}_{\text{Ga}}$ centers.

4.2.1 Experimental

The investigated samples were prepared using VGF boron-encapsulated crystals grown in the Crystal Growth Laboratory of the Department of Materials Science at the University of Erlangen. Their specifications are presented in Table 4.1. The Si and free charge carrier concentrations were determined by SSMS (Spark Source Mass Spectrometry, Dr. Wiedemann, Frankfurt University) and by Hall effect measurements (Dr. B. Birkmann, Erlangen University). The concentration of boron was in the same order of magnitude as that of silicon.

Table 4.1 Specifications of the heavily Si-doped GaAs VGF-grown crystals investigated in this work

Si concentration, cm^{-3}	Density of free charge carriers, cm^{-3}	Mobility, cm^2/Vs
1.61×10^{18}	1.40×10^{18}	1994
2.59×10^{18}	2.07×10^{18}	1724
3.55×10^{18}	3.05×10^{18}	1506
9.73×10^{18}	2.82×10^{18}	1085

The samples were investigated by positron lifetime and coincidence Doppler-broadening spectroscopy. The measurement procedure is described in Section 3.4.

4.2.2 Defect identification by means of positron annihilation

Average positron lifetime τ_{av} versus temperature obtained for GaAs doped with silicon at different doses is presented in Fig. 4.2. The temperature dependences of τ_{av} are similar for all samples indicating the same defects configuration. The magnitude of τ_{av} increases with temperature and reaches some value of saturation at $T > 300 \text{ K}$ that is distinctly higher than the bulk positron lifetime in GaAs, $\tau_{\text{b}} = 230 \text{ ps}$ (Gebauer et al. 2000). The increased average lifetime results from positron trapping into vacancy-like defects. The decomposition

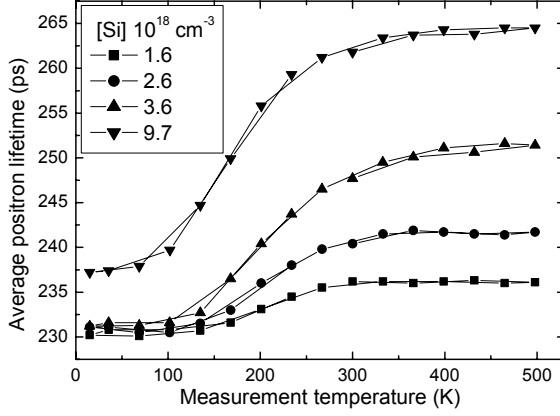


Fig. 4.2: Average positron lifetime as a function of measurement temperature in highly Si-doped VGF-grown GaAs. The concentrations of silicon dopants are indicated. The lines are to guide the eye.

of lifetime spectra by two components yielded the vacancy related lifetime $\tau_v = 262 \pm 5$ ps in all samples except the one with the highest Si content. For this sample, the vacancy concentration exceeded the PALS's sensitivity limit leading to the saturated positron trapping, i.e. the annihilation of all positrons took place in the vacancy-defect. As a result of the saturated trapping, all high temperature spectra had a single component τ_v equal τ_{av} . The lifetime of 262 ps is a typical value for a monovacancy in GaAs. The result gives a certain reason to believe the difference of the τ_{av} values over the range of saturation (see Fig. 4.2) is due to the change of the concentration of the defects having the same configuration.

At low temperatures, τ_{av} is close to τ_b indicating predominant trapping of positrons by non-open volume defects. Such defects are known as positron shallow traps and are commonly attributed to ionized acceptor-like ions, which are able to trap positrons into their negative potential (Saarinen et al. 1989). Since there is no open volume associated with the ions, the positron lifetime τ_{st} related to them is equal τ_b , $\tau_{st} = \tau_b = 230$ ps. Thus, the observed temperature behavior of τ_{av} can be thus explained by competitive positron trapping into two defect types – vacancies and shallow traps:

$$\tau_{av}(T) = (1 - \eta_{st}(T) - \eta_d(T))\tau_b + \eta_{st}(T)\tau_{st} + \eta_v(T)\tau_d, \quad (4.1)$$

where η_{st} and η_v are the fractions of positrons trapped by shallow trap and vacancy-like defects, respectively.

A similar temperature dependence of τ_{av} was observed by J. Gebauer et al. in other heavily Si-doped GaAs samples (Gebauer et al. 1997) investigated by PALS and STM spectroscopy. It was demonstrated rather conclusively that the two defects responsible for positron trapping were $\text{Si}_{\text{Ga}}\text{V}_{\text{Ga}}$ complexes and Si_{As} acceptors. For the vacancy complex, nearly the same positron lifetime ($\tau_v = 262 \pm 2$ ps) as in the samples studied in this work was found. The similar τ_v as well as the qualitative agreement between the τ_{av}

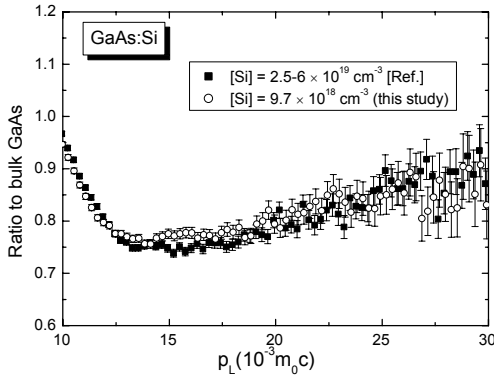


Fig. 4.3: High momentum part of Doppler broadening peak normalized to the data of bulk GaAs. (■) corresponds to GaAs:Si studied by positron annihilation and STM spectroscopy (Gebauer et al. 1997); (○) this study

temperature dependences allows to make the assumption concerning similarity of the microstructure of the defects observed.

In addition, the sample with the highest vacancy concentration was investigated by coincidence Doppler broadening spectroscopy (CDBS). The high momentum part of the annihilation Doppler peak normalized to the data obtained for GaAs reference is shown in Fig. 4.3. Solid squares correspond to the data taken from Ref. (Gebauer et al. 1999), which were obtained for the GaAs:Si sample investigated by STM in Ref. (Gebauer et al. 1997). The momentum distributions of the annihilation radiation in both samples are practically identical. This supports the assumption made above concerning the similar origin of the vacancy defect observed in this study and in the works done earlier (Gebauer et al. 1997). Two types of the point defects detected by positrons in heavily doped GaAs:Si were identified as $\text{Si}_{\text{Ga}}\text{V}_{\text{Ga}}$ complex and Si_{As} acceptor.

4.2.3 Model of the compensation mechanism

In this subsection, a simplified model of the compensation in GaAs:Si is discussed. The main goal of the model is to show that the formation of $\text{Si}_{\text{Ga}}\text{V}_{\text{Ga}}$ complexes can qualitatively explain the strong electrical deactivation of silicon donors (Table 4.1), which can not be understood in terms of autocompensation due to Si_{As} acceptors alone.

Two major assumptions have to be made. Firstly, three types of point defects are taken into account: Si_{Ga}^+ as the dominating donor and Si_{As}^- , $\text{Si}_{\text{Ga}}\text{V}_{\text{Ga}}^{2-}$ as two acceptors. The charge state of the vacancy complex is given as the sum of the charges states of Si_{Ga}^+ and $\text{V}_{\text{Ga}}^{3-}$ (Tan et al. 1993; You et al. 1993). Other Si-related defects (e.g., $\text{Si}_{\text{Ga}}\text{-Si}_{\text{As}}$ pairs and Si clusters) are known to become important for $[\text{Si}] \approx 3 \times 10^{18} \text{ cm}^{-3}$ (Suezawa et al. 1991) and can be neglected in the first approximation. Thus, the free carrier concentration can be evaluated as:

$$n = [\text{Si}_{\text{Ga}}] - [\text{Si}_{\text{As}}] - 2[\text{Si}_{\text{Ga}}\text{V}_{\text{Ga}}]. \quad (4.2)$$

The second assumption is that all silicon atoms are electrically active, i.e.:

$$[Si_{Ga}] = [Si] - [Si_{As}] - [Si_{Ga}V_{Ga}]. \quad (4.3)$$

The concentration of silicon atoms was determined by SIMS measurements (Table 4.1), $[Si_{Ga}V_{Ga}]$ and $[Si_{As}]$ could be extracted from the results of positron annihilation. The vacancy concentrations were calculated according to the one-defect two-component trapping model (Section 3.1.2) using the lifetime spectra measured at 500 K. At this temperature, positron trapping by shallow traps can be neglected due to the temperature detrapping of positron captured into the shallow negative potential of acceptor ions (Eq. 3.16). The decomposition of the spectra was performed at the fixed value of the vacancy-related lifetime, $\tau_{av} = 264$ ps. This lifetime corresponds to the maximum value of τ_{av} for positron saturated trapping (Fig. 4.2). The trapping coefficient μ_v was taken to be $1.7 \times 10^{15} \text{ s}^{-1}$ (Le Berre et al. 1995). After the vacancy concentrations were determined, the density of shallow traps could be obtained at 20 K using the three-state trapping model (Section 3.1.2). In this model, the positron annihilation at vacancy defects, negative ions and in the bulk is considered. According to the temperature dependence of the vacancy trapping coefficient (Puska and Nieminen 1994), the value of $\mu_v(20 \text{ K}) = 1.5 \times 10^{16} \text{ s}^{-1}$ was used. For the ions, $\mu_i(20 \text{ K}) = (5 \pm 2) \times 10^{16} \text{ s}^{-1}$ was taken (Saarinen et al. 1995; Gebauer et al. 1997). The values of concentration obtained by this procedure, $[Si_{Ga}V_{Ga}]$ and $[Si_{As}]$, are plotted in Fig. 4.4. For the highest level of doping, only the lower limit of vacancies concentration could be obtained due to the saturation observed for positron trapping.

As the number of acceptors has been determined, the concentration of free charged carriers may be easily calculated from Eqs. (4.2) and (4.3):

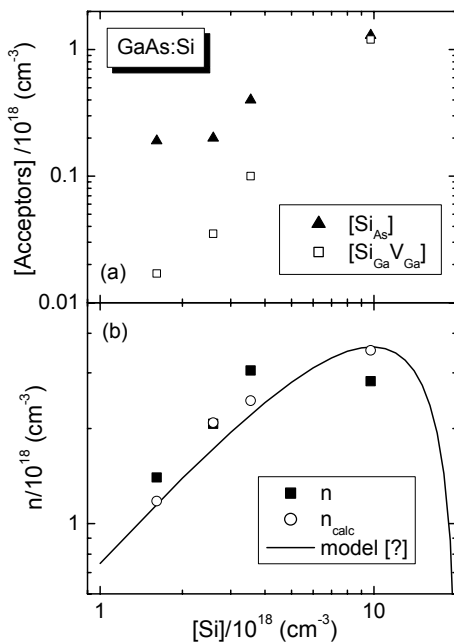


Fig. 4.4: (a) Concentration of acceptor-like defects ($Si_{Ga}V_{Ga}$, and Si_{As}) determined by positron annihilation lifetime spectroscopy as a function of Si concentration.

(b) Free electrons concentration directly measured (\blacksquare) and calculated (\circ) within compensation model using acceptors concentrations shown in (a).

$$n = [Si] - 2[Si_{As}] - 3[Si_{Ga}V_{Ga}]. \quad (4.4)$$

The calculated n_{calc} and directly measured n values of the carrier concentration are shown in Fig. 4.4 (b) as a function of $[Si]$. For the high values of $[Si]$, both n_{calc} and n demonstrate a deviation from the linear increase. This indicates the enhancement of the compensation degree at high doping levels due to the rapid increase of the concentration of the acceptor-like $Si_{Ga}V_{Ga}$ complexes [see Fig. 4.4 (a)]. However, n_{calc} is higher than n obtained for the sample having the highest concentration of silicon. The discrepancy observed can be explained as follows. In this sample, the concentration of $Si_{Ga}V_{Ga}$ complexes was underestimated due to the saturated positron trapping mentioned above; so the concentration of silicon acceptors was also underestimated, since Eq. (3.18) used for its calculation contains the quantity $[Si_{Ga}V_{Ga}]$. Therefore, the concentrations of acceptors used in (4.4) were lower than the real ones and n_{calc} hence higher than the real free electron density n . The solid line in Fig. 4.4(b) represents a compensation model developed in Ref. (Birkmann et al. 2002), which is based on a similar approach under the following assumption made on the acceptors concentrations:

$$[Si_{As}] = [Si]/11, \quad (4.5)$$

$$[Si_{Ga}V_{Ga}] = 2.3 \cdot 10^{16} \text{ cm}^{-3} \cdot ([Si]/10^{18} \text{ cm}^{-3})^{1.82}. \quad (4.6)$$

The dependence (4.5) was deduced from results of LVM measurements (Hannig et al. 1999); (4.6) is just a power-law fit to the published STM (Gebauer et al. 1997) and PALS (Laine et al. 1996; Gebauer et al. 1997) data on $Si_{Ga}V_{Ga}$. The results obtained by these approximations are in good agreement with the magnitudes of the $[Si_{As}]$ and $[Si_{Ga}V_{Ga}]$ concentrations under discussion in this thesis.

Summarizing the results, doping of GaAs by Si impurity results in the formation of acceptor-like $Si_{Ga}V_{Ga}$ complexes. The concentration of this complexes increases rapidly with the increasing doping level. The simplified compensation model based on direct measurements of the concentration $Si_{Ga}V_{Ga}$ by positron annihilation correctly describes the $[Si]$ - n -relationship for the range of concentrations $[Si] < 10^{19} \text{ cm}^{-3}$ (Fig. 4.1 and Fig. 4.4). At higher doping levels, the model is not valid due to the formation of other defects (such as, e.g. Si-pairs and Si-clusters), which were not taken into consideration in the model. Moreover, the vacancy concentrations in GaAs doped with Si at doses higher 10^{19} cm^{-3} exceed the sensitivity limit of positron annihilation and thus cannot be established.

4.3 Influence of dislocations on the lateral distribution of $Si_{Ga}V_{Ga}$ complexes in Si-doped VGF GaAs wafers

The compensation model of GaAs:Si described in the previous section allows us to outline the acceptors concentration as a function of silicon content only. This section dis-

cusses the influence of the dislocation density on the distribution of $\text{Si}_{\text{Ga}}\text{V}_{\text{Ga}}$ complexes. The interrelation between the concentration of $\text{Si}_{\text{Ga}}\text{V}_{\text{Ga}}$ defects and dislocation density was noted by Baeumler et al. in a recent photoluminescence study (Baeumler et al. 2002). They found a variation of a PL (photoluminescence) signal across a GaAs:Si wafer with non-homogeneous distribution of dislocations. The intensity of the 1100 nm peak attributed usually to $\text{Si}_{\text{Ga}}\text{V}_{\text{Ga}}$ complex anticorrelated with the concentration of dislocations. Since PL is a non-quantitative method, series of the samples cut out from the same wafer were studied in this work by means of positron annihilation. (Section 4.3.2). The results of more detailed investigations are presented in Section 4.3.3; in particular, it was shown that the dislocations may induce the variation of $\text{Si}_{\text{Ga}}\text{V}_{\text{Ga}}$ concentration resulting in the variation of compensation degree over GaAs:Si wafer.

4.3.1 Experimental details

Two wafers obtained from different VGF-grown GaAs:Si crystals were investigated. In the following, the wafers are referred as numbers #1 and 2.

Wafer #1 was investigated earlier by photoluminescence spectroscopy (PLS) and by laterally resolved photoluminescence topography (PLT) measurements (Baeumler et al. 2002). PLS and PLT were performed at 2 K using 514 nm Ar^+ laser illumination with 60 μm diameter spot size. The signal was dispersed with 1 m monochromator equipped with grating blazed at 2000 nm (band width 3 nm) and detected with the LN_2 cooled Ge detector.

PLT measurements on wafer #2 were performed at room temperature (RT) with 634 nm laser beam using Si-Detector sensitive over the range of 320 to 1100 nm wavelength. 2D-distribution of free charged carriers' concentration was determined by infrared absorption (IRA) and Hall-Effect measurements at RT. For the IRA, 1064 nm laser was used. The distribution of dislocation density was determined by EPD (etch-pit density) topography measurements.

The silicon content was determined by SIMS (wafer #1) or AtES (Atom emission spectroscopy, wafer #2) and amounted to $1.5 \times 10^{18} \text{ cm}^{-3}$ and $(1.3 \pm 0.1) \times 10^{18} \text{ cm}^{-3}$ in wafers #1 and #2, respectively.

For PALS investigations, several pieces with the size of 5×5 mm were prepared from each wafer. The exact positions of the samples taken from wafers #1 and #2 are indicated in Fig. 4.7 and Fig. 4.10, respectively. The measurement procedure is given in Section 3.4

4.3.2 Correlation between photoluminescence and positron annihilation investigations of silicon doped VGF GaAs

A typical PL spectrum of VGF GaAs:Si contains four luminescence band (Fig. 4.5, Table 4.2).

Table 4.2 - Assignment of photoluminescence lines in VGF GaAs:Si (Williams 1968; Tajima et al. 1994)

Label	Wavelength (nm)	Energy (eV)	Transitions from conduction band and shallow donors (Si_{Ga}) to valence band and shallow acceptors (Si_{As}^0 and B_{As}^0)
BN	832	1.49	
e, B_{As}^-	922	1.34	B_{As}^-
Si-Y	1100	1.13	$\text{Si}_{\text{Ga}}\text{V}_{\text{Ga}}$ acceptor level
X	1250	0.99	Undefined deep center, X

The luminescence intensities of these bands were found to be dependent on the position of the measurement on the wafer. The intensities of Si-Y and X bands increase from the wafer's center towards its edge whereas the intensities of BN and (e, B_{As}^-) bands were found to be higher at the center of the wafer (Fig. 4.5).

Full wafer topograms of wafer #1 shown in Fig. 4.6 present a more detailed pic-

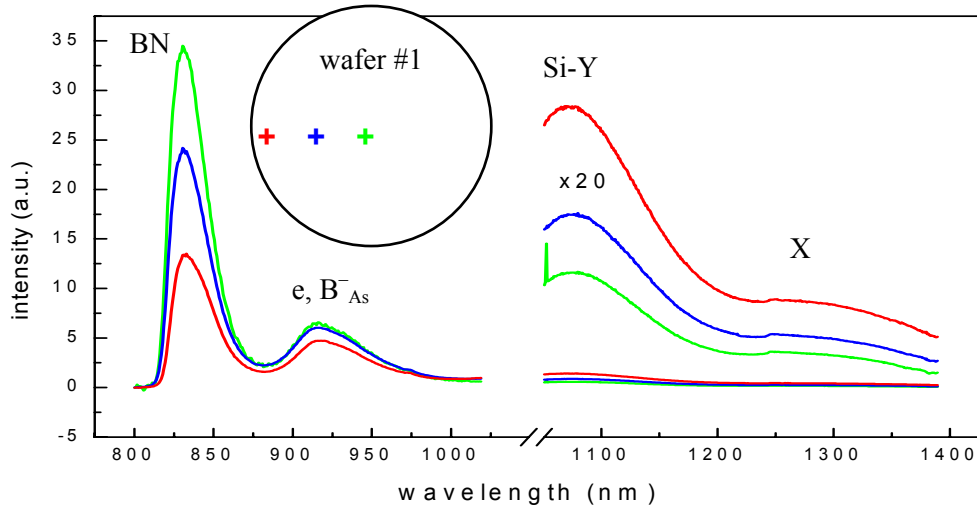


Fig. 4.5: Photoluminescence spectra measured in VGF GaAs:Si wafer #1. Curves of different colors correspond to different measurement positions on the wafer as indicated schematically by the colored crosses. Intensities of the bands with wavelengths higher 1050 nm are shown explicitly with 20 \times magnification. The spectra were not normalized. (From Ref. (Baeumler et al. 2002))

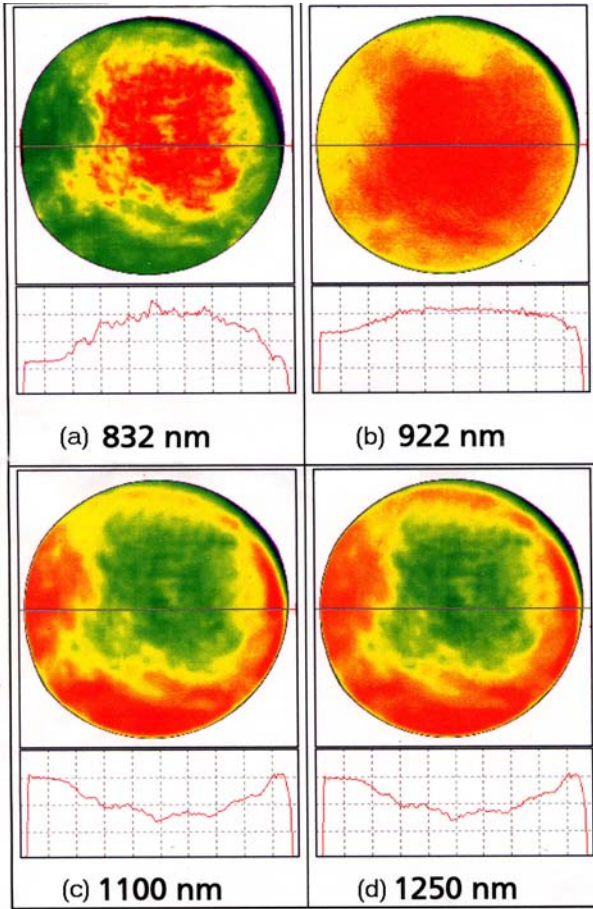


Fig. 4.5: Photoluminescence topograms of wafer #1 measured for the four luminescence lines occurring in GaAs:Si (see Fig. 4.5). (From Ref. (Baeumler et al. 2002)). The assignments of each PL-band are given in Table 4.2.

ture of the lateral intensity variation of each luminescence line. The variations were not connected with the distribution of silicon dopants across the wafer, since the latter was constant as determined by SIMS. In contrast, etching experiments revealed non-homogeneous distribution of local dislocation density. It was found that the intensity of the shallow (832 nm and 922 nm) transitions correlates whereas its value for the deep transitions (1100 nm and 1250 nm) anticorrelates with the EPD patterns. Such intensity variation can be explained either with the concentration variation of transition centers itself or by the presence of some non-homogeneously distributed non-radiative recombination center (NRRC). Thus, the dislocations can act as NRRCs in GaAs (Hoering 2001). On the other hand, dislocations are known to change the stoichiometry in the surrounding volume (Weyher et al. 1992). The area around the dislocations may contain less gallium vacancies and thus less $\text{Si}_{\text{Ga}}\text{V}_{\text{Ga}}$ resulting in a reduction of the 1100 nm photoluminescence peak. The problem can be resolved by direct measurement of the $\text{Si}_{\text{Ga}}\text{V}_{\text{Ga}}$ distribution by positron annihilation measurements.

For PALS investigation, the central part of the wafer #1 was cut into 15 sample pairs as shown in Fig. 4.7. Average positron lifetime τ_{av} is presented in Fig. 4.8 as a function of measurement temperature. The dashed line indicates the positron lifetime in the bulk GaAs, τ_{b} . The temperature behavior of τ_{av} is similar to the one observed in heavily

doped GaAs:Si investigated in the previous section. At high temperatures, τ_{av} is distinctly higher than τ_b due to positron trapping into vacancies. The decrease of τ_{av} towards low temperatures is evidence of the presence of positron shallow traps, i.e., as it is generally accepted, negatively charged ions. Silicon and boron acceptors are good candidates for these shallow trap defects. The decomposition of the lifetime spectra has revealed the presence of a vacancy-like defect with positron lifetime close to 260 ps. It is in good agreement with the value of 262 ps found for $\text{Si}_{\text{Ga}}\text{V}_{\text{Ga}}$ (Section 4.2). By using the analogy with the heavily doped GaAs:Si, the vacancy defect observed in wafer #1 was also identified as silicon donor-gallium vacancy complex; the shallow positron traps were attributed to silicon and boron acceptors.

At this point, it is worth to draw the reader's attention to the small hysteresis of τ_{av} , observed for the sample pairs 1-2 and 29-30 at high temperature region (Fig. 4.8). Obviously, some vacancy-like defects were annealed during the measurement at 500 K. This cannot be the $\text{Si}_{\text{Ga}}\text{V}_{\text{Ga}}$ complex, since $\text{Si}_{\text{Ga}}\text{V}_{\text{Ga}}$ was found to be thermally stable up to 500 K (see Section 4.2, Fig. 4.2). Since the decomposition of the lifetime spectra into more than two components (i.e. more than one defect) was impossible, the positron lifetime related to the annealed defects should be in the order of that one for the monovacancy. The average positron lifetime measured in other samples did not demonstrate such hysteresis behavior indicating the positron trapping into the one type of defect only. Possibly, the concentration of the second defect in those samples was under the sensitivity limit of positron annihilation. The PL topogram recorded at the 1250 nm PL line shows the maximum of the luminescence intensity at the edges and minimum in the middle of the wafer [Fig. 4.6 (d)]. Since sample pairs 1-2 and 29-30 correspond to the wafer edges (Fig. 4.7), it is reasonable to suggest that the unknown defect gives rise to the 1250 nm photoluminescence peak. The origin of this peak is currently unknown (X-defect in Table 4.2). A more detailed discussion on this question is given in Section 4.4. At this stage, it should be noted that the X-center is a vacancy-like defect and its concentration in most of

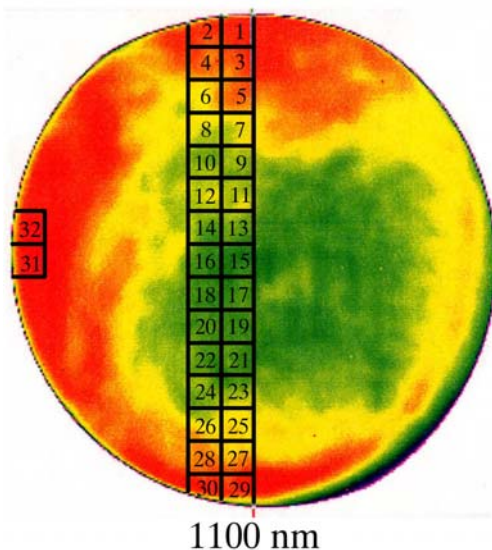


Fig. 4.7: Photoluminescence topogram image of wafer #1 recorded at the luminescence line of 1100 nm. Exact positions of the sample pairs taken for PALS measurements are indicated. The area of each single sample equaled 5×5 mm.

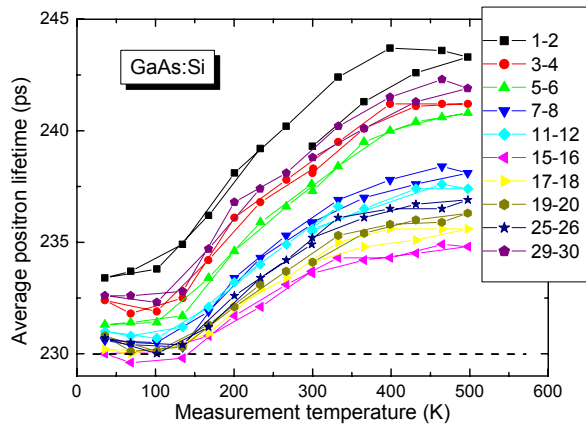


Fig. 4.8: Average positron lifetime vs temperature measured across the wafer #1. The sample numbers correspond to those shown in Fig. 4.7. The data points are connected by the lines in just the same consequence, the temperature measurements has been carried out (see Section 3.4).

the samples is too low to be detected by positrons.

The concentration of the $\text{Si}_{\text{Ga}}\text{V}_{\text{Ga}}$ complexes in each sample could be estimated from the lifetime data, as described in Section 4.2.3. For the samples 1-2 and 29-30, the vacancy concentration was determined after annealing of the X-defect. The obtained concentrations are plotted versus sample position in Fig. 4.9(a). As can be seen, the distribution of the vacancy complex is not constant, but reveals a minimum in the middle of the wafer replicating the intensity variation of the 1100 nm photoluminescence peak [fig. 4.9(b)]. The calculations of the concentrations of positron shallow trap performed by the three-state positron trapping model at 20 K yielded unrealistically large numbers (up to 10^{18} cm^{-3}) of the negative ions. Most probably, this is due to relatively low $\text{Si}_{\text{Ga}}\text{V}_{\text{Ga}}$ concentrations, at which the application of the three-state model is not possible.

Thus, we can conclude that the observed contrast of the 1100 nm (and, probably, of the 1250 nm) luminescence is caused by a non-uniform distribution of the deep centers, $\text{Si}_{\text{Ga}}\text{V}_{\text{Ga}}$ and the X-defect. The inverted contrast of the shallow transitions [Fig. 4.6 (a

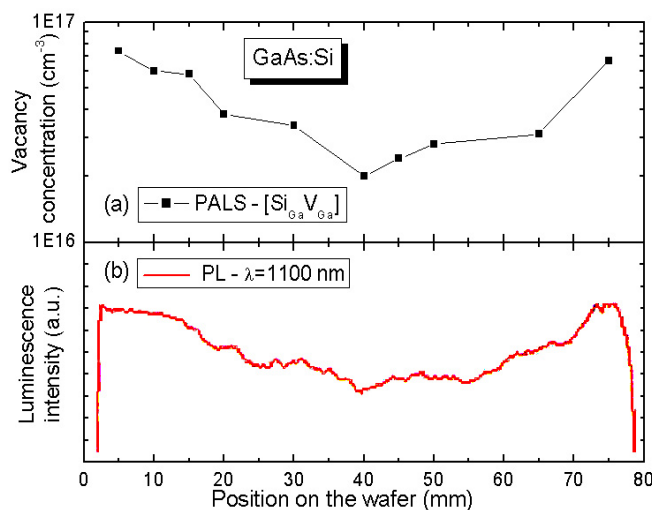


Fig. 4.6: (a) The distribution of $\text{Si}_{\text{Ga}}\text{V}_{\text{Ga}}$ complexes across the wafer #1, as determined by PALS

(b) intensity variation of the 1100 nm photoluminescence band, measured across wafer # 1 (From Ref. (Baeumler et al. 2002))

and b)] can be explained as a result of recombination competition, whence 832 nm and 922 nm intensity variations were caused indirectly by the variation of the deep centers concentration described above (Baeumler et al. 2002).

4.3.3 Lateral variation of the compensation degree in VGF GaAs:Si

This subsection continues the discussion on the influence of local dislocation density on the point defects formation in silicon doped VGF GaAs.

The combined photoluminescence and positron annihilation investigations (previous section) have rather clearly demonstrated the anticorrelation of the dislocation density and $\text{Si}_{\text{Ga}}\text{V}_{\text{Ga}}$ complexes distributions. However, these methods have not answered the question, whether the concentration of other point defects (Si_{Ga} and Si_{As}) and thus the compensation degree is also influenced by dislocations. This problem has been touched in this work by a systematic investigation of a VGF GaAs wafer (#2) with the help of SIMS, PALS, CDBS, IR absorption and electrical measurements (Bondarenko et al. to be published).

The EPD-topogram of wafers #2 (Fig. 4.10) revealed large variations of the local dislocation density in both wafers. The IR absorption measurements have shown a variation of the free electron concentration that replicated the EPD contrast (Fig. 4.11). In order to explain such correlation between n and EPD, two possible scenarios have been considered. Firstly, the increase of n may be merely due to non-homogeneous dopant (Si) distribution. The dislocation-rich regions thus have to have higher Si concentration than the rest of the wafer. The second scenario suggests lateral variation of the degree of compensation caused by dislocations-induced changes in concentration of electrically active point defects, i.e. Si_{Ga} , Si_{As} and $\text{Si}_{\text{Ga}}\text{V}_{\text{Ga}}$ (Section 4.2).

The first hypothesis has been examined by direct measurements of Si content; atom emission spectroscopy (AtES) has been applied. The analyzed samples were pre-

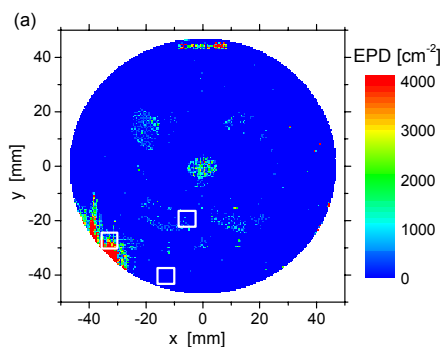


Fig. 4.7: Dislocation density distribution in wafer #2 obtained by EPD measurements. White squares denote the positions, from which the samples for PALS and AtES investigations were taken.

pared from wafers as shown by white squares in Fig. 4.10. Silicon concentration was

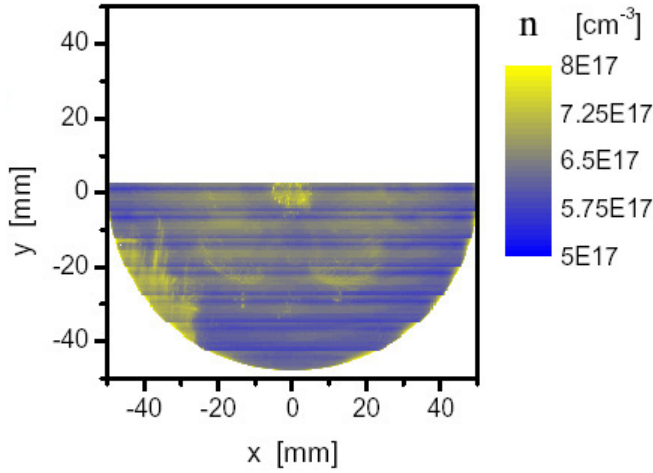


Fig. 4.8: Distribution of free charge carrier concentration in wafer #2 determined by IR absorption measurements.

found to be constant* in all samples and equaled $(1.3 \pm 0.1) \times 10^{18} \text{ cm}^{-3}$. Thus, the dislocation density does not influence the Si distribution and, therefore, the first scenario must be rejected. Consequently, the observed variation of n is due to different compensation ratios in dislocation-rich and dislocation-free regions. In order to give a quantitative interpretation of this discrepancy, one should identify the type of each defect participating in compensation as well as to evaluate their concentrations. As was shown in Section 4.2, for heavily-doped GaAs:Si these are single silicon donors, Si_{Ga} and two acceptors, Si_{As} and $\text{Si}_{\text{Ga}}\text{V}_{\text{Ga}}$.

Firstly, the type and concentration of the vacancy-complexes were determined by positron annihilation. Results of the lifetime measurements in the samples taken from wafer #2 are shown in Fig. 4.12. The vacancy-related defect, to be observed as the increase of τ_{av} over the bulk value ($\tau_{\text{b}} = 230 \text{ ps}$), has a positron lifetime τ_{v} close to 260 ps in all samples. This value is similar to $\tau_{\text{v}} = 262 \pm 5 \text{ ps}$ found for $\text{Si}_{\text{Ga}}\text{V}_{\text{Ga}}$ complexes (see Sections 4.2.2 and Ref. (Gebauer et al. 1997)). Also, the temperature dependence of τ_{av} is in good agreement with one observed in heavily doped GaAs:Si (Fig. 4.2). Therefore, the vacancies have also been identified as the Si_{Ga} -donor- V_{Ga} -vacancy complexes. The strong decrease of τ_{av} at low temperatures is due to the positron trapping by the Si_{As} acceptors acting as positron shallow traps with the positron lifetime close to τ_{b} .

The concentration of the vacancy complexes has been calculated according to the two-state one-defect trapping model using the lifetime data obtained at 300 K (Table 4.3). Similar to the results discussed in the previous section, the concentration of $\text{Si}_{\text{Ga}}\text{V}_{\text{Ga}}$ defects decreases with the increase of the dislocation density (Fig. 4.12). Bearing in mind the homogeneous distribution of the silicon dopants, the local reduction of $\text{Si}_{\text{Ga}}\text{V}_{\text{Ga}}$ concentration can explain the enhancement of free electron density observed in the dislocation-rich regions. However, this suggestion is valid only if the number of silicon donors

* Note: this observation is in agreement with constant silicon distribution found in wafer #1, Sec.4.3.2.

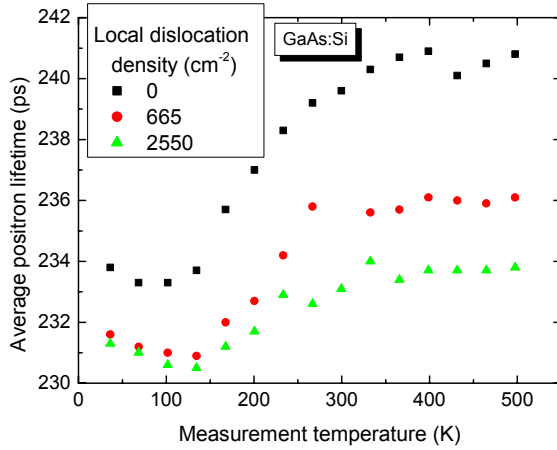


Fig. 4.12 Average positron lifetime vs temperature measured in three samples cut out from the regions of the wafer #2 having different concentration of dislocations. The sample positions are shown in **Fig. 4.10**. Dislocation densities are given in the legend.

and acceptors is constant across the wafer. It can be proved in the framework of the compensation model described in Section 4.2.3. Once the concentrations of free electrons, silicon and vacancy complexes are known, the concentrations of the silicon donors and acceptors can be calculated using the following linear system of equations:

$$\begin{aligned} [Si] &= [Si_{Ga}] + [Si_{As}] + [Si_{Ga}V_{Ga}] \\ n &= [Si_{Ga}] - [Si_{As}] - 2[Si_{Ga}V_{Ga}] \end{aligned} \quad (4.7)$$

The results of calculations and direct measurements are summarized in Table 4.3 and presented in Fig. 4.13. Si_{Ga} and Si_{As} concentrations are practically independent of dislocation density, whereas the formation of $Si_{Ga}V_{Ga}$ is found to be strongly suppressed by high concentration of dislocations.

Table 4.3 – Summary of directly measured and calculated data for VGF GaAs:Si samples with different dislocation density (wafer #2).

EPD (cm^{-2}) (measured)	n (cm^{-3}) (measured)	$[Si]$ (cm^{-3}) (measured)	$[Si_{Ga}V_{Ga}]$ (cm^{-3}) (measured)	$[Si_{As}]$ (cm^{-3}) (calculated)	$[Si_{Ga}]$ (cm^{-3}) (calculated)
0	8.77×10^{17}	1.3×10^{18}	5.7×10^{16}	1.26×10^{17}	1.12×10^{18}
665	1×10^{18}	1.3×10^{18}	3.1×10^{16}	1.0×10^{17}	1.17×10^{18}
2550	1.02×10^{18}	1.3×10^{18}	1.5×10^{16}	1.18×10^{17}	1.17×10^{18}

In summary, the correlation between local electrical properties and the dislocation density distribution was observed in silicon doped VGF GaAs wafers. It was shown that the correlation was not imposed by non-uniform distribution of silicon atoms, but related to the lateral variation of the degree of compensation. The latter is due to the suppression of formation of acceptor-like $Si_{Ga}V_{Ga}$ complexes by the high dislocation density. The concentration of $Si_{Ga}V_{Ga}$ complexes in dislocation-rich regions was reduced by 70% in

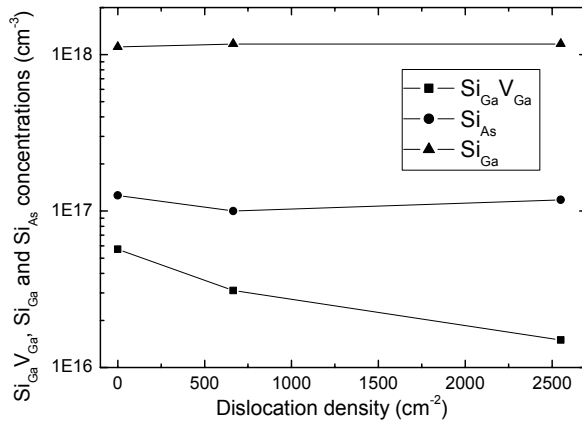


Fig. 4.13: Concentrations of donors (Si_{Ga}) and acceptors (Si_{As} , $Si_{Ga}V_{Ga}$) in silicon doped VGF GaAs as a function of the dislocation density.

comparison with the dislocations-free samples. In contrast to this, the incorporation of silicon as Si_{Ga} -donors or Si_{As} -acceptors was not affected much by dislocations.

4.4 Identification of the 0.95 eV luminescence band in VGF GaAs:Si

The discussion on point defects in silicon doped GaAs would be incomplete without a mention of the defect, which gives rise to 1250 nm (0.95 eV) luminescence band (Table 4.2). Though the occurrence of this band in n-type GaAs (e.g. in GaAs:Si, GaAs:Te or GaAs:S) has been known for a long time (Suezawa et al. 1994; Reshchikov et al. 1995; Toba et al. 1995), the attempts to attribute it to a certain defect are still controversial. A variety of defect types were proposed, e.g. acceptor-like ions (Toba et al. 1995), a $V_{As}Si_{Ga}V_{Ga}$ complex (Reshchikov et al. 1995) or $Si_{Ga}-Si_{As}$ pairs (Suezawa et al. 1994). However, neither of these defects was found to be consistent with the results of cathodoluminescence and positron annihilation investigations presented in this section. Instead, the set of possible candidates responsible for the illumination at 1250 nm is enriched by an additional defect type, the gallium vacancy.

4.4.1 Experimental

Two sets of samples have been investigated by the positron annihilation and cathodoluminescence spectroscopy. The first set corresponded to the one prepared from the VGF GaAs:Si wafer #1 (Section 4.3.1). Six samples of the second set have also been cut from a VGF GaAs:Si wafer. In order to avoid confusions, this wafer is referred in the following as wafer #3 keeping the general wafers numerating order of this chapter. In comparison to wafer #1 ($[Si] = 1.5 \times 10^{18} \text{ cm}^{-3}$, $n = 7.8 \times 10^{17} \text{ cm}^{-3}$), wafer #3 had lower concentration of

silicon dopants ($n = 1 \times 10^{17} \text{ cm}^{-3}$). However, exact Si-content in wafer #3 was not measured.

The cathodoluminescence spectroscopy was performed with a JSM 6400 scanning electron microscope (SEM) equipped with an Oxford monochromatic system. The range of temperatures from 20 K to 100 K was investigated. 20 keV electron beam was selected to excite the sample. A germanium (Ge) detector was used for collecting the corresponding CL spectra.

PALS measurements were performed according to the procedure described in section 3.4. The time resolution of the spectrometer was 240 ps.

Coincidence Doppler broadening spectroscopy (CDBS) was performed at 400 K and 200 K for the samples cut from wafer #1 and #3, respectively. The piece of undoped semi-insulating GaAs was taken as the material of reference and measured at room temperature. About 6×10^7 annihilation events were accumulated in each spectrum.

4.4.2 Cathodoluminescence spectroscopy

Fig. 4.14 represents the cathodoluminescence spectra measured in samples taken from wafers #1 and #4. Four luminescence bands denoted as A-D are assigned as given in Table 4.2. The origin of the defect responsible for the band D is unknown. For the sake of convenience, it will be further referred as X. The intensity of the band D is much higher in wafer #4 than in #1. In contrast, the band C related to $\text{Si}_{\text{Ga}}\text{V}_{\text{Ga}}$ complex is much

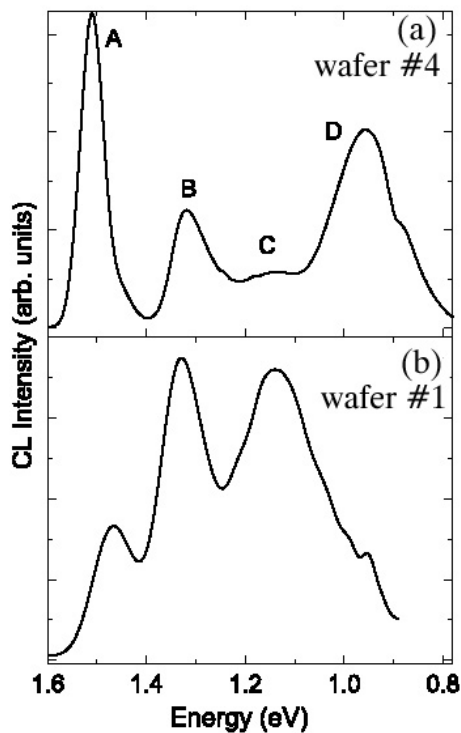


Fig. 4.14: Cathodoluminescence spectroscopy measurements on (a) wafer #4 and (b) wafer #1. Sample 2 was taken for investigation of wafer #1. CL spectroscopy was performed after PALS measurements. (From (Lei et al. 2003))

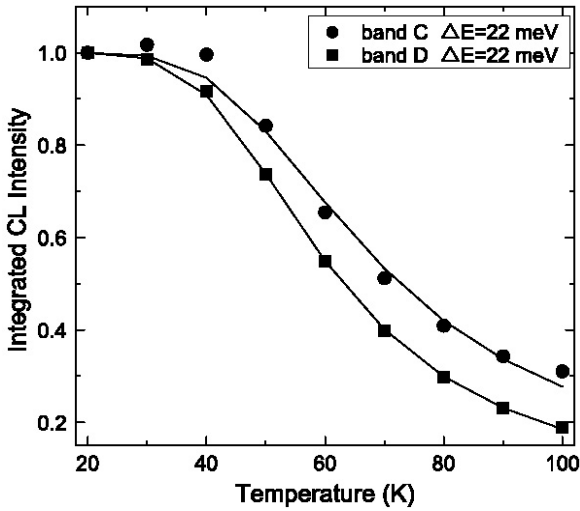


Fig. 4.15: Integral CL intensity of the luminescence bands C and D (see Fig. 4.14) as a function of temperature obtained in wafer #3. Intensity was normalized to the one at 20 K. Solid lines represent a fit according to Eq. 4.8

stronger in wafer #1. The intensity differences are due to the different concentrations of the corresponding defects (Yacobi and Holt 1990).

For the wafer #3, the luminescence bands C and D were measured in temperature interval from 20 K to 100 K. Their CL intensities vs temperature are shown in Fig. 4.15. Both intensities are characterized by the exponential decay:

$$I = I_0 [1 + C \cdot \exp(-\Delta E / k_B T)]^{-1}, \quad (4.8)$$

where C is a temperature-independent constant; k_B is Boltzmann constant and T is temperature; ΔE is an activation energy for thermal quenching processes introduced within the framework of configurational-coordinate (CC) model (for the model description see Ref. (Williams and Mackintosh 1968)). The model assumes that the light emission occurs by transition of the electron from the excited state associated with the donor atom to the ground state of the acceptor-like gallium vacancy. (Shionoya 1966). The ΔE is related to the position of the donor level in the band gap (Williams and Mackintosh 1968).

The value of ΔE can be determined by the analysis of the luminescence intensity as a function of temperature. A least-squares fitting according to Eq. (4.8) yielded the same $\Delta E = 22 \text{ meV}$ for both luminescence bands. This value is in good agreement with $\Delta E = 19 \pm 2 \text{ meV}$ found for $\text{Si}_{\text{Ga}}\text{V}_{\text{Ga}}$ complex in heavily silicon-doped GaAs (Sauncy et al. 1996). Similar ΔE implies the same position of the upper excited energy state for each recombination center, $\approx 20 \text{ meV}$ below the conduction band. The lower level of $\text{Si}_{\text{Ga}}\text{V}_{\text{Ga}}$ complex is known to be at about 0.3 eV above the valence band (Sauncy et al. 1996). Since the emission energy of the X defect (0.95 eV) is smaller than that for $\text{Si}_{\text{Ga}}\text{V}_{\text{Ga}}$ (1.2 eV), its ground state must be at $\approx 0.5 \text{ eV}$ above the valence band.

4.4.3 Defect identification by positron annihilation

The results of positron annihilation lifetime measurements are sufficiently different for wafers #1 and #3 (Fig. 4.8 and Fig. 4.16). The average positron lifetime τ_{av} increases continuously with increasing temperature in wafer #1, whereas the pronounced maximum at 200 K followed by a considerable decrease of τ_{av} is observed in wafer #4. Such large discrepancy of the τ_{av} temperature behavior points to a different nature of positron annihilation centers in both wafers. However, their vacancy-related lifetimes provided by one-defect spectra decomposition were found to be similar, $\tau_v = 260 \pm 5$ ps, the typical value for a monovacancy in GaAs. The vacancy-like defect in wafer #1 was previously identified as the $\text{Si}_{\text{Ga}}\text{V}_{\text{Ga}}$ complex (Section 4.2.2). The configuration of the vacancy-like defect in wafer #3 is currently unknown. It is reasonable to attribute the origin of this defect to the X-center that is responsible for the 0.95 eV luminescence band. Let us consider some aspects supporting this point.

First of all, the detailed investigation of the τ_{av} hysteresis observed in samples 1-2 and 29-30 of wafer #1 (Fig. 4.8) has led to the conclusion that some vacancy-like defects were annealed during the measurements at 400-500 K. As has already been noted in Section 4.3.2, this temperature is not high enough to cause the annealing of $\text{Si}_{\text{Ga}}\text{V}_{\text{Ga}}$ complexes. Hence, some other type of defects must be present. Since τ_{av} measured in other samples did not demonstrate such hysteresis, concentration of this defect must be higher at the wafers edge and too low to be detected with positrons in the middle of the wafer. Such lateral distribution is in agreement with the intensity variation of the 1250 nm (0.95 eV) photoluminescence line [Fig. 4.6 (d)]. As a check, one more pair of samples was cut from the edge of wafer #1 (samples 31-32, Fig. 4.7) and measured at temperatures from 300 K to 600 K. The expected hysteresis was indeed observed (Fig. 4.17). Thereafter the sample 2 (sample pair 1-2, wafer #1) was measured with cathodoluminescence at 75 K. As Fig. 4.14 (b) shows, the 0.95 eV CL peak disappeared. Thus, the assignment of the X-

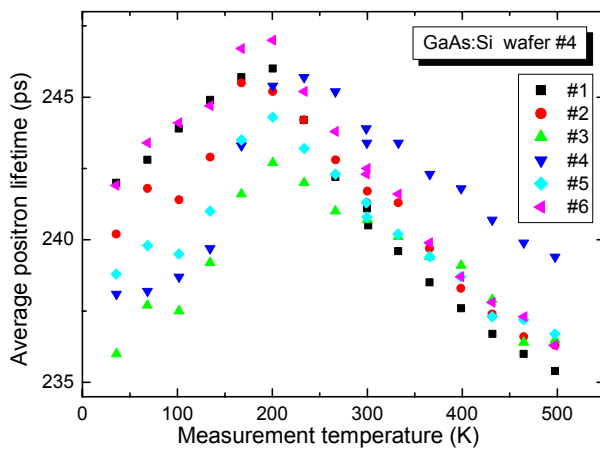


Fig. 4.9: Average positron lifetime as a function of temperature measured in the samples cut from silicon doped GaAs wafer #3.

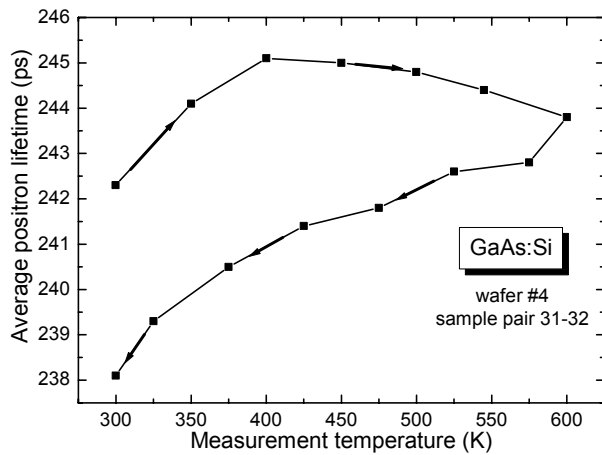


Fig. 4.10: The hysteresis of the average positron lifetime observed by temperature-dependent PALS-measurements performed on the sample pair 31-32 of GaAs:Si wafer #3. Samples position is shown in Fig. 4.7 The arrows indicate the order in which the measurements were performed.

defect responsible for 0.95 eV CL band to the unidentified vacancy-like defect observed with positron annihilation is justified.

As the next step, coincidence Doppler broadening (CDBS) measurements were performed in order to get additional information on electron momentum distribution at detected vacancies. Actually, the annihilation with core electrons, which are atom specific, is of interest here. In the case of a vacancy neighbored by some impurity or dopant atom (e.g., $\text{Te}_{\text{As}}\text{V}_{\text{Ga}}$ complex in GaAs:Te), the annihilation momentum distribution at vacancy-complex will differ from that of a single vacancy due to annihilation of positrons with core electrons of a foreign atom (Gebauer et al. 1999). Moreover, gallium and arsenic vacancies can be in principle differentiated with CDBS, since the core electron momentum distribution for As atoms surrounding V_{Ga} is different from that for Ga atoms, which are in the direct vicinity of V_{As} (Gebauer et al. 2001). Results of CDBS measurements revealed the same shape of annihilation momentum distribution for both wafers

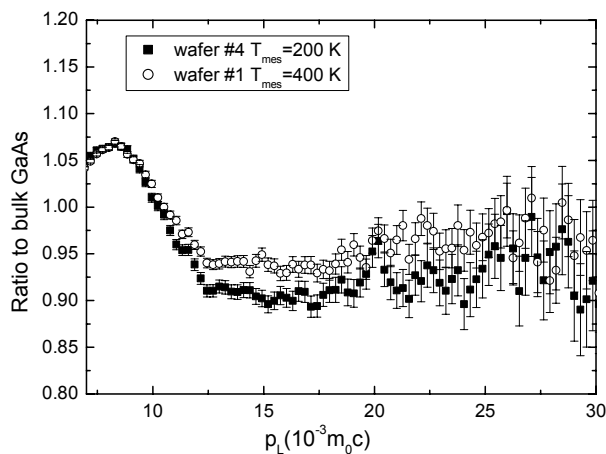


Fig. 4.18: Momentum distribution of the annihilation radiation obtained in the samples of wafers #1 and #3. The measurement temperature corresponded to the maximum trapping rate, i.e. to the longest τ_{av} (see Fig. 4.8 and Fig. 4.16).

(Fig. 4.18). This means the vacancy-like defects in wafer #1 ($\text{Si}_{\text{Ga}}\text{V}_{\text{Ga}}$) and in #3 (X-defect) belong to the same sublattice. Thus the X-defect must contain a gallium vacancy.

Summarizing the results of positron annihilation, photo- and cathodoluminescence spectroscopy, the following observations on the X-defect may be made: X represents a monovacancy-like defect that is mobile at 400-500 K. The electron momentum distribution at X is similar to that one measured for $\text{Si}_{\text{Ga}}\text{V}_{\text{Ga}}$ complex. Thus, X must be related to a gallium vacancy. However, τ_{av} demonstrates a quite different temperature dependence of positron trapping into X than into $\text{Si}_{\text{Ga}}\text{V}_{\text{Ga}}$ complex pointing to a different charge state of these defects. According to CL and PL measurements, the energy level of X lies approximately at 0.5 eV above the valence band; this is in good agreement with the ionization level provided by some calculations for triply negative V_{Ga} (Fig. 2.5). Formation of X is suppressed with increasing silicon concentration. Previously, X was always ascribed to some complex involving a donor-atom. However, in this work the same CL band was found in initially-undoped As-rich p-type GaAs (Section **Fehler! Verweisquelle konnte nicht gefunden werden.**, Fig. 6.7), which has low concentration of donor atoms. A monovacancy-like defect was found also in that material. Since the undoped GaAs was As-rich, the origin of the defect was attributed to the gallium vacancy. This is in agreement with the interpretation of the results discussed above. Thus, the X-defect relates to V_{Ga} and is not necessarily connected to a Si_{Ga} -donor. Taking into account that X was found also in p-type GaAs and bearing in mind it is mobile already at 500 K, it is reasonable to suggest that X does not belong to a donor- V_{Ga} complex but represents an isolated gallium vacancy.

4.5 Discussion: defects formation in VGF GaAs:Si

On the basis of the results of positron annihilation, photo- and cathodoluminescence spectroscopy the following mechanism of defect formation in silicon-doped GaAs is proposed. Since the growth takes place under As-rich conditions (Section 2), a large number of gallium vacancies V_{Ga} is present in the crystal. These vacancies can exist in different charge states: neutral, $-e$, $-2e$ or $-3e$. According to theoretical calculations of Tan et al. (Ref. (Tan et al. 1993)) triply-negatively-charged V_{Ga} dominate over the other charge states (Fig. 2.3). In an intrinsic, i.e. undoped, crystal the vacancy concentration decreases with decreasing temperature during cooling down the crystal. In the case of a doped crystal, the concentration of charged vacancies depends on the charge carrier concentration or on the position of the Fermi level, which is the so-called Fermi-level effect (Section 2.3). The equilibrium V_{Ga} concentration increases as n increases in n-type GaAs. Moreover, Tan et. al. showed that due to the Fermi-level effect the concentration of $\text{V}_{\text{Ga}}^{3-}$ is either independent of temperature or even shows a small negative temperature dependence. That is, as the temperature is lowered, the $[\text{V}_{\text{Ga}}^{3-}]$ is either unchanged or increases (Fig. 2.3).

Thus, Si doping increases the solubility of V_{Ga}^{3-} at the growth temperature. At high doping levels ($[\text{Si}] > 10^{18} \text{ cm}^{-3}$) gallium vacancies form $\text{Si}_{\text{Ga}}V_{\text{Ga}}$ acceptor complexes due to Coulomb attraction of Si_{Ga}^+ -donors and V_{Ga}^{3-} -acceptors. These complexes give rise to the 1100 nm luminescence band. At moderate level of doping, not all gallium vacancies are able to find a Si_{Ga} neighbor. It does not necessary mean that the vacancy concentration is higher than that of Si. Most probably, the density of Si donors is not high enough for a negative vacancy to feel the positive charge of a Si_{Ga} -donor. According to the Fermi-level effect, V_{Ga}^{3-} remains stable also after cooling down of the crystal. The monovacancies are seen as 1300 nm luminescence band in wafers #1 and #4. If the concentration of Si dopants is further decreased, the number of monovacancies will dominate over that of $\text{Si}_{\text{Ga}}V_{\text{Ga}}$ complexes. This results in a higher intensity of the 1300 nm luminescence band in comparison with the 1100 nm band in wafer #3.

The main argument against the interpretation given above consists in the commonly accepted fact that isolated Ga vacancies are not stable at temperatures above room temperature. Hautojärvi et al. observed annealing of monovacancy-type defects, which had been introduced by low-temperature electron irradiation, at 400 K. In the samples investigated in this study, vacancy-like defects have been found to be stable up to 500 K (the highest measurement temperature). However, the vacancies observed by Hautojärvi et al. had been created at low temperatures and hence were not in thermodynamic equilibrium. Therefore, there was a “thermodynamic driving force” tending to move the crystal into the equilibrium state by eliminating of excess vacancies. In contrast, the vacancies in the as-grown crystal studied here had been formed at high temperature and remained after the cooling down the crystal, because their presence is energetically favorable, as explained above.

5. Vacancy formation in semi-insulating and silicon-doped GaAs under equilibrium conditions

5.1 Experimental

At temperatures lower than 1240° C (melting-point), the GaAs system consists of two phases – solid and gas – and has according to Gibbs' phase rule two degrees of freedom. In other words, it is necessary to fix two independent parameters, in order to adjust certain equilibrium state of the samples. The most convenient way is to choose sample temperature and the ambient gas pressure. At elevated temperatures, the gas phase consists predominantly of the arsenic tetramer As_4 and the partial vapor pressure of gallium can be neglected (Arthur 1967). The defect concentrations at equilibrium will then be a function of the sample temperature and the arsenic ambient vapor pressure. Holding the sample temperature fixed and varying the arsenic pressure, one can change the chemical composition of the crystal. This makes it possible to investigate the formation of point defects as a function of crystal stoichiometry. However, direct measurements of defect concentrations at the high temperatures necessary for their formation are difficult. Therefore, one often tries to “freeze” the high-temperature defect configuration by quenching of an investigated crystal from high to low (room) temperatures. This method was also used in this work.

The studied samples were cut from the semi-insulating undoped and silicon doped LEC grown GaAs wafers (5×5×0.5 mm). The wafers were supplied by FCM (Freiberger Compound Materials GmbH). The resistivity of undoped material was about $10^6 - 10^7 \Omega\text{cm}$. The concentrations of Si and free electrons in GaAs:Si were equal to $1,2 \times 10^{19} \text{ cm}^{-3}$ and $5 \times 10^{18} \text{ cm}^{-3}$ respectively. For the annealing, two identical samples with

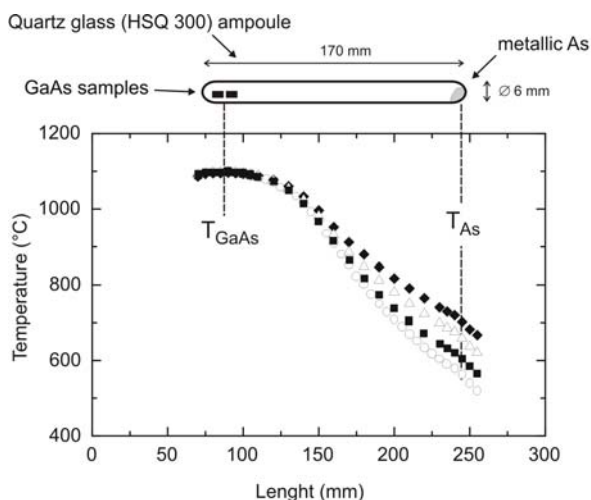


Fig. 5.1: Temperature profile of the two-zone furnace used for the annealing of GaAs samples under different As pressures. Positions of the samples and As-source are shown by vertical lines.

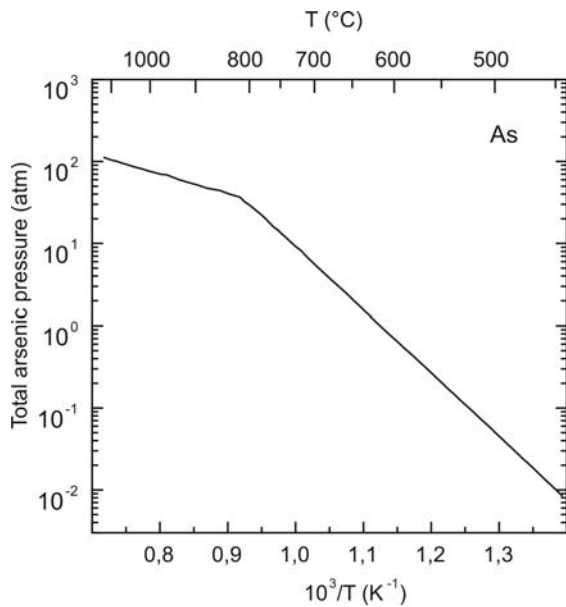


Fig. 5.2: Vapor pressure of metallic As versus temperature (from Ref. (Gokcen 1989)). The sharp bend of the curve corresponds to the melting point of arsenic (817°C).

a piece of metallic arsenic were sealed in the quartz ampoule and placed into a two-zone temperature furnace, as Fig. 5.1 shows. The arsenic vapor pressure is determined by the temperature at the coldest part of the ampoule and corresponds thus to the temperature of the metallic arsenic (T_{As} in Fig. 5.1) (Kröger 1964) providing the arsenic quantity is high enough to prevent its complete sublimation. The samples temperature was 1100°C for each annealing, whereas the temperature of As-source was varied over the range of $550^\circ\text{C} - 740^\circ\text{C}$. Corresponding arsenic pressure values were determined with the help of the $p_{\text{As}}(T)$ dependence taken from Ref. (Gokcen 1989) (Fig. 5.2).

Since semi-insulating GaAs material was investigated, the purity of the annealing experiments was of special importance. The introduction of an electrically active impurity in concentration of 0.1 ppm (10^{15} cm^{-3}) changes immediately the conductivity type of GaAs from semi-insulating to semi-conducting by jump-like transition of the Fermi-level position, which in turn affects the formation of point defects (Tan et al. 1993; Hurle 1999). Copper is known as an often occurring impurity in the annealing experiments due to its ubiquity and high diffusive coefficient. In this connection, the high purity copper-free quartz ampoules HSQ300 (Heraeus Quarzglas GMBH&Co) have been used. The ampoules have been etched for 2 hours in nitrohydrochloric acid ($3\text{HCl}:1\text{HNO}_3$), rinsed three times with distilled water and two times with ethanol whereupon dried in air for 24 hours. The samples were etched in 2% of bromine methanol solution and bathed in methanol just before and after annealing. The etching time was about 5 min, which corresponded to the removing of $\approx 40\ \mu\text{m}$ of the surface layer. Two identical samples with the piece of pure As (99,999%) were placed in the quartz ampoules, which were filled three times with argon and then they were sealed under a pressure of 10^{-3} Torr using a conventional gas-burner.

However, despite all the precautions a sample contamination with copper in the order of 10^{16} atoms/cm³ occurred usually during the annealing (Section 5.3.2). Most probably, the source of copper atoms was the brass head of the gas-burner. Moreover, about 10^{15} copper atoms/cm² can be adsorbed from alcohol used for the sample and ampoule cleaning (Hall and Racette 1964). In order to reduce the level of contamination, a new sample preparation procedure was developed. A different burner with a head made of quartz glass (Herbert Arnold GmbH) was used. Only high-purity distilled water and no ethanol was used in the ampoule cleaning procedure. The SI GaAs samples were prepared and packed under “clean-room” conditions at FCM. Immediately after unpacking, they were sealed in the ampoules and annealed. As a result, the copper contamination was indeed reduced and amounted to 10^{14} atom/cm³. This had a great influence on the quality of the experimental data and has helped significantly in the interpretation of the results. (Section 5.3.3)

5.2 Defects detected by PALS in annealed GaAs

5.2.1 Si-doped GaAs

Average positron lifetime curves versus measurement temperature for silicon doped GaAs in the as-grown state and after annealing under different As-pressures are presented in Fig. 5.3. The temperature dependent behavior of the average positron lifetime in as-grown and annealed samples is similar to that observed for GaAs:Si material studied in Section 4. At high temperatures, it is distinctly larger than that of bulk GaAs due to positron trapping into vacancy type defects. The decrease of the average positron lifetime with decreasing temperature is related to the positron trapping at negative ions that act as shallow positron traps at low temperatures having positron lifetime close to bulk value $\tau_b=230$ ps (Saarinen et al. 1989). This means that at low temperatures, positrons are trapped by two kinds of defects, namely by vacancies and negative ions, whereas at high

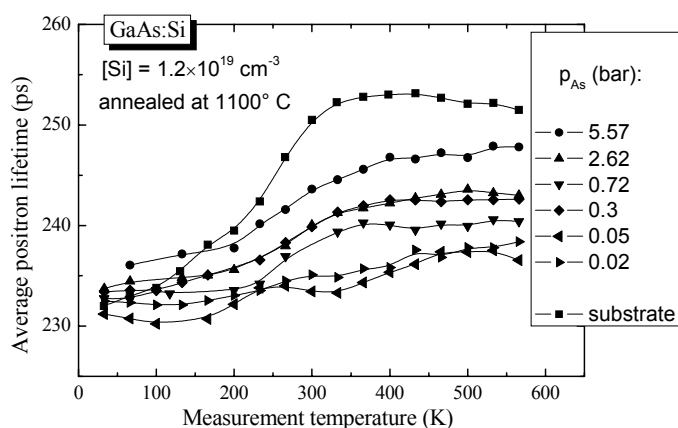


Fig. 5.3: Average positron lifetime versus temperature obtained in GaAs:Si annealed at different arsenic pressures p_{As} . Lines are to guide the eye only.

temperatures, the trapping by the negative ions is negligibly small.

The origin of the observed vacancy-type defects and the shallow traps in as-grown material is well known from the previous positron annihilation and scanning tunneling microscopy studies of GaAs:Si and has been discussed in detail in Section 4. The vacancies are related to Ga-vacancy–Si_{Ga}-donor complexes (Si_{Ga}V_{Ga}) with a defect-related lifetime of $\tau_v = 262 \pm 5$ ps (Gebauer et al. 1997). A similar τ_{vac} was found in both as-grown and annealed samples. On this basis, vacancy defects in annealed GaAs:Si have been attributed to V_{Ga}-Si_{Ga} defect complexes, too. The negative ions observed at low temperatures correspond to silicon acceptors mentioned above and probably to the acceptor-type impurities (C_{As}, Cu_{Ga}) that might be unintentionally introduced during sample handling.

5.2.2 Undoped semi-insulating GaAs

No vacancy defects were observed in as-grown semi-insulating GaAs (Fig. 5.4). The average positron lifetime τ_{av} was close to τ_b at all temperatures of measurement. This observation itself represents an important result. In earlier positron annihilation studies of undoped SI GaAs, there were always some vacancy-like defects found (Saarinen et al. 1993; Chen et al. 1996; Kuisma et al. 1996). In the annealed samples, τ_{av} is strongly enhanced indicating positron trapping at vacancies. A defect-related lifetime of 293 ± 10 ps was found. This value is distinctly larger than that for V_{Ga}-Si_{Ga} complex in GaAs:Si indicating a larger open volume of the vacancy, but still below the value calculated for a divacancy in GaAs (e.g., 332 ps in Ref. (Gebauer et al. 1999)). Thus, the observed vacancies should also be monovacancies. The decrease of the average positron lifetime toward low temperatures is due to the positron trapping at negative ions. The origin of the negative ions was attributed to the copper double acceptors, Cu_{Ga}²⁻, as it is discussed in Section

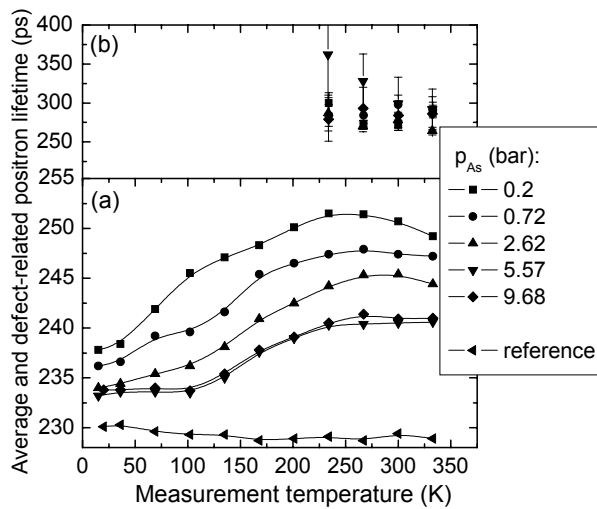


Fig. 5.4: (a) Average and (b) defect-related positron lifetime versus temperature obtained in undoped semi-insulating GaAs annealed at different arsenic pressures, p_{As} . The not annealed material is denoted as reference. Lines are to guide the eye only.

5.3.2.

In contrast to the Si-doped GaAs (Fig. 5.3), the average positron lifetime in the annealed undoped GaAs decreases with the increasing arsenic vapor pressure during annealing. The maximal τ_{av} was observed after the annealing at 0.2 bar (Fig. 5.4), whereas GaAs:Si annealed at this pressure reveals almost no positron trapping. Since the average positron lifetime determines the magnitude of the positron trapping rate (Eq. 3.6) and thus the concentration of the vacancy-like defects (Eq. 3.4), the pressure dependence of τ_{av} reflects a relation between the concentration of the vacancy defects at 1100° C and the arsenic vapor pressure. The enhancement of the vacancy concentration towards higher arsenic pressures in n-type GaAs had also been observed in previous positron annihilation studies (Gebauer 2000; Gebauer et al. 2003) and attributed to the formation of complexes containing gallium vacancies. This is consistent with the results obtained in this work for the annealed GaAs:Si. The reduction of the vacancy concentration by an increase of the arsenic pressure observed in SI GaAs represents an important result that was not reported before. Therefore, the following discussion concentrates mostly on the defects observed in the annealed SI GaAs.

5.2.3 Reproducibility of results for annealed SI GaAs

While the results of positron annihilation measurements in annealed GaAs:Si were found to be in good accordance with the previous annealing studies of n-type GaAs (Gebauer 2000) and hence may be considered as well-reproducible, the pressure dependence of the vacancy-related signal observed in semi-insulating GaAs should be subjected, as a qualitatively new result, to a reproducibility test. During the two year investigation of SI GaAs, several sample series were prepared and annealed under similar conditions. Subsequently, the temperature dependent positron annihilation measurements were performed. In contrast to silicon-doped GaAs, rather bad reproducibility of the positron annihilation results was found. The $\tau_{av}(T)$ curves obtained for three measurement series are shown in Fig. 5.5. As can be seen, both absolute values of the average positron lifetime and also its arsenic pressure dependence demonstrate very big fluctuations from one set of samples to another. However, it is important to note that the tendency of the highest τ_{av} at the lowest p_{As} , is preserved for each annealing series.

There are several reasons for the observed irreproducibility:

- 1) Uncertainties of the arsenic pressure. The temperature profile in the two-zone oven (Fig. 5.1) has a plateau only in the high-temperature region (at $T_{GaAs} = 1100^\circ C$), whereas it demonstrates a rather big gradient in the low-temperature zone, at T_{As} . Therefore, small variations in the position of the arsenic source, i.e. in the ampoule length, have a relatively big effect on its temperature and hence on the whole pressure in the ampoule. Thus, the typical temperature error amounting to 10 K corresponds to $\Delta p_{As} \approx 0.5$ bar (Fig. 5.2).

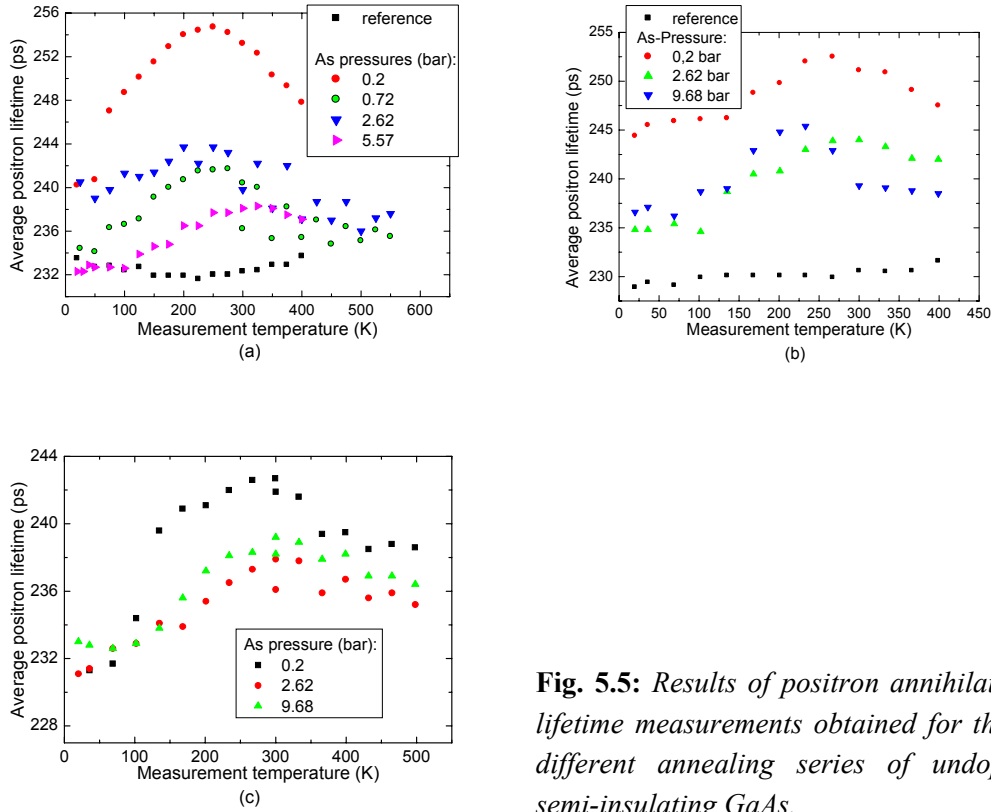


Fig. 5.5: Results of positron annihilation lifetime measurements obtained for three different annealing series of undoped semi-insulating GaAs.

2) Uncertainties of the quenching rate. After each annealing, the ampoules were quenched into the water at room temperature to preserve the high temperature defect configuration. Even though the cooling was done as quickly as possible, it is rather improbable that the quenching rate at each quenching was the same.

3) Uncertainties of the position of the Fermi-level. In annealed samples, the Fermi-level was found to be in the lower part of the band-gap (Sect. 5.3, Table 5.1). Its exact position may have a big influence on the concentrations of point defects.

Obviously, the first two reasons are of a minor significance. They can lead to insignificant fluctuations but they are unable to explain the big discrepancies observed in Fig. 5.5. The third argument seems to be the most important one. Before the annealing, the Fermi-level in SI GaAs samples is pinned by deep EL2 donors in the middle of the band-gap. The annealing at 1100° C with subsequent quenching destroys the EL2 centers (Hurle 1999). In this state, the position of the Fermi-level is not fixed any more but determined by the ratio between the concentrations of donors and acceptors present in a crystal. Since SI GaAs is usually intentionally doped by carbon atoms, which form C_{As} -acceptors (Section 6.2), the acceptor concentration dominates and the Fermi-level moves from the mid-gap position towards the valence band. The position of E_F becomes then very sensitive to the number of acceptor-like defects, which in its turn is defined by the purity conditions of the annealing experiments. The initial carbon content in as-grown SI

GaAs amounts normally to 10^{14} - 10^{15} cm^{-3} (Korb et al. 1999), whereas the concentration of impurity atoms introduced unintentionally during the sample handling may exceed this value by one order of magnitude. The chemical analysis of the annealed samples showed concentrations of copper atoms, $[\text{Cu}] \approx 10^{16}$ cm^{-3} , i.e. an enhanced value with respect to the as-grown sample having $[\text{Cu}] \approx 10^{13}$ cm^{-3} . Cu in GaAs is known to be sited on the gallium sublattice, Cu_{Ga} , forming an acceptor-like level at 0.5 eV above the valence band (Tin et al. 1987; Kuriyama et al. 1994; Leon et al. 1995) (for more detailed discussion of the Cu-contamination see Section 5.3.2). In such a way, uncontrolled contamination in the range of 1 ppm only, being the source of the dominating acceptor-like impurities, represents the main factor determining the electronic properties of annealed SI GaAs samples. This was not the case in the investigations of n-type GaAs mentioned above, where the Fermi-level position was expelled into the conduction band by high (up to 10^{19} cm^{-3}) concentrations of Te_{As} -donors, and where contamination with impurities in the order of 10^{16} cm^{-3} did not play significant role.

It turned out, that the electronic properties of a crystal (i.e. Fermi-level position) have a profound effect on the formation of vacancy-like defects in GaAs. The following two examples demonstrate this fact. Three $\tau_{\text{av}}(T)$ curves shown in Fig. 5.6 represent the results obtained for three SI GaAs samples, which were prepared and annealed under very similar conditions. The arsenic pressure was equal to 0.2 bar, the annealing time was 2 hours for each annealing. However, the PALS results for one of the samples (\blacktriangle , Fig. 5.6) were found to be quite different from those obtained for the other two specimens. Hall-Effect measurements showed that all the samples became p-type, whereas the hole concentrations were practically equal in the samples demonstrating similar $\tau_{\text{av}}(T)$ dependence ($[p] \approx 2 \times 10^{12}$ cm^{-3}) and two orders of magnitude lower ($[p] \approx 4 \times 10^{10}$ cm^{-3}) in the third sample. Obviously, the vacancy concentration is a function of chemical potential (i.e. crystal composition), which can be controlled by maintaining the arsenic vapour pressure, and it depends also on the Fermi level position. This was also confirmed by the results of

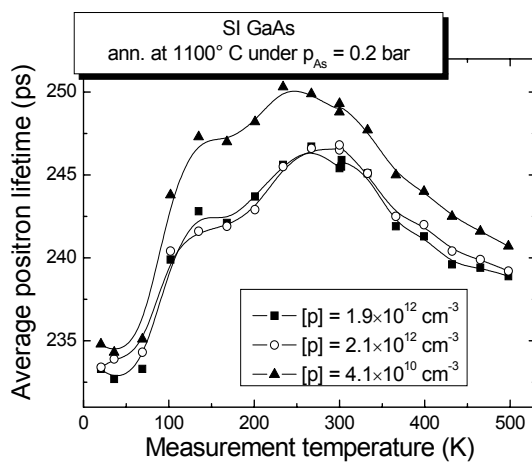


Fig. 5.6: Average positron lifetime as a function of measurement temperature in three SI GaAs samples prepared under identical conditions and annealed for 2 hours at 1100°C under arsenic pressure of 0.2 bar. Hole concentrations are indicated.

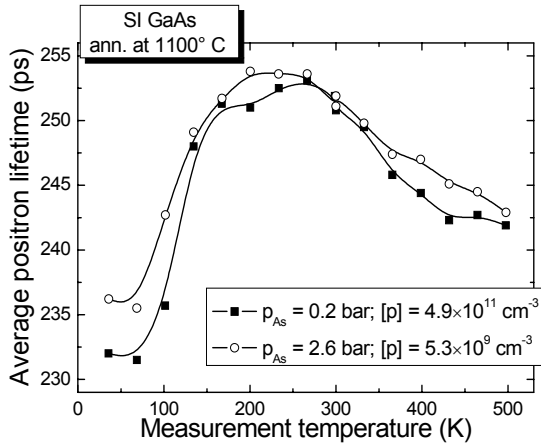


Fig. 5.7: Average positron lifetime as a function of measurement temperature in two SI GaAs samples annealed for 2 hours at 1100° C at 0.2 and 2.6 bar. Hole concentrations corresponding to each samples are indicated.

the lifetime measurements performed on two GaAs samples annealed under different arsenic pressures – 0.2 and 2.6 bar (Fig. 5.7). Surprisingly, both the samples demonstrated very similar values of τ_{av} . It should be that the concentrations of the vacancy-like defects in these samples have been nearly the same. However, electrical measurements revealed hole concentrations, which differed by two orders of magnitude, $4.9 \times 10^{11} \text{ cm}^{-3}$ and $5.3 \times 10^9 \text{ cm}^{-3}$ for crystals annealed at 0.2 and 2.6 bar, respectively. The difference in the free charge carrier concentrations reflects the different positions of the Fermi-level, E_F , in these samples, which obviously has an effect on the vacancy concentration. Note that the different hole densities cannot be directly related to the numbers of the vacancy-like defects, since the concentration change in the region of $10^9 - 10^{11} \text{ cm}^{-3}$ is well under the sensitivity limit of positron annihilation.

The existence of an interrelation between the Fermi-level and the concentration of vacancies was predicted by Tan in Ref. (Tan et al. 1993) for n-type GaAs. It was shown that in highly n-doped crystals, the concentration of gallium vacancies, $[V_{Ga}]$, does not increase with increasing temperature, T , as one would expect according to $[V_{Ga}] \sim \exp(-E/k_B T)$, where E is the formation energy and k_B is the Boltzmann constant, but remains constant or even decreases slightly. This phenomenon, called Fermi-level effect,

Table 5.1 – Results of the room-temperature Hall measurements on the undoped SI GaAs samples annealed at defined As-pressure. The sample series corresponds to that shown in Fig. 5.4

P_{As} , bar	$[p]$, cm^{-3}	μ , cm^2/Vs	ρ , Ωcm
0.2	7.28×10^{11}	333	2.57×10^4
0.7	4.74×10^{10}	191	6.87×10^5
2.6	1.42×10^{11}	176	2.47×10^5
5.6	7.18×10^{10}	203	4.27×10^5
9.7	5.35×10^{11}	407	2.86×10^4

was confirmed experimentally by J. Gebauer in a positron annihilation study of GaAs:Te (Gebauer et al. 2003). The results presented in this subsection demonstrated that the Fermi-level has a certain effect on the vacancy formation also in p-type GaAs. Obviously, the influence of the location of E_F may be compared with that of the chemical potential, i.e. p_{As} (Fig. 5.6 and Fig. 5.7). In principle, the vacancy concentration must be then treated as a function of p_{As} and E_F , i.e. $[V] = f(p_{As}, E_F)$. However, control over the Fermi level in annealed SI samples is hardly possible, first of all due to its high sensitivity to the concentration of impurities unintentionally introduced during sample handling. Obviously, the contamination level in the samples, the results of which are presented in Fig. 5.4, was nearly constant, since their electrical properties were found to be very similar (Table 5.1). This enables the analysis of the vacancy concentration as a function of p_{As} only, given in the next section.

5.3 Defect identification in annealed n-type and SI GaAs

5.3.1 Identification of vacancies

This subsection discusses the dependence of vacancy-like defects concentration on arsenic ambient pressure in the undoped and silicon-doped GaAs samples. The concentrations were calculated from the data of decomposition of positron lifetimes spectra via the Eq. 3.4 at 300 K and 500 K for undoped and silicon doped samples, respectively. At these temperatures the spectra were found to have only two components, i.e. no positron trapping into shallow traps was observed. The C_{vac} vs p_{As} plot, presented in Fig. 5.8, reveals an opposite behavior of the concentrations of the vacancy-like defects with increasing As pressure for undoped and silicon doped GaAs. This difference points to a different origin of the vacancies observed in these two kinds of samples. According to the mass-action law reactions (2.11) and (2.12):

$$\begin{aligned} [V_{Ga}] &= K_{VGa} \times p_{As}^{1/4} \\ [V_{As}] &= K_{VAS} \times p_{As}^{-1/4} \end{aligned}$$

where K_{VGa} and K_{VAS} are the mass action constants for the gallium and arsenic vacancy at a certain temperature and p_{As} is the ambient arsenic vapor pressure.

It follows that $[V_{Ga}]$ should increase and $[V_{As}]$ decrease with arsenic pressure as a power of +1/4 and -1/4, respectively. The fit to the experimental data (solid lines in Fig. 5.8) have indeed yielded an exponent close to 0.25 for GaAs:Si and -0.25 for SI GaAs.

Based on these results, the origin of vacancy-type defects in silicon doped GaAs was attributed to V_{Ga} , whereas in annealed SI GaAs formation of V_{As} was assumed. While this assignment in the case of GaAs:Si is in agreement with the interpretation of the positron lifetime data given earlier (see Section 5.2.1), the observation of As vacancies is more surprising than expected. The point is that according to theoretical calculations, the

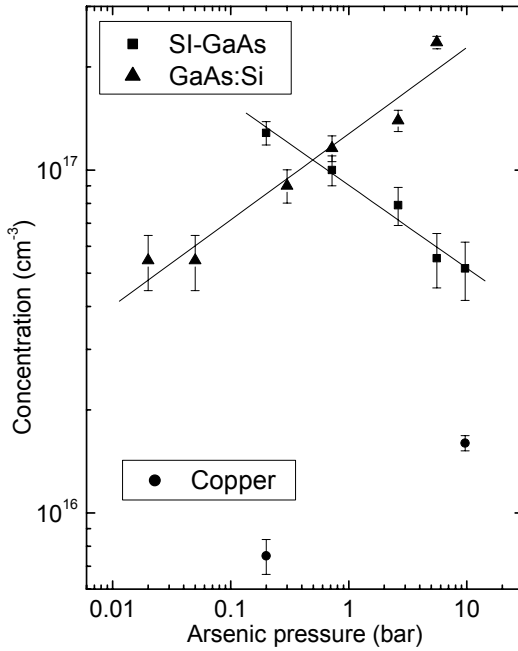


Fig. 5.8: Vacancy-defects concentrations in annealed GaAs:Si and SI GaAs extracted from the positron lifetime data presented in fig. 5.3 and 5.4. Solid lines represent power law fit to data corresponding data point. Full circles present the concentration of copper impurities obtained with the help of titration measurements.

ionization levels of V_{As} are in the upper part of the energy gap, close to the conduction band (Baraff and Schlüter 1985; Puska 1989; Xu 1990) (Fig. 2.5). The theoretical expectations were supported by a few positron studies, where observation of V_{As} in n-type (Saarinen et al. 1991; Ambigapathy et al. 1994) or in *photoexcited* semi-insulating material (Peng et al. 1994; Kuisma et al. 1996) were reported. There had been two defect-related lifetimes found, 295 ps and 257 ps, which were attributed to neutral and negative charge states of the arsenic vacancy (Saarinen et al. 1991). The value of 295 ps is in good agreement with the defect-related lifetime, $\tau_v = 293 \pm 10$ ps, found in this study for annealed SI GaAs, supporting thereby the identification of the observed vacancy defect as V_{As} . However, earlier investigations revealed the ionization levels of V_{As} at $E_C - 140$ meV (Saarinen et al. 1991) for $+0$ and $E_C - 30$ meV (Saarinen et al. 1991) and $E_C - 60$ meV (Kuisma et al. 1996) for $0/-$ transitions, respectively, which were in good qualitative agreement with theoretical calculations mentioned above. Consequently, arsenic vacancies should be positive (and thus not detectable with positrons) in semi-insulating or in p-type GaAs, where the position of Fermi level is in the middle or in the lower part of the band gap. The Hall-effect measurements of the samples investigated in this study (Table 5.1) have shown that all annealed samples became slightly p-type with $[p] = 10^{11} - 10^{12} \text{ cm}^{-3}$ that corresponds to the position of Fermi level at 0.4-0.5 eV above the valence band. It is worth to note, that this is the first time vacancy-like defects were observed with positrons in as-grown *p-type* GaAs. These results can be explained by the formation of V_{As} -X defect complex, where the X represents another at least one time negatively charged defect that compensates the positive charge of the arsenic vacancy. The possibilities for X to be a native or impurity-kind defect are discussed in the following.

As far as the investigated crystals were cut from undoped semi-insulating commercially available wafers, the concentration of the residual impurities in the samples was extremely small – below 10^{15} cm^{-3} – and thus not able to explain the occurrence of 10^{17} cm^{-3} (s. Fig. 5.8) vacancy-complexes. Other impurity sources are an uncontrolled contamination that might happen during the samples preparation. Copper is a good candidate for such kind of contaminations, because of its high diffusion coefficient and high solubility in GaAs (Tin et al. 1987; Kuriyama et al. 1994; Leon et al. 1995). Cu atoms are incorporated on the Ga sublattice as double acceptors $\text{Cu}_{\text{Ga}}^{2-}$ (Leon et al. 1995), which can form electrically active complexes with positively charged arsenic vacancies due to their Coulomb attraction. Different structures of such complexes have been proposed in the literature: $\text{Cu}_{\text{Ga}}\text{V}_{\text{As}}$ (Tin et al. 1987; Kuriyama et al. 1994), $\text{V}_{\text{As}}\text{Cu}_{\text{Ga}}\text{V}_{\text{As}}$ (Tin et al. 1987).

The chemical analysis of the annealed SI GaAs samples has indeed shown a distinct increase of their Cu content (full circles in Fig. 5.8) after annealing. However, the Cu concentration was about 10^{16} cm^{-3} only; that is one order of magnitude lower than the measured number of vacancies. Independent of the concentration arguments, there exists another possibility to check whether the As vacancy is neighbored by a Cu atom. The high momentum part of the Doppler broadening of 511 keV annihilation line carries information on the chemical surrounding of positron trapping centers (Section 3.3). This method was found to be successful in identification of donor- V_{Ga} complexes in n-type GaAs (Gebauer et al. 1999; Gebauer 2000; Gebauer et al. 2001). Results of Doppler broadening measurements normalized to the data obtained for as-grown SI GaAs reference sample are shown in Fig. 5.9. In the upper part of the figure the ratio curve of anni-

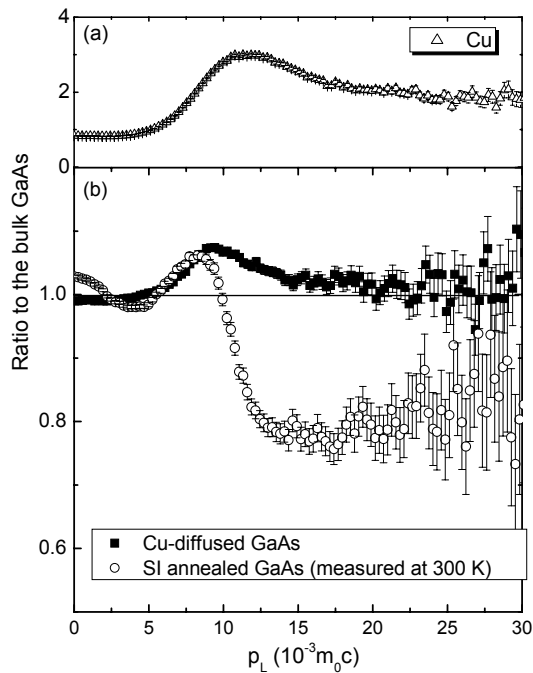


Fig. 5.9: Normalized annihilation momentum distribution measured at room temperature in a) pure Cu; b) SI GaAs annealed at $p_{\text{As}} = 0.2$ bar (\circ) and in SI GaAs after Cu in-diffusion experiment (\blacksquare)

hilation momentum distribution obtained in pure copper is shown. In Fig. 5.9 (b), two kind of samples are compared – SI GaAs annealed at $p_{As} = 0.2$ bar (\circ) and GaAs crystal after copper in-diffusion (\blacksquare). In the latter, the formation of the vacancy clusters neighbored by copper precipitates was observed (Krause-Rehberg et al. 1999; Bondarenko et al. 2001). In the case of the positron annihilation with electrons of copper, the intensity in the high momentum region of Doppler peak, $(10-20) \times 10^{-3} m_0c$, is higher than in bulk GaAs [ratio is larger than 1, Fig. 5.9 (a)]. Thus, the presence of Cu atoms in the immediate vicinity of a positron trap can be seen as such characteristic increase of the intensity of the electron-positron momentum distribution like it was observed for Cu-diffused GaAs. In annealed GaAs in contrast, no sign of Cu in the neighborhood of detected vacancies was observed [Fig. 5.9 (b), (\circ)]. This result provides us with additional support for the assumption that copper is not responsible for the observed vacancy-like defect complex in annealed semi-insulating GaAs.

There were no other foreign atoms with a concentration about that of V_{As} found. Thus, we can exclude impurities from the possible candidates for the defect X. The observed V_{As} -like defect must be related to a native defect-complex. The exact nature of this complex is impossible to determine from results of positron annihilation alone.

5.3.2 Identification of shallow traps in undoped annealed GaAs

The conversion of electrical conductivity from semi-insulating to p-type in annealed GaAs samples is connected with the decrease of the number of EL2 donors and increase of the acceptor-like ion concentration after annealing (Section 5.2.3). The acceptors rep-

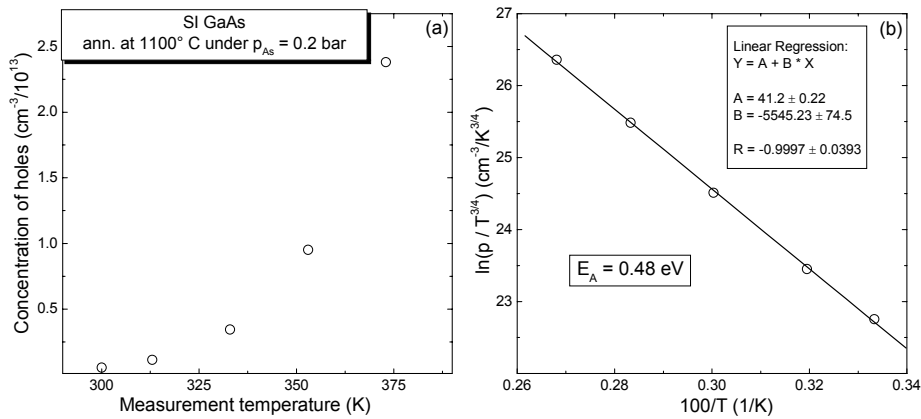


Fig. 5.10: Results of the temperature-dependent Hall-effect measurements on SI GaAs annealed at 1100°C under 0.2 bar of arsenic vapour pressure. Solid line represent a fit to experimental data. By the fit, the activation energy of 0.48 eV above the valence band was determined (see text).

resent positron shallow trap defects and are seen in lifetime measurements as a decrease of the average positron lifetime at low temperatures (Fig. 5.4). However, they cannot be directly identified by PALS because the positron lifetime related to them is close to the bulk value. In this subsection, this question is addressed by determination of the acceptor ionization level with the help of temperature-dependent Hall-effect measurements (TDH) and by the observation of changes of the annihilation momentum distribution by the coincidence Doppler broadening spectroscopy.

Fig. 5.10 (a) shows the temperature dependence of the hole concentration, p , in the SI GaAs annealed at $p_{As} = 0.2$ bar. The dependence $\ln(p \cdot T^{-3/4})(1/T)$ represents a straight line [Fig. 5.10 (b)], which slope corresponds to the activation energy of the acceptor defect. The energy $E_A = 0.48$ eV above the valence band was found. In the literature, this energy level is attributed to the Cu_{Ga} acceptor (Tin et al. 1987; Leon et al. 1995). As was mentioned in the previous subsection, copper is a frequently occurring contaminant in annealing studies due to its ubiquity and high diffusion coefficient, $D = 1.1 \times 10^{-5} \text{ cm}^2 \text{ s}^{-1}$ at 500° C (Hall and Racette 1964). The chemical analysis of the samples annealed at 0.2 and 9.7 bar revealed a distinct enhancement of the copper content (Fig. 5.8). On this basis, the observed shallow trap defects were attributed to negative copper ions.

Additional support for this assumption comes from the results of the coincidence Doppler broadening (CDB) investigation (Fig. 5.11). The curve consisting of the open symbols represents the measurement of the annealed GaAs samples performed at 20 K. At this temperature, negative ions are dominating positron trapping centers, as can be seen from lifetime measurements (Fig. 5.4) – $\tau_{av}(20 \text{ K})$ is close to τ_b value. Thus, the observed annihilation momentum distribution corresponds to annihilation of positrons with the electrons of acceptor-like atoms. Note the difference to the CDB measurement performed on the same sample at the temperature of 300 K corresponding to positron trapping into vacancies (Fig. 5.9). The second curve in Fig. 5.11 (■) is the same one shown in

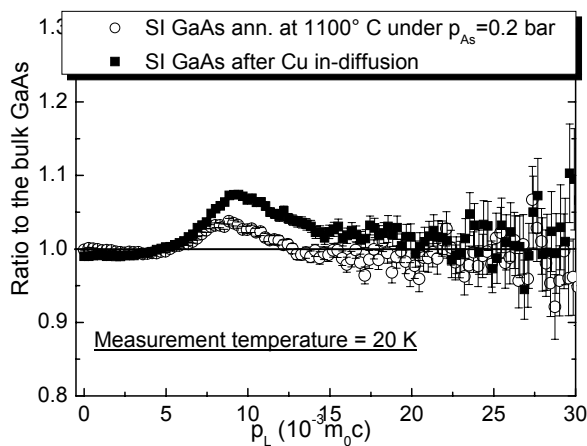


Fig. 5.11: Normalized annihilation momentum distribution in (■) SI GaAs after Cu in-diffusion (Bondarenko et al. 2001) and (○) in annealed in this work SI GaAs. The temperature of measurement was 20 K.

Fig. 5.9 and corresponds to annihilation of positrons with the electrons of Cu atoms. As can be seen, annihilation momentum distribution in the annealed SI GaAs measured at 20 K demonstrates the intensity increase characteristic for the presence of copper atoms in the neighborhood of the annihilation site. Hence, the assignment of shallow trap defects to copper acceptors is justified.

5.3.3 Charge state of the V_{As} complex

The presence of high concentrations of shallow positron traps, identified in the previous subsection as Cu_{Ga} -acceptors, hampers the investigations of vacancy-like defects in the annealed GaAs. Firstly, copper atoms being an uncontrolled impurity influence the reproducibility of the annealing experiments (Section 5.2.3). Secondly, lifetime measurements were found to be affected by positron trapping into shallow positron traps already at temperatures slightly below 300 K (Fig. 5.4). This makes the quantitative analysis of the low-temperature spectra extremely difficult. At the same time, the low-temperature region is the most important, since it corresponds to the highest sensitivity of positron annihilation to open-volume defects (Section 3.2). In order to get rid of copper contamination, a new copper-free annealing procedure was applied (Section 5.1). According to chemical analysis of the samples prepared and annealed under high-purity conditions, it was possible to decrease the number of Cu impurities by two orders of magnitude, from 10^{16} cm^{-3} to 10^{14} cm^{-3} .

Also the PALS results, shown in Fig. 5.12, were found to be qualitatively quite different from those obtained previously (Fig. 5.4). The average positron lifetime increases as the temperature decreases from 500 K to 300 K showing a plateau at $T = 150\text{--}300 \text{ K}$ and decreases rapidly at $T < 150$. The presence of a plateau of such a kind has not been reported in previous positron studies of GaAs and is hence of a special interest. According to the theoretical calculations, the temperature independent positron trapping is expected for the neutral vacancy (Section 3.2.1). Hence, it is reasonable to suggest that at

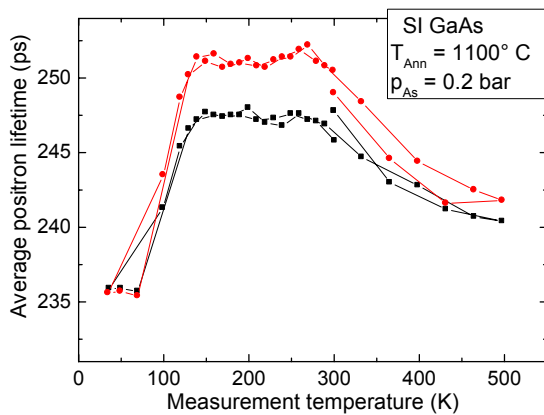


Fig. 5.12: Average positron lifetime vs measurement temperature in SI GaAs after high-purity annealing at 1100°C at $p_{As} = 0.2 \text{ bar}$.

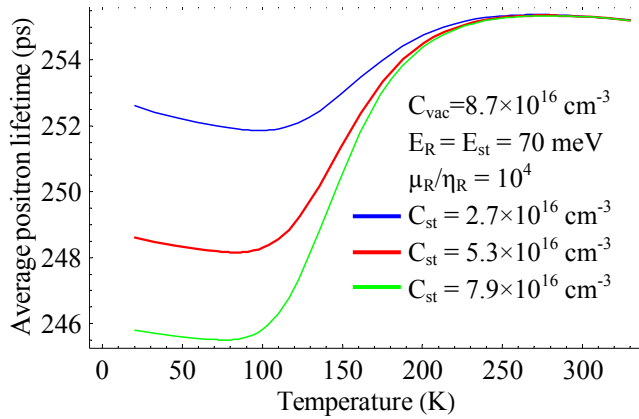


Fig. 5.13: Results of the simulation of the average positron lifetime as a function of temperature for different concentrations of shallow trap defects C_{st} . The model used is described in section 3.2.2. Model parameters are denoted.

150-300 K the dominating trapping center is a neutral vacancy complex. Obviously, the plateau was not observed by previous measurements (Fig. 5.4) due to high shallow trap (Cu_{Ga}) concentrations, which caused the continuous decrease of the positron average lifetime at temperature less than 300 K.

Shallow positron traps, however, can not explain the rapid drop of τ_{av} observed in Fig. 5.12 as temperature lowers from 150 K to 120. Taking into account the decreased concentrations of acceptor-like impurities, the decrease of τ_{av} is simply too abrupt to be imposed by a competitive positron trapping into vacancy and shallow trap defects. Even much higher acceptors concentration could not cause such a steep decrease of τ_{av} . This is demonstrated in Fig. 5.13 by modeling of the $\tau_{av}(T)$ for different concentrations of shallow traps. The model used is described in Section 3.2.2. As can be seen, the presence of shallow positron traps with concentration as high as $8 \times 10^{16} \text{ cm}^{-3}$ can reduce τ_{av} by 10 ps over the temperature decrease of 150 K. This is clearly far from the observed dynamics of $\tau_{av}(T)$ – decrease of 15 ps in 30 K.

Most probably, there is a temperature driven $+/0$ charge transition of the detected vacancy-complex. When the temperature falls below 150 K, the Fermi-level crosses the defect ionization energy level evoking the change of the defect charge state from neutral to positive. Since positrons are repelled by positively charged defects, most of them will annihilate in the crystal bulk or will be trapped and annihilate at shallow traps resulting in the observed quick decrease of $\tau_{av}(T)$. The neutral charge state of the V_{As} complex is in agreement with the results of the Hall-effect measurements (Table 5.1), according to which the hole concentrations do not correlate with the concentrations of the vacancy defects.

5.3.4 Gibbs free energy of V_{As} formation

Having identified the origin of the detected vacancy as V_{As} (Section 5.3.1) and determined its charge state (previous section) it is possible to obtain the formation energy of arsenic vacancies by analyzing the pressure dependence of their concentration. According to the thermodynamic model of defects in GaAs (Section 2.3), the concentration of neutral arsenic vacancies is defined by Eq. 2.19:

$$[V_{As}^0] = K_{V_{As}} / p_{As_4}^{1/4} = (B_{As_4} / p_{As_4})^{1/4} \exp[-(H_f - TS_f) / kT],$$

where H_f and S_f are the formation enthalpy and entropy, respectively. B_{As_4} is the gas pressure constant determined as (Tan 1994)

$$B_{As_4} = (2\pi m_{As_4} / h^2)^{3/2} (kT)^{5/2} = 131.5 T^{5/2}$$

The difference $H_f - TS_f$ represents Gibbs free formation energy, G_f , which one can find from a fit to experimental data according to 2.19 for T equal $T_{ann} = 1100^\circ \text{C}$ and using G_f as the only fitting parameter. The fit yielded $G_f = 3.94 \text{ eV}$ (fig. 5.14).

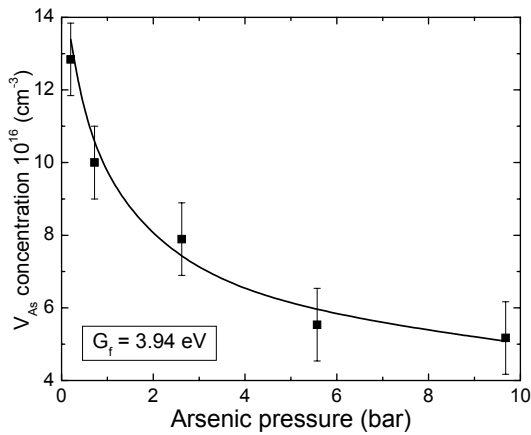


Fig. 5.14: Concentration of As vacancies at 1100°C in SI GaAs as a function of arsenic vapour pressure. Fit to experimental data (solid line) yielded the value of 3.94 eV for Gibbs' free energy of formation of V_{As}

6. Defects study in intentionally undoped VCz-grown GaAs

This chapter contains the results of an extensive systematic study of undoped GaAs grown by the vapor pressure-controlled Czochralski technique, which is a modification of the liquid-encapsulated Czochralski growth method (Section 6.1). Several tens of as-grown crystals were investigated by a variety of experimental methods (PALS, LVM, SIMS GDMS, Hall-measurements), resulting in a large number of experimental data. The discussion in this chapter is concentrated on the PALS results concerning processes of formation of vacancy-like defects in GaAs material of different conductivity types and stoichiometry (Sections 6.2-**Fehler! Verweisquelle konnte nicht gefunden werden.**). Since the large number and detailed analysis of PALS data may confuse a reader inexperienced with the methods of positron annihilation, there were only a few conclusions drawn (Section 6.6).

6.1 Growth method

The Vapor Pressure Controlled Czochralski method (VCz) is a modified LEC crystal growth procedure, which allows growing of GaAs crystals with and without B_2O_3 encapsulation (Tatsumi et al. 1994). By conventional LEC-growth, the boric oxide is utilized to prevent the vaporization of arsenic, which is a highly volatile component at high temperatures, from the GaAs melt. However, the use of B_2O_3 has a series of disadvantages. Firstly, LEC-grown GaAs crystals contain high concentrations of boron, which is an amphoteric impurity in GaAs. It can be incorporated either as a neutral substitutional atom B_{Ga} or as an acceptor B_{As} . Boron acceptors contribute to electrical deactivation of donor atoms in n-type GaAs decreasing thereby the doping efficiency. B_{Ga} are known to have a negative effect on the implantation coefficient in the production of FET-elements (Tomizawa et al. 1987). Secondly, due to the large thermal gradients on the melt- B_2O_3 encapsulant boundary, high thermo-mechanical stresses are introduced into the periphery of the growing crystal. This promotes the formation of a large number of dislocations in the grown crystals, which in its turn may have an influence on the radial homogeneity of wafers electrical properties, as was shown for GaAs:Si in Section 4.3. The VCz growth method is an efficient technique to modify the well-established LEC-method towards crystal pulling under markedly reduced thermo-mechanical stress.

The VCz technique makes use of B_2O_3 encapsulation optional. Growing without boric oxide, As-loss from a free melt surface is prevented by maintaining an arsenic vapor pressure in the growth chamber. For several years, this method has been under development at the Institute for Crystal Growth (ICG) in Berlin (Rudolph et al. 1997). The sche-

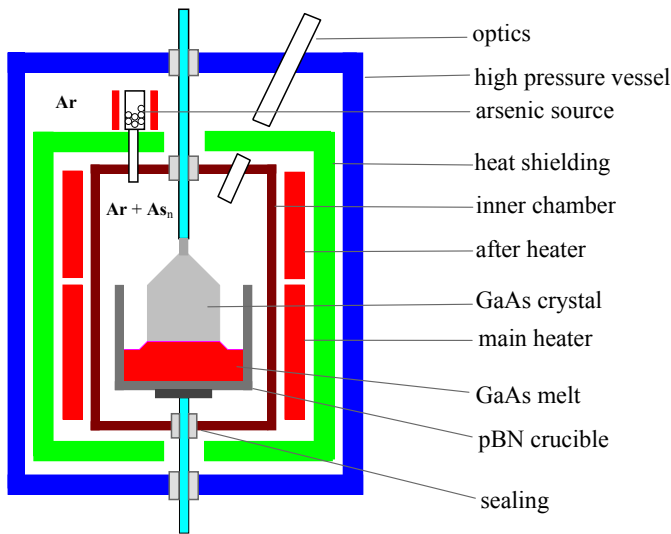


Fig. 6.1: Scheme of the VCz arrangement used for growth of GaAs without B_2O_3 encapsulant (From Ref. (Kiessling et al.))

matic drawing of the VCz arrangement used at ICG for GaAs growth without B_2O_3 encapsulant is given in fig. 6.1. The main constructive difference from the LEC-setup is the presence of an inner chamber, which is used for temperature shielding of the growing crystal. This allows remarkable reduction of temperature gradients in axial and radial directions. The whole system is placed inside a high-pressure vessel, since the growth is performed under high pressures of an inert gas, usually argon or nitrogen. The heat shielding, main heater and inner chamber are made of high-pure graphite. Two crucible types, made of high purity pyrolytic boron nitride (pBN) or silicon dioxide (SiO_2), can be applied. Special solid sealing for the feed through mechanisms for translational and rotational movement of a growing crystal and crucible were developed which results in a quasi non-conservative system. The As-source is positioned outside the inner chamber and heat shielding, in order to prevent thermal contact between the source and main heater. Thus, the temperature of the As-source, T_{As} , and hence As vapour pressure in the inner chamber, p_{As} , can be adjusted independently.

Main advantages of VCz method are (i) low level of residual strains and (ii) reduced dislocation density due to reduced thermal stresses. GaAs crystals of diameters 100-150 mm with dislocation density in the range of 10^4 cm^{-2} were obtained (Neubert and Rudolph 2001). Moreover, control over p_{As} provides an additional (iii) advantage of crystal growth from different melt compositions. However at present, the latter may also be considered as a disadvantage, since the introduction of one more parameter, p_{As} , increases the complexity of the growth system, whereas the current state of knowledge about the interaction mechanisms between point defects and the melt composition is still rather poor. Other VCz disadvantages are (i) relatively high complexity of the equipment and therefore increased investment costs and (ii) enlarged process time and high operational costs.

6.2 Carbon controlled growth

Nowadays, the LEC and consequently VCz growth methods are used predominantly for the production of SI GaAs wafers (Rudolph and Jurisch 1999). The main intrinsic point defect in SI GaAs that governs its electronic properties is the deep double donor EL2 with two energy levels in the band gap EL2^{+/+} at 0.54 eV and EL2^{+/0} at 0.75 eV (Hurle 1999), which, according to the current state of knowledge, is attributed to the arsenic antisite defect, As_{Ga} (Krause-Rehberg et al. 1994; Hurle 1999). The EL2 provides free electrons to the conduction band and determines thus the n-conductivity type of GaAs. However, in order to produce semi-insulating high resistive crystals ($\rho \approx 10^6$ - 10^8 Ωcm), the main part of EL2 donors must be compensated. This is usually done by intentional doping of GaAs crystals with carbon atoms, which are incorporated exclusively on the As sublattice forming shallow acceptor-like defects, C_{As} (Hurle 1999). The typical values of EL2 and C_{As} concentrations in SI GaAs amount to 10^{16} cm^{-3} and 10^{15} cm^{-3} , respectively.

By conventional LEC-growth, the carbon-doping is performed by adjusting a certain CO-partial vapour pressure in the inert-gas atmosphere under simultaneous introduction of an oxygen potential (water content of B₂O₃, adding of Ga₂O₃). The quantity of carbon absorbed by the melt is determined by thermodynamic reactions within the multi-component system Ga-As-B-O-H-N-C. Also by growing without boric oxide encapsulation, the carbon content may be controlled by the CO-pressure, as was firstly shown in Ref. (Kiessling et al. 2003) and discussed in the following.

The positron annihilation lifetime spectroscopy can be useful in two ways in such kind of studies. Firstly, deviation of the crystal composition from stoichiometry should influence in the first place the concentration of vacancy defects, which is perfectly seen in positron annihilation measurements. Secondly, negatively charged C_{As} are shallow positron traps and hence seen as a decrease of positron lifetime at low temperatures providing there is trapping into open-volume defects as well (similar to Si_{As} in GaAs:Si, Section 4.2.2). The lower sensitivity limit of positron annihilation, $2\text{-}5 \times 10^{15}$ cm^{-3} , fits perfectly to the carbon concentrations lying in the range of interest. Curiously, positron sensitivity to negative ions appears often as a disadvantage making difficult the study of the subject of main interest – vacancy like defects. This study of carbon-controlled growth, in contrast, takes an advantage of the PALS ability to detect C_{As} acceptors. However, it should be noted that the discussion is constrained to a qualitative analysis only. Determination of absolute concentrations of carbon atom by means of positron annihilation is not possible due to the difficulties of spectra decompositions at low temperatures.

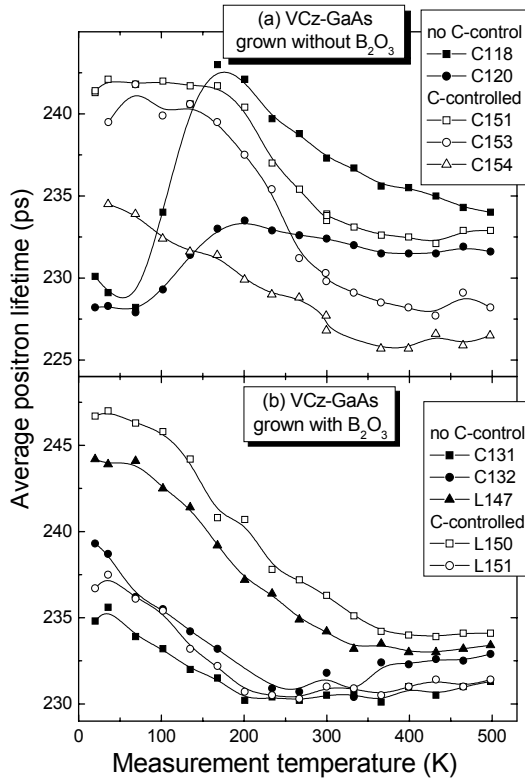


Fig. 6.2: Temperature dependence of the average positron lifetime measured in VCz-GaAs grown (a) with and (b) without B_2O_3 encapsulation under and without control of CO pressure. The lines are to guide the eye.

The results of positron lifetime measurements in VCz-GaAs crystals grown with and without B_2O_3 -encapsulation with and without application of carbon control are presented in Fig. 6.2. In all samples, open-volume defects were observed – the average positron lifetime was higher than the value of bulk lifetime in GaAs ($\tau_b = 230$ ps). Two-component decomposition of the lifetime spectra yielded the defect-related lifetime of 270 ± 10 ps, pointing to the presence of monovacancy-type defects. The increase of the average positron lifetime toward lower temperatures is an indication of the negative charge of the detected vacancies. Only two samples [C118 and C120, Fig. 6.2 (a)], grown without B_2O_3 -encapsulation and also without control over the CO-vapour pressure, demonstrate the pronounced decrease of the positron lifetime at temperatures below 200 K. This decrease is explained by positron trapping at negative ions, C_{As}^- , which concentration in these samples must be about 10^{16} cm^{-3} to produce such an effect. It was confirmed by LVM measurements (Table 6.1). The carbon content in the melt and hence in the crystal can significantly be reduced by decreasing the CO-pressure during the crystal growth. There was no shallow trap related decrease of the positron lifetime observed in the samples grown under C-control conditions [open symbols in Fig. 6.2 (a)]. This means that the concentration of shallow trap defects (i.e. C_{As}^-) is under the sensitivity limit of positron annihilation, $5 \times 10^{15} \text{ cm}^{-3}$. It is interesting to note, that carbon incorporation seems to be

Table 6.1 – Growth parameters, carbon and free charged carriers concentrations of VCz-GaAs samples investigated in this section

Sample #	B ₂ O ₃ encapsulation	Carbon control	[C _{As}], cm ⁻³	Conductivity type and carriers concentration, cm ⁻³
C151	No	Yes	1.4×10 ¹⁵	[n] = 4×10 ¹⁴
C153	No	Yes	0.9×10 ¹⁵	[n] = 6×10 ¹⁴
C154	No	Yes	1.3×10 ¹⁵	[n] = 7×10 ¹³
C118	No	No	< 3.3×10 ¹⁶	[p] = 8.2×10 ¹⁵
C120	No	No	< 1.9×10 ¹⁶	[p] = 4.2×10 ¹⁵
L150	Yes	Yes	5.5×10 ¹⁴	[n] = 5.8×10 ¹⁴
L151	Yes	Yes	0.7×10 ¹⁴	[n] = 5.8×10 ¹⁴
C131	Yes	No	7.8×10 ¹⁴	[n] = ?
C132	Yes	No	5.2×10 ¹⁴	SI [n] ≈ 10 ⁷
L147	Yes	No	1×10 ¹⁵	SI [n] ≈ 4×10 ⁷

suppressed by the presence of B₂O₃ layer. Positron annihilation measurements did not show the presence of negative ions in any crystal grown with boric oxide encapsulation regardless whether C-control was applied [Fig. 6.2 (b), Table 6.1].

6.3 Influence of the melt stoichiometry and unintentional doping on vacancy formation

One of the advantages of the VCz growth method is the possibility of the in-situ control of the melt composition during the growth without the boric oxide encapsulation. This is realized by adjusting an appropriate arsenic vapour pressure in the growth chamber. The higher the As-pressure, the more As-rich is the GaAs melt. As-pressure is controlled in turn by the temperature of a reservoir with pure metallic arsenic (arsenic source in fig. 6.1), T_{As}. The crystals investigated in this work were grown at T_{As}, varying between 590° C and 660° C corresponding to Ga- and As-rich melts (Wenzl et al. 1991). A melt of a nearly stoichiometric composition was obtained at T_{As} = 630° C (Kiessling et al.). Control over the melt composition provides an indirect possibility to influence the composition of the grown crystals. The possibility is called “indirect”, since there is no exact knowledge about the phase extent of GaAs at present (Fig. 2.1). Moreover, Ga-rich melt does not necessarily mean that the crystal is Ga-rich (Section 2.1). Deviation from stoichiometry in a crystal is realized through formation of point defects (Eq. 2.1). Thus Ga-rich crystals should have markedly less Ga vacancies than the As-rich one. However, it is not always the case, as demonstrated in the following.

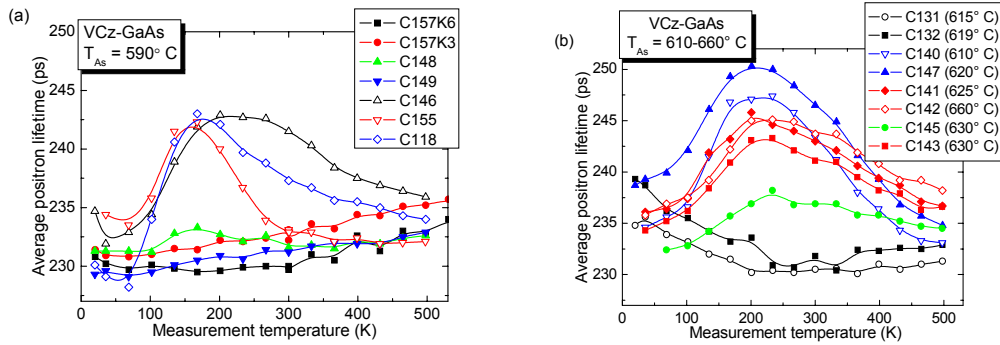


Fig. 6.3: Average positron lifetime as a function of temperature measured in VCz-GaAs grown at (a) $T_{As} = 590^\circ\text{C}$ and (b) $T_{As} = 610-660^\circ\text{C}$ (T_{As} is indicated). The lines are drawn to guide the eye.

Fig. 6.3 shows the results of positron annihilation lifetime measurements obtained for some of the crystals grown at different temperatures of the arsenic source. Fig. 6.3 (a) corresponds to crystals grown from Ga-rich melt ($T_{As} = 590^\circ\text{C}$). The crystals presented in Fig. 6.3 (b) were grown from the melt, which composition varied from light- to heavy As-rich by increasing T_{As} from 610°C to 660°C . As can be seen, average positron lifetime reveals very pronounced differences for the samples within each group indicating large variations in concentrations of vacancy-like defects. Thus, τ_{av} in most of the 590°C crystals has rather low values, $\tau_{av}(300\text{ K}) \approx 230 - 233\text{ ps}$ [solid symbols in Fig. 6.3 (a)]. However, three samples demonstrated distinctly higher τ_{av} with strong temperature dependence. The longest τ_{av} observed for sample C146 was very close to those obtained in some crystals of the second group [red symbols in Fig. 6.3 (b)]. Note the similar great differences between the samples in this group, which can not be related to T_{As} . Obviously, formation of vacancies is determined not only by arsenic activity. The second deciding factor is the position of the Fermi level (Section 2.3). In undoped material, the Fermi level may be easily shifted by a relatively small number of electrically active impurities¹. Chemical analysis did indeed revealed presence of $10^{16}-10^{17}$ silicon atoms in the 5 samples, which demonstrate the longest τ_{av} in Fig. 6.3 (b). The point is that these crystals were grown in a crucible made of SiO_2 material, which was the source of the Si-contamination. Since silicon in As-rich GaAs is incorporated mostly as Si_{Ga} -donor (Section 4.1), all these samples became n-type semiconductors (Table 6.2).

Interestingly, the C146 sample [Fig. 6.3 (a)] was grown from a Ga-rich melt that was *intentionally doped* with a small amount of silicon. Despite the melt composition enriched with Ga, this crystal was found to be also n-type (Table 6.2) and had approximately the same number of vacancy-like defects as the mentioned above crystals grown in SiO_2 -crucible from As-rich melt. Obviously, silicon incorporation is not affected much

¹ Similar observation was also made in the annealing experiments of undoped SI GaAs described in Section 5.2.3.

Table 6.2 – Growth conditions, concentrations of major dopants and electrical characteristics of VCz-GaAs crystals presented in Fig. xx.

Sample	T _{As} (° C)	Crucible	Si (cm ⁻³)	C _{As} (cm ⁻³)	n (cm ⁻³)	μ (cm ² /Vs)
C140	610	SiO ₂	2.3×10 ¹⁶	1.4×10 ¹⁶	5×10 ¹⁶	4420
C141	625	SiO ₂	not measured	1.7×10 ¹⁶	6×10 ¹⁶	3200
C142	660	SiO ₂	1.5×10 ¹⁷	1.5×10 ¹⁶	8×10 ¹⁶	3510
C143	630	SiO ₂	1.5×10 ¹⁷	1.2×10 ¹⁶	9.2×10 ¹⁶	3550
C147	620	SiO ₂	not measured	1.4×10 ¹⁶	3.5×10 ¹⁶	4190
C146	590	pBN	5.3×10 ¹⁶	2.5×10 ¹⁶	3.1×10 ¹⁶	3420

by the melt composition and is hence the *determining factor* in the process of vacancy formation. Discussion of the origin of these vacancies is postponed to the following subsections. At this stage, it is just worth to note that they represent a monovacancy-like defect, which is negatively charged.

The other samples presented in Fig. 6.3 were found to be semi-insulating (C131, C132 and C148) or p-type. The results of positron annihilation observed in these samples are very much different from those obtained in n-type specimens. This again demonstrates quite clearly that the formation of vacancies in as-grown GaAs is governed by the electronic properties of the crystals. The following subsection is devoted to this subject.

6.4 Results of PALS measurements

6.4.1 Semi-insulating GaAs

Semi-insulating GaAs samples demonstrated very short positron lifetimes (Fig. 6.4). The room temperature τ_{av} did not exceed 232 ps. Such a short positron lifetime means that the concentration of vacancy-like defects is near or below the sensitivity limit of positron annihilation, $2\cdot6\times10^{-8}$ a.u. (Krause-Rehberg and Leipner 1999). In GaAs, the limit corresponds to $\approx 0.8\text{--}3\times10^{15}$ cm⁻³. This is in agreement with earlier observations on as-grown SI GaAs (West 1979). The presence of vacancies is seen clearly as the increase of positron lifetime with decreasing temperature, observed for the samples C131 and C132 (Fig. 6.4) in the temperature interval of 20–250 K. The other two samples, however, do not reveal such an increase. This discrepancy is discussed in the following.

Increasing τ_{av} with lowering sample temperature designates enhancement of positron trapping rate (K_d in eq. 3.14). A similar temperature behavior of K_d was reported in earlier studies of SI GaAs studies by means of positron lifetime (Saarinen et al. 1993; Kuisma et al. 1996) and Doppler-broadening spectroscopy (Chen et al. 1996). There, this temperature effect was attributed to positron trapping into negatively charged *Ga monovacancies*. Although, positron annihilation experiments are unable to identify,

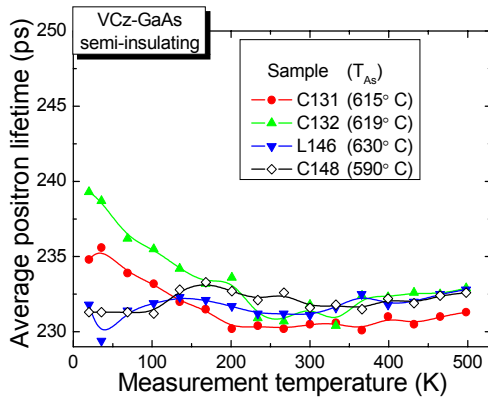


Fig. 6.4: Average positron lifetime measured as a function of temperature in as-grown SI GaAs. Temperatures of arsenic source (T_{As}) applied during the growth is indicated.

whether the V_{Ga} are isolated or bound to a defect complex. Occurrence of an isolated gallium vacancy seems to be more probable. Its concentration ($2\text{-}3 \times 10^{15} \text{ cm}^{-3}$) is less than that of the EL2 center, which is the dominating intrinsic point defect in SI GaAs (Table 6.3). Out of the probable impurities, only carbon acceptors are present in concentrations in the order of 10^{15} cm^{-3} . However, an increase of the carbon content suppresses the intensity of the vacancy signal (Table 6.1 and Fig. 6.4). Thus, the possibility of the formation of a $C_{As}V_{Ga}$ complex can be excluded.

Table 6.3 – Concentrations of carbon acceptors and neutral EL2 centers, resistivity and electron mobility measured in SI GaAs crystals grown from As- and Ga-rich melts

Sample	Melt composition	C_{As} (cm^{-3})	EL2 ^o (cm^{-3})	ρ (Ωcm)	μ (cm^2/Vs)
C131	As-rich	7.8×10^{14}	0.8×10^{16}	4×10^7	6500
C132	As-rich	5.2×10^{14}	1×10^{16}	1×10^7	4500
L146	As-rich	2.5×10^{15}	0.9×10^{16}	1×10^8	5000
C148	Ga-rich	6.3×10^{15}	0.8×10^{16}	3×10^8	2700

On the other side, carbon plays an important role for the electrical properties of semi-insulating GaAs. The resistivity of SI crystals is increased by orders of magnitude with increasing of the carbon concentration from 10^{14} to 10^{15} cm^{-3} (Table 6.3). The high-resistivity samples do not show the characteristic increase of positron lifetime at low temperatures. There are two possible explanations. Firstly, these crystals contain less V_{Ga} . Secondly, the decrease is not seen due to a higher concentration of carbon acceptors, which trap positron into their shallow negative potential at low temperatures.

No correlation of vacancy formation as well as crystal electrical properties to the composition of the melt, from which the crystals were grown, could be established.

6.4.2 p-type GaAs

Electrical properties of a series of p-type grown GaAs samples are summarized in Table 6.4.

Table 6.4 – *Electrical characteristics of p-type VCz-samples grown from As- and Ga-rich melt*

Sample	Melt composition	ρ (cm^{-3})	μ_h (cm^2/Vs)	ρ_h (Ωcm)
C118	As-rich	8.2×10^{15}	304	2.5
C120	As-rich	4.2×10^{15}	48	31
C145	As-rich	1.4×10^{16}	285	1.6
C155	Ga-rich	2.5×10^{13}	113	2.2×10^3
C149	Ga-rich	3.2×10^{16}	320	0.6
C157K3	Ga-rich	1.4×10^{15}	113	39
C157K6	Ga-rich	6×10^{15}	108	10

According to the results of positron annihilation lifetime measurements (Fig. 6.5) it is possible to divide the investigated samples in two groups. For the first group, which is represented by solid symbols, a short positron lifetime increasing monotonously with temperature was observed. The samples of the second group (open symbols) demonstrate, in contrast, a pronounced maximum of τ_{av} at $T \approx 200$ K.

The first group represents results, which were often reported for p-type GaAs (e.g., in Refs. (Le Berre et al. 1995; Gebauer et al. 2000)). The short average positron lifetime is usually ascribed to positrons annihilating from the delocalized state in the lattice, whereas the increase of τ_{av} to higher temperatures – to temperature lattice expansion. A theoretical value for delocalized positron lifetime can be written as (Hautojärvi 1979):

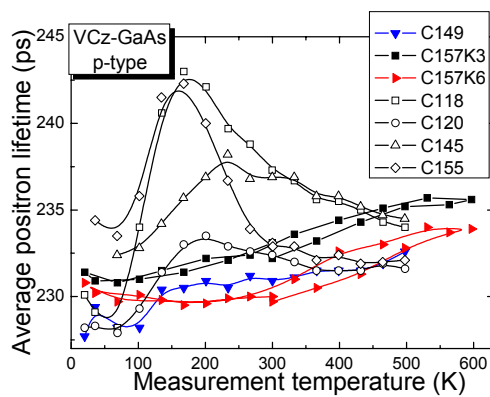


Fig. 6.5: *Average positron lifetime measured as a function of temperature in p-type VCz-grown GaAs.*

$$\tau_{th} = \frac{a^3}{\sigma v N_e}, \quad (6.1)$$

where a^3 is the volume of the cubic cell, N_e is the number of electrons in this volume, σ is the cross section of the e^+e^- annihilation, and v is the positron velocity relatively to the electron. Le Berry et al. were the first who performed such analysis for p-type GaAs using the temperature dependence of the cell parameter a obtained from the thermal-expansion coefficient values given in Ref. (Weyrizli 1989). However, it turned out that the average positron lifetime increased more rapidly with temperature than the $\Delta a^3/a^3$ parameter (Krambrock et al.). To explain the discrepancy, Le Berry resorted to the argument of positron-phonon coupling. According to Stott (Stott and West 1978) lattice vibrations play a role in the positron distribution by temporarily expanding the interstitial spaces. The duration of these momentary expansions is long enough for positrons to annihilate, so that the electron density seen by positrons is lower than that due only to the continuous thermal expansion of the lattice. However, the results presented in Fig. 6.5 were found to be completely inconsistent with such interpretation. Firstly, the average positron lifetime in the samples of the second group does not increase but decreases continuously in the high-temperature region. Note the intersection of the $\tau_{av}(T)$ curves of group 1 and group 2 samples. Also, semi-insulating GaAs crystals did not show such remarkable change of positron lifetime with increasing temperature (Fig. 6.4). Secondly, measurements of the C157K3&K6 samples revealed a distinct hysteresis of τ_{av} at high temperatures, which can not be explained in terms of lattice thermal expansion. Thus, the temperature increase of τ_{av} can not be ascribed to a temperature increase of the lattice constant. Consequently, there should exist an open-volume defect with positron trapping coefficient μ increasing towards higher temperatures. The defect annealed partially during the high-temperature measurements causing the hysteresis of τ_{av} observed in Fig. 6.5 According to theoretical considerations (Section 3.2.1), the temperature increase of μ is expected for neutral (Fig. 3.5) or *positive* vacancies. Since the C157 crystal was grown from Ga-rich melt, the *arsenic vacancy* is the most likely assignment for the defect observed.

The samples of the *second group* demonstrates τ_{av} temperature dependence characteristic for positron trapping into a negative vacancy and shallow trap defect. The latter is most probably represented by carbon acceptors, high concentrations of which must be present in p-type crystals. The occurrence of negative vacancies in as-grown p-type GaAs was never reported before. Two component decomposition of lifetime spectra yielded defect-related lifetime of 270 ± 15 ps pointing to monovacancy type of the defect detected in these samples. The origin of this defect was attributed to the gallium vacancy. This argumentation is based on the results of CL spectroscopy given in the following subsection.

It is interesting to note the relation between positron lifetime and crystals electronic properties. Two samples, C118 and C145, having very similar values of hole con-

centrations and mobility (Table 6.4) demonstrated similar τ_{av} curves in the temperature region of 300-500 K (Fig. 6.5). A much shorter positron lifetime was detected in the sample C120. This sample had nearly the same carrier concentration as C118 and C145 crystals, but the mobility was found to be ~ 6 times less. Sample C155 differs from other p-type specimens by the strongest temperature dependence of positron lifetimes. This sample has also the highest resistivity value (Table 6.4). Unfortunately, the mechanism lying behind the interrelation of positron trapping and electronic properties of semiconducting crystals is not understood sufficiently well.

6.4.3 n-type GaAs

There were two kinds of donor-like impurities observed in n-type VCz-GaAs: silicon and sulfur. Silicon was the dominating impurity in crystals grown in a SiO_2 -crucible (see Section 6.3). Free electron concentration in these crystals was in the order of 10^{16} cm^{-3} (Table 6.2). In crystals grown in a pBN-crucible, the silicon concentration was significantly reduced. The major donor species in these samples was represented by sulfur atoms, as GDMS analysis showed. It is not quite clear what was the origin of the sulfur contamination. Most probably, the metallic arsenic used as arsenic source (Fig. 6.1) contained small amounts of S (Neubert and Rudolph 2001). However, the concentration of S atoms was much less than that of Si in crystals grown in a SiO_2 crucible. Also the free electron density was found to be at least two orders of magnitude less than that of silicon-contaminated samples. The electrical characteristics of the n-type GaAs samples investigated in this work are summarized in Table 6.5. It is worth to note, that all n-type material was grown from the melt, the composition (i.e. T_{As}) of which corresponded to As-rich crystals. The only exception was the C146 crystal that was grown from Ga-rich melt ($T_{As} = 590^\circ \text{ C}$). But n-type conductivity of this crystal was imposed by high concentrations of silicon presented in the melt, as was mentioned in section 6.3.

Results of positron annihilation measurements performed on n-type GaAs-crystals are presented in fig. 6.6. In order not to encumber the graph, silicon contaminated

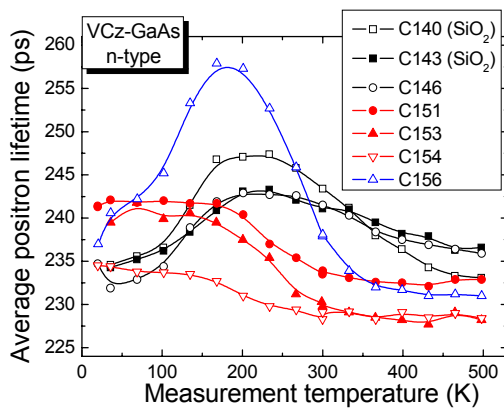


Fig. 6.6: Average positron lifetime measured as a function of temperature in n-type VCz-grown GaAs. Crystals grown in a SiO_2 -crucible are indicated. All other crystals were grown in a pBN-crucible.

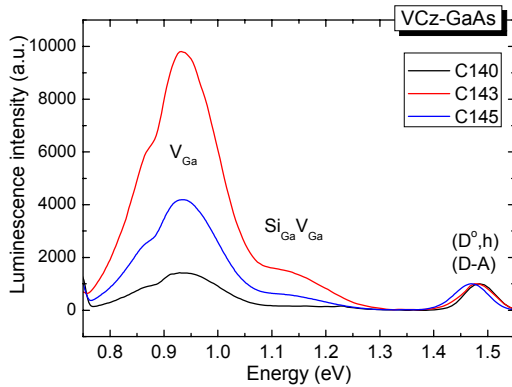
Table 6.5 – Electrical characteristics of the investigated n-type VCz-grown GaAs crystals

Sample	Crucible	Crystal stoichiometry	n (cm ⁻³)	μ _e (cm ² /Vs)	ρ _e (Ωcm)
C140	SiO ₂	As-rich	5×10 ¹⁶	4420	28×10 ⁻³
C143	SiO ₂	As-rich	9.2×10 ¹⁶	3550	19×10 ⁻³
C146	pBN	Ga-rich	3.1×10 ¹⁶	3420	59×10 ⁻³
C151	pBN	As-rich	4×10 ¹⁴	4440	3.5
C153	pBN	As-rich	6×10 ¹⁴	6180	1.7
C154	pBN	As-rich	7×10 ¹³	2370	37.6
C156	pBN	As-rich	1.5×10 ¹⁵	5180	0.8

samples were presented by three $\tau_{av}(T)$ curves only. Measurement results obtained for other crystals of this type are shown in Fig. 6.3.

The average positron lifetime in all the samples demonstrated a general increase towards low temperatures. The increase indicates the presence of vacancy defects, which are negatively charged (Section 3.2). The temperature decrease of the positron lifetime observed in some samples in the 20-200 K temperature region is connected with the influence of negative acceptors acting as shallow positron traps (Section 3.2.2). Thus, Si-containing samples, C140/C143/C146, demonstrate the characteristic decrease, which is usually ascribed to positron annihilating at Si_{As}-acceptors (Section 4.2.2). Also the high-temperature behavior of the average positron lifetime is similar to that observed in lightly silicon-doped GaAs crystals (Fig. 4.16), indicating a similar nature of the open-volume defects detected in these materials. This assumption was supported also by CL-measurements.

As discussed in Section 4.4, the vacancy defect observed in GaAs:Si is responsible for the 0.95 eV luminescence band (Fig. 4.14). A luminescence peak at this energy was also found in VCz-grown Si-contaminated GaAs (Fig. 6.7). In section 4.5, the supposition was made that the defect giving rise to the observed luminescence band is a

**Fig. 6.7:** Cathodoluminescence spectra measured in VCz-grown GaAs. Data were normalized to the intensity peak corresponding to band-band transition (1.48 eV)

sition was made that the defect giving rise to the observed luminescence band is a single gallium vacancy, which is not bound to a silicon atom. The CL measurements of C145 sample provided an excellent proof for this assumption. This crystal was grown with a pBN-crucible and was, hence, free from silicon impurity atoms. Moreover, C145 belongs to the “anomalous” p-type crystals, which demonstrated the presence of negative vacancies (Section 6.4.2, Fig. 6.5). According to theoretical calculations (Section 2.4), only V_{Ga} can be negatively charged in p-type samples. Thus, negative vacancy defects observed in n- and p-type material were attributed to *gallium vacancies*.

Comparing the intensity of the room temperature positron annihilation signal (fig. 6.6) with the values of charge carrier concentrations, one can see that an increase of the free electron density imposes also an increase of vacancy concentrations, which is seen as a longer positron lifetime. This may be connected with the Fermi-level effect, according to which concentrations of gallium vacancies increase with increasing Fermi energy (Section 2.3 and 4.5).

6.5 Validity of positron annihilation for determination of vacancy concentration

Positron annihilation is often claimed as the unique tool for determination of the absolute concentrations of open-volume defects. However, defect concentrations are not measured directly in positron lifetime measurements. The real measurable quantity is the positron trapping rate k , which is assumed to be proportional to concentrations of vacancy-like defects (Eq. 3.4). The coefficient of proportionality μ is called trapping coefficient. μ is a parameter specific for a certain defect type and must be determined by means of an independent method. Since there are no other reliable methods for vacancy detection, the information used for μ determination is always indirect (Krause-Rehberg and Leipner 1997). Therefore, the trapping coefficient is usually known with an accuracy factor not better than two. Consequently, absolute vacancy concentrations determined with Eq. 3.4 are connected with relatively big uncertainties.

The situation becomes more complicated, since different defects demonstrate different temperature dependence of the positron trapping coefficient, $\mu(T)$. Let's consider Fig. 6.3 (b). The average positron lifetime demonstrates temperature behavior in samples C140 and C147 (blue symbols) clearly different from that C141, C142, C143 (red symbols). Corresponding $\tau_{\text{av}}(T)$ curves intercept with the effect that the average lifetime at the maximum of $\tau_{\text{av}}(T)$ curve is higher in the samples C140/C147, whereas positron lifetime at 500 K is distinctly longer in crystals C141-C143. The question arises quite naturally: which kind of samples contains larger number of vacancies? Taking the same trapping coefficient for all samples, the answer would be – vacancy concentration is higher in samples C140/C147. However, the intensity of the CL-peak was found to be higher in sample C143 than in C147, anticorrelating with the τ_{av} values. Fig. 6.3 (a) demonstrates

an even more extreme discrepancy. The average positron lifetime in the samples presented by open symbols is very different at 300 K, but very similar at the maximum of $\tau_{av}(T)$ curves. Similar examples can be found in all other graphs of this section, in which $\tau_{av}(T)$ curves are shown, leading to two main conclusions:

- 1) Even qualitative analysis of defects concentrations by means of positron lifetime spectroscopy is justified only if the defects demonstrate similar dependence of positron trapping coefficient¹. Thus, it is always important to perform temperature dependent PALS measurements.
- 2) Temperature dependence of positron trapping in semiconductors carries important information about the defect structure of positron trapping centers. This information is, however, difficult to extract, since $\mu(T)$ was found to be in addition influenced by crystals electronic properties.

The next section is devoted to temperature dependent positron trapping in GaAs.

6.6 Summary

The study presented in this chapter had two main goals. Firstly, it was aimed to contribute to better understanding of the connections between formation of point defects and crystal growth conditions in VCz-GaAs. In particular, control of carbon content during the growth without boric oxide encapsulation (Section 6.3), influence of the arsenic activity and unintentional impurities on crystals defect properties were subjects of interest. Secondly, the systematic investigation of great variety of as-grown crystals with the help of positron annihilation lifetime spectroscopy together with many other characterisation techniques provided large number of experimental data, which could significantly extend the state of our knowledge about the interaction between positrons and semiconducting matter. Vacancy formation in both semi-conducting (n- as well as p-type) and semi-insulating material was studied. In general, about 30 different GaAs crystals were studied by several experimental methods: PALS to investigate open-volume defects, CL as a complimentary method for defects identification, local vibrational mode spectroscopy (LVM) for detection of acceptor-like impurities, infrared absorption spectroscopy (IRA) to obtain concentrations of EL2⁰ centers, glow discharge and secondary ion mass spectrometry (GDMS and SIMS) for the crystals chemical analysis. The LVM, IRA, GDMS and SIMS data were taken from Ref. (Kiessling et al.).

Vacancies on both sublattices, V_{Ga} and V_{As} , were detected in as-grown GaAs by means of positron lifetime spectroscopy. The following conclusions were made:

- 1) Arsenic vacancies were found in Ga-rich p-conducting GaAs. According to the temperature dependence of positron trapping, V_{As} must be present in neutral or positive charge state (Section 6.4.2).

¹ This condition was satisfied in the investigations presented in Chapters 4 and 5

-
- 2) In p-type *As-rich* crystals, formation of negatively charged gallium vacancies was observed (Section 6.4.2).
 - 3) Negative V_{Ga} were also found in semi-insulating (Section 6.4.1) and n-GaAs (Section 6.4.3) regardless of the melt composition, from which the crystals were grown.
 - 4) The concentration of Ga vacancies depends on the position of Fermi level in a crystal and is the higher the more pronounced its n-type characteristics are. In other words, the concentration of gallium vacancies in GaAs increases with the transition of its conductivity type from semi-insulating to highly semi-conducting (Section 6.4.1).
 - 5) It would be very interesting to perform a quantitative analysis of this dependence. However, possibilities of positron annihilation for determination of vacancy concentrations are constrained, as discussed in the Section 6.5.

7. On the temperature dependence of positron trapping in GaAs

The practical importance of positron annihilation as a method for semiconductor studies lies in its unique ability to measure the absolute concentrations of vacancy-like defects and depends extremely on the accuracy of these measurements. The latter is constrained by the knowledge of the trapping coefficient μ , which represents a constant of proportionality between the measured trapping rate K and concentration C_d of a certain defect-type. (Eq. 3.4). In order to determine the trapping coefficient, the vacancy concentration must be measured independently of the positron experiment by using a reference method (Krause-Rehberg and Leipner 1997). Unfortunately, the information provided by such methods is always indirect. Therefore, μ is *at best* known with an accuracy factor of two. Moreover, the trapping coefficient is usually obtained at room temperature, whereas positron annihilation is often most sensitive and hence its results are most reliable at low temperatures. These uncertainties invalidate the significance of positron annihilation as a quantitative method, despite the high precision of measurements (about 1% for positron annihilation lifetime spectroscopy).

In this respect, the information obtained from temperature-dependent measurements can have more deterministic and quantitative character than the determined absolute vacancy concentrations, since these results represent just the change of annihilation parameters (τ_{av} or K) with temperature, whereas no normalization on positron trapping coefficient is necessary. However, despite the fact that positron annihilation has been applied to study of semiconducting materials for more than 30 years, the influence of the temperature on the positron trapping rate in semiconducting materials is still not well understood. Theoretical works performed in the late 80's (Section 3.2.1) provided description of the positron trapping temperature dependence in good (at least qualitative) agreement with experimental results available at those times. This enabled developing of simple trapping models for fitting to the experimental data (Section 3.2.2). Satisfied with this success, both theoretical and experimental investigations of the essence of the positron trapping coefficient temperature dependence were stopped. Experimentalists dealing with positron annihilation temperature-dependent measurements interpret their results either in the frameworks of the positron trapping models mentioned above or resort to purely qualitative arguments, such as temperature-driven defect charge transition (Gebauer et al. 2001) or resonance trapping (Shirai and Takamura 1989), if these models turn out to be not applicable. The present author strongly believes that the valuable information about positron-defects interaction contained in the temperature behavior of positron trapping remains unused due to a lack of understanding.

It is the goal of this chapter to demonstrate the importance of temperature influence on positron annihilation parameters and to show the necessity of its further theoretic-

cal and experimental investigations. Two expedients are used to achieve the task. Firstly, inconsistency of the existing model of temperature-dependent positron trapping with some experimental results is shown (Section 7.1). No theoretical development of a new trapping model was intended here. This subject deserves an individual investigation. Secondly, all the positron annihilation lifetime results obtained in this work were systematized according to the temperature dependence of the trapping rate, i.e. average positron lifetime. It is the authors hope that such analysis will contribute to a better understanding of the temperature dependence of positron trapping in semiconductors. In particular, the following questions were discussed:

- 1) How does the temperature dependence of the trapping rate $K(T)$ depend on the concentration of vacancy-like defects?
- 2) What is the influence of the defect charge state on $K(T)$?
- 3) Does $K(T)$ depend on the vacancy charge state?
- 4) Below which temperatures are positrons effectively trapped by shallow traps?
- 5) How does the shallow trap concentration influence these temperatures?

7.1 GaAs:Si vs GaAs:Te

The defect structure of silicon- and tellurium-doped GaAs are very similar. Both these materials are self-compensated n-type semiconductors, in which Si_{Ga} or Te_{As} donors are partly deactivated due to formation of acceptor-like donor-gallium vacancy complexes, $\text{Si}_{\text{Ga}}\text{V}_{\text{Ga}}$ and $\text{Te}_{\text{As}}\text{V}_{\text{Ga}}$, and, in case of GaAs:Si, additionally by silicon acceptors, Si_{As} ¹. The formation of donor- V_{Ga} pairs was first proposed in order to explain the occurrence of a broad luminescence band at approximately 1100 nm (1.12 eV) in n-doped GaAs (Williams 1968). But the final prove of the existence of these vacancy complexes was provided by a series of positron annihilation lifetime measurements, in which vacancy concentrations could be measured directly (Gebauer et al. 1997, Gebauer et al. 1999). It is commonly assumed that both $\text{Si}_{\text{Ga}}\text{V}_{\text{Ga}}$ and $\text{Te}_{\text{As}}\text{V}_{\text{Ga}}$ are two times negatively charged, as one would expect for the complex consisting of a singly positive donor and triply negative V_{Ga} . The charge of a gallium vacancy in n-type GaAs was determined in a theoretical study (Baraff and Schlüter 1985) and in a recent positron work (Gebauer et al. 2003). The same charge state (-2e) for vacancy-complexes in both silicon- and tellurium-doped GaAs was found to be consistent with the compensation model based on results of electrical measurements in these materials and with the model of self-activated luminescence developed for the interpretation of the results of luminescence experiments in n-doped GaAs (Williams and Mackintosh 1968). As one can see, structure and electronic properties of $\text{Si}_{\text{Ga}}\text{V}_{\text{Ga}}$ and $\text{Te}_{\text{As}}\text{V}_{\text{Ga}}$ seem to be very similar. However, results of temperature-dependent positron annihilation measurements in GaAs:Si and GaAs:Te turned out to be quite different.

¹ Defects in GaAs:Si are discussed in details in Section 3.

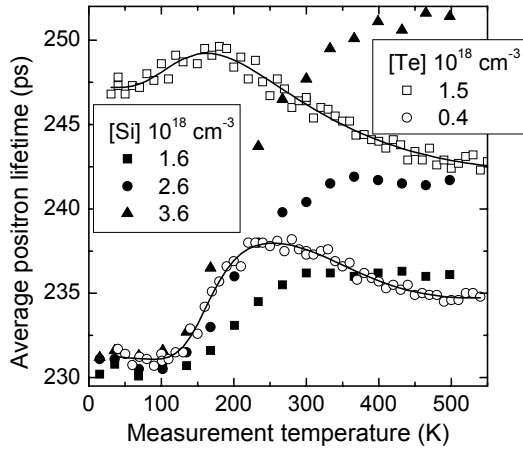


Fig. 7.1: Average positron lifetime as a function of measurement temperature for as-grown Si- and Te-doped GaAs. The data for GaAs:Te are taken from (Gebauer et al. 2003)

Fig. 7.1 shows average positron lifetime measured as a function of temperature in GaAs doped with different doses of tellurium (solid symbols) or silicon (open symbols). The data corresponding to GaAs:Si were obtained in this work (Fig. 4.2). Positron lifetime results in GaAs:Te originate from the PhD work of J. Gebauer (Gebauer 2000) and were published in Refs. (Gebauer et al. 1997; Gebauer et al. 2003). In both materials, average positron lifetime measured at room temperature is distinctly higher than the bulk lifetime of GaAs, indicating positron trapping into vacancy-like defects. The trapping rate, which can be determined from τ_{av} with the Eq. 3.6, increases to higher doping levels, indicating thereby the increase of the vacancy-like defect concentration. The decrease of τ_{av} to low temperatures indicates positron trapping by shallow traps represented by acceptor-like ions (e.g. C_{As} or Cu_{Ga}). In GaAs:Si, silicon doping itself is a source of Si_{As} -acceptors. Therefore, shallow traps concentration is always higher, and thus the decrease of τ_{av} is more pronounced in Si-doped than in Te-doped GaAs. The shallow trap defects have a considerable influence on positron trapping at temperatures ≤ 300 K. At higher temperatures, positron detrapping from the weak Coulomb potential of negative ions dominates and positron annihilation at shallow traps can be neglected. Thus, the behavior of τ_{av} at $T \geq 300$ K is governed by positron trapping into vacancy like defects and is the subject of interest for the following discussion.

In Te-doped GaAs, τ_{av} continuously decreases with increasing temperature (Fig. 7.1). Such $\tau_{av}(T)$ behavior was also often observed in positron annihilation lifetime studies of GaAs (e.g., in intentionally undoped GaAs (Krause-Rehberg and Leipner 1999) or in electron-irradiated GaAs (Polity et al. 1997)) and other semiconductors (e.g., in neutron irradiated silicon). According to theoretical trapping model (Section 3.2.1), a decrease of the positron trapping coefficient, and consequently a decrease of τ_{av} , is expected for a negative vacancy (Fig. 3.5). This is in agreement with the assumed negative charge state for the $Te_{As}V_{Ga}$ complex. The validity of the trapping model is corroborated by the good fit of the experimental data (solid lines in fig. 7.1) according to the two-defect trap-

ping model considering negative vacancies and shallow trap defects (Section 3.2.2). However, the model was found to be inapplicable for interpretation of $\tau_{av}(T)$ curves in Si-doped GaAs.

As fig. 7.1 shows, lifetime measurements in GaAs:Si reveal no decrease of the average positron lifetime in the high-temperature region. This is surprising, since one expected the same $\tau_{av}(T)$ dependence as in GaAs:Te due to the equal charge states of the vacancy-defects in these materials. But in contrast to GaAs:Te, τ_{av} in GaAs:Si remains constant or even slightly increases at temperatures above room temperature. Such $\tau_{av}(T)$ behavior is considered to be characteristic for a neutral, not a negative vacancy (Fig. 3.5). All attempts to apply the model of positron trapping by negative vacancies and shallow traps to the results obtained for GaAs:Si ended in failure. The best possible fit yielded unreasonably high concentrations of acceptor-like defects – two orders of magnitude higher than the vacancy concentration. This is obviously just a mathematical artifact. The $\tau_{av}(T)$ represent a competitive process of positron trapping into vacancy and shallow trap defects. In order to produce the $\tau_{av}(T)$ dependence similar to the one measured in GaAs:Si, the $T^{-1/2}$ increase of the trapping rate of negative vacancy, K_v and K_R in Eq. 3.15, must be compensated by positron trapping into shallow trap defects (Fig. 3.7) up to the temperatures of 600 K. For this, the positron detrapping rate (δ_{st} in Eq. 3.16) must be reduced by increasing the shallow trap concentration, C_{st} .

Thus, it was shown that the model of positron trapping into a negative vacancy is inconsistent with the results of positron lifetime measurements in GaAs:Si. There are two possible explanations of this disagreement:

- 1) The theoretical considerations of the temperature dependence of positron trapping are correct and thus $Si_{Ga}V_{Ga}$ -complex must be neutral;
- 2) $Si_{Ga}V_{Ga}$ is negative. In this case, the theory must be reconsidered.

7.2 Positron trapping in GaAs doped with Si and Te simultaneously

7.2.1 Experimental

The samples investigated were cut from a GaAs single crystal doped with silicon and tellurium atoms simultaneously (GaAs:Si&Te). The crystal was grown using VGF-technique and characterized by means of chemical analysis (AtES – atom emission spectroscopy) and electrical measurements (Hall-effect) at FCM. AtES measurements revealed large variation of the dopants concentration over the crystal length. Therefore, five samples were taken from different axial positions of the crystal for positron annihilation investigations. In the following, the samples are referred according to their position with integers 1-5, whereas 1 and 5 correspond to the ingot seed and tail, respectively.

Despite large concentration gradients of Si- and Te- donors, free electron density was found to be nearly the same in all samples pointing to high electrical compensation in this material. The results of SIMS and Hall-effect measurements for three of samples are summarized in Table 7.1.

Table 7.1 – Dopant and free electron concentrations and electron mobility measured in the GaAs:Si&Te samples investigated in this work

Sample #	[Si] (cm ⁻³)	[Te] (cm ⁻³)	n (cm ⁻³)	μ (cm ² /Vs)
1	1.5×10 ¹⁷	9.3×10 ¹⁷	9.37×10 ¹⁷	3116
4	2.0×10 ¹⁷	1.0×10 ¹⁸	1.19×10 ¹⁸	2481
5	9.0×10 ¹⁷	8.5×10 ¹⁸	1.27×10 ¹⁸	1556

Temperature-dependent positron annihilation lifetime measurements were performed according to the general measurement procedure (Section 3.4) on the experimental setup with time-resolution of 241 ps.

7.2.2 Results of temperature-dependent PALS measurements

Results of two-component analysis of the lifetime spectra obtained for GaAs:Si&Te samples at different measurement temperatures are shown in fig. 7.2. The decomposition was successful only for high-temperature spectra ($T > 300$ K), while for the lower temperatures large scattering of the fitting parameters, defect-related lifetime τ_d and its intensity, was observed [fig. 7.2 (a)]. Obviously at low temperatures, positron trapping into more than one defect occurs and hence the one-defect (two-component) trapping model can not be applied. However, it was impossible to decompose the spectra into more than two components. This indicates the small difference between positron lifetimes corresponding to the different types of positron traps. Due to the small difference, the individual lifetimes could not be separated. Thus, positrons trapped by negative ions (shallow positron traps) annihilate within the same time period as those annihilating from the bulk. At higher temperatures, positrons were trapped predominantly by a defect with $\tau_d = 265 \pm 5$ ps [fig. 7.2 (a)]. In GaAs, positron lifetimes of this order are attributed to a monovacancy-type defect [calculation]. Note that the same defect-related lifetime was obtained also for GaAs:Si (Chapter 4).

The average positron lifetime reveals complicated temperature and doping dose dependence [fig. 7.2 (b)]. The lowest τ_{av} is observed in the sample #1 doped with the smallest numbers of Si and Te atoms. $\tau_{av}(T)$ curve demonstrates a plateau at about 234 ps in 500 K – 330 K temperature region, increases as temperature decreases from 330 K down to 200 K and decreases with the further lowering of the measurement temperature. The latter decrease is ascribed to positron trapping into shallow trap defects as discussed for GaAs:Si in section 4.2.2. the two next samples #2 and #3 demonstrate a $\tau_{av}(T)$ behavior qualitatively similar to that of #1. The only difference is the shift of the τ_{av} to higher

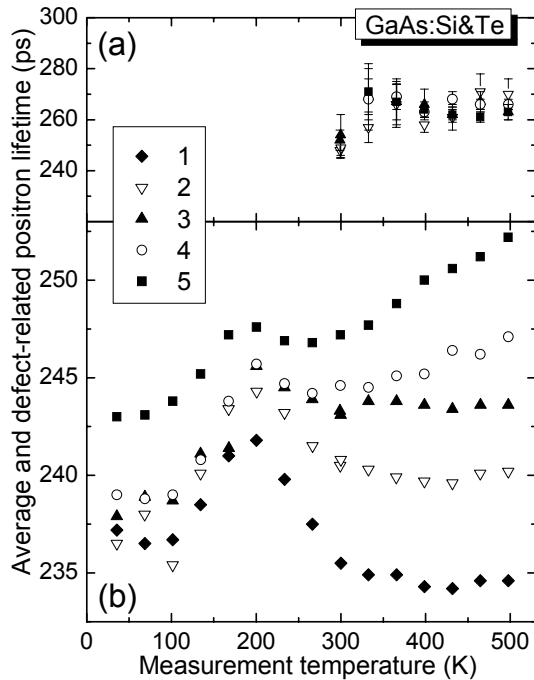


Fig. 7.2: Results of the temperature-dependent positron lifetime measurements obtained in GaAs doped with Si and Te atoms.

(a) defect-related lifetime;

(b) average positron lifetime.

values that is especially remarkable in the high-temperature region, where the influence of shallow positron traps is negligibly small. One should also note the extension of the plateau interval down to 300 K in sample #3. The enhancement of the average positron lifetime values to higher doping levels corresponds to an increase of the vacancy-like defects concentration. This tendency is also preserved for the last two samples #4 and #5. However, there are no plateau-regions observed for these specimens. Instead, τ_{av} demonstrates a continuous increase in high-temperature interval, giving rise to the minimum in the $\tau_{av}(T)$ function at the temperature of about 270 K.

7.2.3 Discussion

The temperature dependence of the positron trapping in GaAs:Si&Te represents an important result enlarging significantly the state of our knowledge on positron trapping in semiconductors and also on point defects in heavily n-doped GaAs. There were three main conclusions made: (i) the temperature behavior of τ_{av} cannot be explained in terms of two-defect trapping model assuming positron capture by negative ions (shallow traps) and open-volume defects (vacancies). Hence, (ii) there are more than one vacancy-type defects present in GaAs:Si&Te crystals. It is the first time, that the presence of more than one monovacancy-like defects in a single sample can be unambiguously demonstrated by PALS measurements. This is possible due to the different temperature behavior of positron trapping coefficient corresponding to these defects. (iii) The results support the as-

sumption of different defect properties of Si- and Te-doped GaAs. The conclusions stated above are based on the following arguments:

(i) Inconsistence of two-defect model.

The following reasons often used for interpretation of τ_{av} T-dependence were found to be **not** applicable:

- 1) *Competitive trapping into negative vacancy-like defects and shallow positron traps.* At best, this is demonstrated by $\tau_{av}(T)$ curves measured in samples #4 and #5 (Fig. 7.2). The two extremes observed at 200 K and 270 K cannot be modeled principally under the assumption of a single open-volume positron trap.
- 2) *Temperature-induced change of defect charge state.* Due to the high doping range, 10^{18} - 10^{19} cm⁻³ (Table 7.1), the Fermi level position in all samples was in the conduction band and could not be significantly affected by the temperature change in the interval of 300-500 K concerned here. Hence, no recharging effect could have taken place.
- 3) *Electron screening effect*, which can change the effective charge of defects felt by positrons and lead to a different temperature dependence of τ_{av} in differently doped samples. However, the free electron concentration was found to be nearly the same in all samples (Table 7.1). Thus the screening effect in sample #5 cannot be much larger than that in sample #1 to explain the profound difference in $\tau_{av}(T)$.

(ii) Presence of several types of open-volume defects.

- 4) Consequently, more than one kind of vacancy-like defects should exist in the crystal. The positron trapping into these defects has a different temperature dependence resulting in the complex behavior of $\tau_{av}(T)$ observed.
- 5) The positron lifetimes related to these defects could not be separated, i.e. have similar values. Hence, the defects must of a similar type. The found defect-related lifetime $\tau_d=264$ ps corresponds to a monovacancy in GaAs.
- 6) It is the first time the simultaneous presence of such defects is observed in a semiconducting crystal by positrons.

(iii) Consequences for Si- and Te-doped GaAs:

- 7) Obviously, the defect causing the increase of τ_{av} with increasing temperature (samples #4 and #5) must dominate positron trapping in the heavily-doped GaAs:Si. In GaAs:Te, in contrast, the other defect type is the dominating positron trapping center which demonstrates a strong decrease of the average positron lifetime towards higher temperatures. The superposition of positron trapping into the two defect types results in the temperature dependence $\tau_{av}(T)$ in GaAs:Si&Te.
- 8) A possible explanation for the different temperature dependence of positron trapping demonstrated by these defects is their different charge states. According to theoretical calculations (Section 3.2.1) increase of τ_{av} with increasing temperature is expected for

the neutral (or positive!) vacancy, while decreasing τ_{av} corresponds to trapping by the negative vacancy.

The latter item represents the subject of discussion for the following subsection.

7.3 Systematization of results

The results presented in the previous section have clearly demonstrated that the temperature dependence of positron trapping contains important information about the defect configuration in the GaAs crystals doped with Si or Te. In this section, the features of the $\tau_{av}(T)$ curves obtained for a great variety of samples studied in this work are examined in details. Most of the experimental data originated from the study of VCz-grown GaAs (Chapter 6). Therefore, it is reasonable to consider in the first place the lifetime spectra presented in that chapter. As far as vacancy-like defects are the subject of interest, only the high temperature ($T > 200$ K) part of $\tau_{av}(T)$ have to be considered. At temperatures below 200 K, positron trapping into shallow traps can not be neglected and dominates the temperature behavior of τ_{av} . As the main parameter, the slope of a $\tau_{av}(T)$ curve will be discussed. For the sake of convenience, a special designation for the parameter has been introduced:

$$Y = \frac{d}{dT} \tau_{av}(T) \quad (7.1)$$

Let's call Y the temperature decay of τ_{av} .

In a first approximation, the Y estimation could be done just by the fitting of the increasing part of the τ_{av} curves with a simple linear function. Surprisingly, such rather qualitative analysis performed for each sample revealed a presence of three *discreet* temperature decays (linear slopes) of the average positron lifetime. In other words there were three different temperature dependencies of τ_{av} observed, as demonstrated by the example $\tau_{av}(T)$ curves in Fig. 7.3. Y_i is represented by two curves, corresponding to the samples

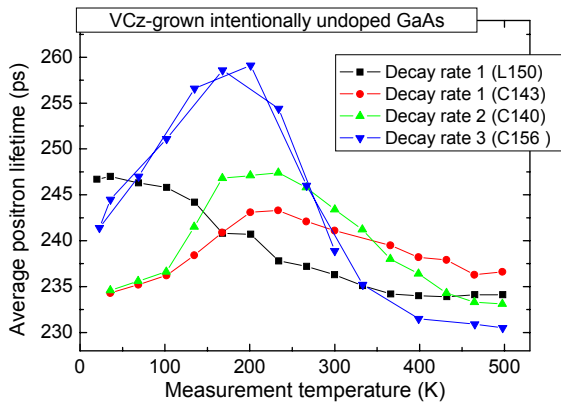


Fig. 7.3: Three typical temperature dependences of the average positron lifetime found in intentionally undoped GaAs. The lines are drawn to guide the eye.

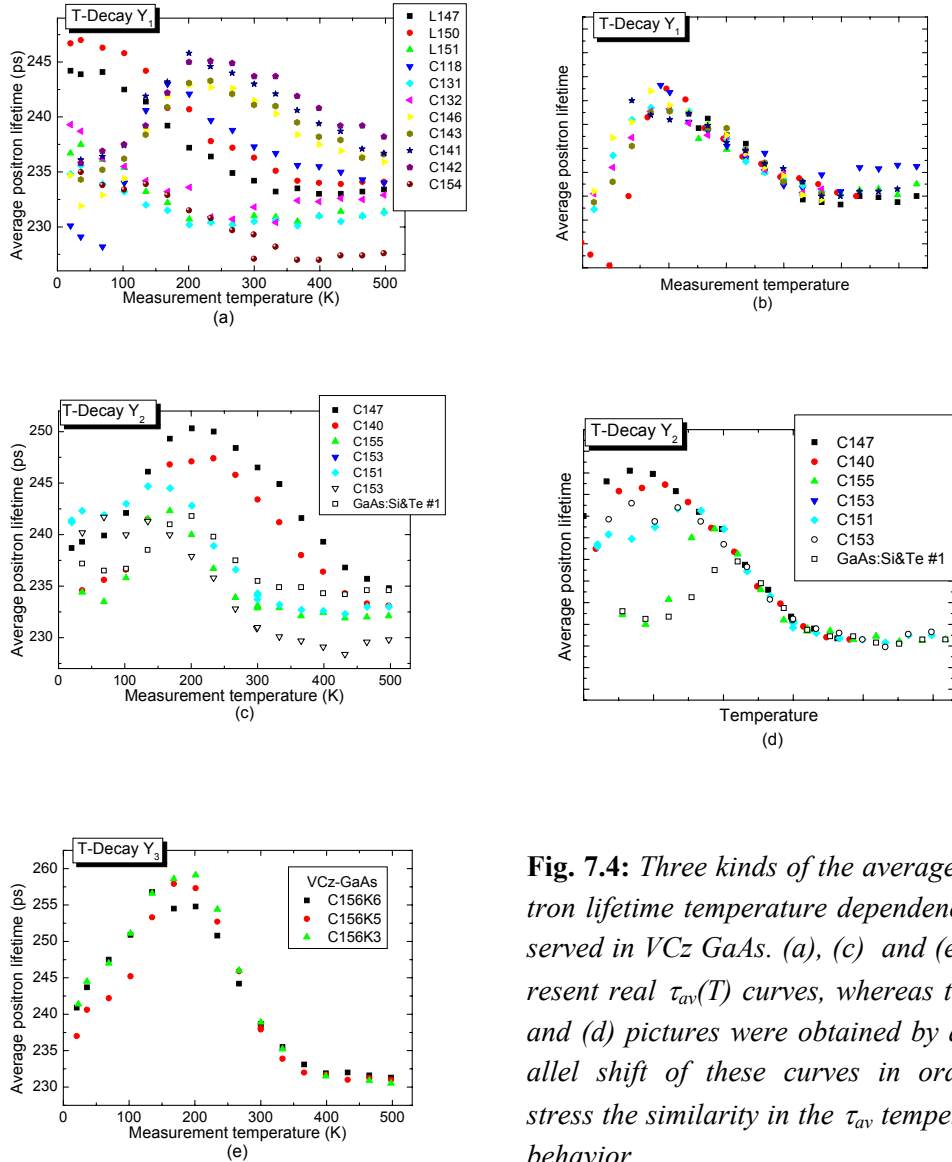


Fig. 7.4: Three kinds of the average positron lifetime temperature dependence observed in VCz GaAs. (a), (c) and (e) represent real $\tau_{av}(T)$ curves, whereas the (b) and (d) pictures were obtained by a parallel shift of these curves in order to stress the similarity in the τ_{av} temperature behavior.

with (red symbols) and without (black symbols) shallow traps. Fig. 7.4 shows the existence of the *discreet* decays more clearly. Parts (a), (c) and (e) present “real” τ_{av} curves related to Y_1 , Y_2 and Y_3 respectively. The (b) and (d) parts were constructed manually with the help of a simple parallel shift of the measurement curves in order to make the similarity of their temperature slopes obvious. The decay Y_3 was observed only in three samples cut from the same crystal (C156).

Similar analysis was performed for the results obtained in the other samples investigated in this work. It turned out, that all the samples can be classified in four groups according to the kind of temperature τ_{av} temperature dependence (Table 7.2). Most of the investigated samples belong to the first group, for which τ_{av} demonstrates the smallest decay (Y_1) – 3 to 4 ps per temperature increase of 100 K. For the samples of the group II,

Table 7.2 –GaAs crystals investigated in this work grouped according to the temperature decays of $\tau_{av}(T)$. The numbers in the column captions correspond to the change of the value of τ_{av} per 100 K

I (0.03-0.04 ps)	II (0.07-0.08 ps)	III (0.17-0.19 ps)	IV T-independent
L147	C147	C156	Heavily-doped
L150	C140	(K3, K6, K9)	GaAs:Si
L151	C153		Sections 4.2 and 4.3
C118	C155		
C131	C151		
C132	GaAs:Si&Te #1		
C146			
C143			
C141			
C142			
C155			
C154			
GaAs:Si (Section 4.4)			
SI annealed GaAs (Section 5.2.2)			

τ_{av} decreases faster, at the rate of 7-8 ps/100 K. But the highest temperature decay was observed for the three samples of group 3 and amounted to 17-19 ps per 100 K.

The occurrence of the discrete decay rates was never reported before (at least, such reports are not known to the author). Such behavior of τ_{av} was also not predicted by theoretical calculations. It seems to be a completely new experimental observation.

There are three possible explanations of the observed four kinds of temperature dependences:

- 1) different types of the vacancy-like defects responsible for positron trapping;
- 2) different concentrations of the vacancy and/or shallow trap defects;
- 3) different charge states of the vacancy defects.

The first two variants are hardly probable. Firstly, there are only *two* principle vacancy types in GaAs – gallium and arsenic vacancies – and *three* different decay rates. Naturally, the vacancies can form complexes with other intrinsic or extrinsic point defects, such as impurity atoms or antisites, which could have different positron trapping coefficients. But it is hardly possible, that the same defect complex is formed in very different GaAs samples of the group I and group II, which have different concentrations of impurities and free charge carriers and even different conductivity type. The second vari-

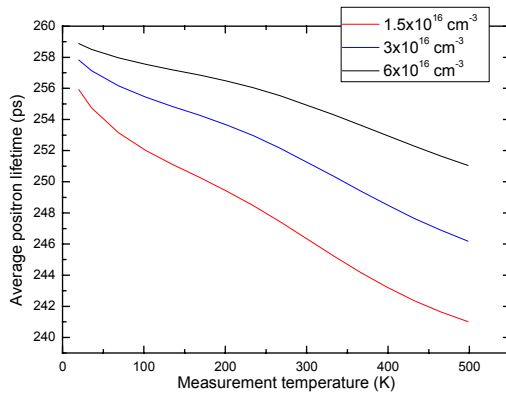


Fig. 7.5: Average positron lifetime calculated as a function of temperature for different vacancy concentrations. One-defect trapping model was used. Trapping into a negative vacancy was assumed.

ant must be also discarded as inappropriate, since it is rather improbable that the ratio between the concentrations of vacancy and shallow trap defects would amount to constant, moreover discrete values in order to explain the occurrence of only three slopes. Moreover, according to the theoretical model described in section 3.2, the vacancy concentration does not influence the slope of the $\tau_{av}(T)$ curve that much. This is demonstrated in Fig. 7.5 with the help of simulation of the $\tau_{av}(T)$ curves for the case of positron trapping by a single defect-type, negative vacancy, presented in different concentrations. As can be seen, concentration variations in the range of observed vacancy concentrations are not strong enough to cause the remarkable changes in the decay rate. Even if it was, we would end up with a continuous distribution of the slopes of the $\tau_{av}(T)$ curves due to continuous distribution of the concentrations of vacancies and shallow traps in investigated samples. This was not observed. More probable, the variation of the vacancy concentrations leads to a parallel vertical shift of the whole $\tau_{av}(T)$ curve which can be clearly seen for some of the samples (e.g., L147 and L150 of group I; C147 and C140 of group 2).

The third variant is the most reasonable one. Obviously, each discrete $\tau_{av}(T)$ decay rate corresponds to a specific defect configuration of studied crystal. The question is: which defect property can vary in a discrete way? This can be only the charge state. However, theoretical calculations (Section 3.2.1) did not predict different temperature dependences of the positron trapping rate for single and double negative vacancies. In contrary, for both vacancies charge states the same $T^{-1/2}$ dependence of the positron trapping rate should be expected (Fig. 3.5). This is in direct contradiction to the experimental results obtained in this work. It is the author's opinion, that the present theoretical model of positron capture does not correctly describe the temperature dependence of the process of positron trapping and must be reconsidered. The improvement of the model will allow to extract much more information from the results of temperature dependent positron lifetime measurements concerning the microstructure of the detected positron trapping centers.

8. Summary

Native defects in as-grown GaAs material were studied in this work. In particular, formation of equilibrium vacancy-like defects was investigated by positron annihilation lifetime spectroscopy (PALS). The obtained results allowed to draw the following conclusions:

- 1) $\text{Si}_{\text{Ga}}\text{V}_{\text{Ga}}$ complexes were found to be responsible for the rapid increase of the compensation degree in heavily silicon-doped GaAs. The compensation model based on the PALS-results was found to be in reasonable agreement with the experiment (Section 4.2)
- 2) The interrelation between the formation of $\text{Si}_{\text{Ga}}\text{V}_{\text{Ga}}$ complexes and dislocation density was established. It was found that the concentration of the vacancy-complexes was strongly suppressed in dislocation-rich regions of the GaAs:Si wafers (Section 4.3).
- 3) Based on the results of positron annihilation and cathodoluminescence spectroscopy, the defect responsible for the 0.95 eV luminescence band was attributed to the isolated gallium vacancy, V_{Ga} (Section 4.4).
- 4) It was demonstrated that vacancy-like defects formed in n-type GaAs:Si and SI undoped GaAs at elevated temperatures (1100° C) are related to different sublattices. In silicon-doped GaAs, $\text{Si}_{\text{Ga}}\text{V}_{\text{Ga}}$ complexes are formed, whereas a defect complex containing arsenic vacancy, V_{As} was detected in annealed SI GaAs. It has been established that this complex is neutral. The Gibbs' free formation energy G_f of V_{As} was determined as $G_f = 3.9$ eV (Chapter 5)
- 5) The shallow trap defects, which can not be identified by PALS measurements can be characterized by Coincidence Doppler-broadening spectroscopy (CDB) measurements performed at low temperatures (20 K). Thus, Cu-acceptors were identified by CDB measurements in section 5.3.2.
- 6) A large variety of crystals grown by Vapor Pressure Controlled Czochralski method (VCz) were studied by several experimental methods. A systematic study of GaAs material possessing all three types of conductivity, i.e. n-, p-type as well as semi-insulating material, was performed (Chapter 6).

- 7) The increase of positron average lifetime towards high temperatures was observed in several p-type samples. It was clearly shown that this increase could not correspond to the temperature expansion of the crystal lattice. Instead, this increase was attributed to positron trapping into negatively or even positively charged defects. Positron capture by positively charged defects is predicted by theory but was never observed experimentally (Section 6.4.2).
- 8) Concentration of vacancy-like defects in n-type material increases with increasing conductivity. It was concluded, that the vacancies are related to negatively charged V_{Ga} , the concentration of which increases due to the Fermi-level effect (Section 6.4.3).
- 9) It was demonstrated that the vacancy complexes in Si- and Te-doped GaAs have different efficiencies of positron capture as a function of temperature. The reasons for this were discussed (Section 7.2).
- 10) It was established that the theoretical consideration of temperature-dependent positron trapping are not always appropriate to describe the temperature behavior of the average positron lifetime. The contradictions of the experiment and model were emphasized (Section 7.3).

References

- M. Alatalo, P. Asoka-Kumar, V. J. Ghosh, B. Nielsen, K. G. Lynn, A. C. Kruseman, A. Van Veen, T. Korhonen and M. J. Puska; *Journal of the Physics and Chemistry of Solids* **59**(1), 55-9 (1998).
- M. Alatalo, B. Barbiellini, M. Hakala, H. Kaupinen, T. Korhonen, M. J. Puska, K. Saari-
nen, P. Hautojärvi and R. M. Nieminen; *Phys. Rev. B* **54**(4), 2397 (1996).
- M. Alatalo, H. Kauppinen, K. Saarinen, M. J. Puska, J. Mäkinen, P. Hautojärvi and R. M.
Nieminen; *Phys. Rev. B* **51**(7), 4176-85 (1995).
- R. Ambigapathy, A. A. Manuel, P. Hautojärvi, K. Saarinen and C. Corbel; *Phys. Rev. B*
50(4), 2188-99 (1994).
- C. D. Anderson; *Science* **76**, 238 (1932).
- J. R. Arthur; *J. Phys. Chem. Solids* **28**, 2257-2267 (1967).
- M. Baeumler, M. Maier, N. Herres, T. Buenger, J. Stenzenberger and W. Jantz; *Materials
Science and Engineering* **B91-92**, 16-20 (2002).
- G. A. Baraff and M. Schlüter; *Phys. Rev. Lett.* **55**(21), 2340-3 (1985).
- G. A. Baraff and M. Schlüter; *Phys. Rev. Lett.* **55**(12), 1327 (1985).
- B. Birkmann, R. Weingaertner, P. Wellmann, B. Wiedemann and G. Mueller; *Journal of
Crystal Growth* **237-239**, 345-349 (2002).
- J. S. Blakemore (1962). *Semiconductor Statistics*, Pergamon Press.
- F. Börner, Th. Bünger, S. Eichler et al. "Laterale Ladungsträgerverteilung in Si-dotierten
GaAs-Wafern". DGKK-Arbeitskreis "Herstellung und Charakterisierung von massi-
ven GaAs-, InP- und SiC-Kristallen". Freiberg, Germany.
- V. Bondarenko, K. Petters, R. Krause-Rehberg, J. Gebauer and H. Leipner; *Physica B*
308-310, 792-795 (2001).
- V. Bondarenko et al. to be published.
- W. Brandt and R. Paulin; *Phys. Rev. B* **5**, 2430 (1972).
- M. R. Brozel and G. E. Stillman (1996). *Properties of GaAs, third edition*. London, IN-
SPEC, The institution of Electrical Engineers.
- Z. Q. Chen, X. W. Hu and S. J. Wang; *Physica Status Solidi A* **156**(2), 277-84 (1996).
- P. A. M. Dirac; *Proc. Roy. Soc.* **117**, 610 (1928).
- P. A. M. Dirac; *Physikalische Zeitschrift* **29**, 561 (1928).
- C. Domke, P. Ebert, M. Heinrich and K. Urban; *Phys. Rev. B* **54**(15), 10288-10291
(1996).
- L. C. Feldman and J. W. Mayer (1986). *Fundamentals of surface and thin film analysis*.
New York, North Holland.
- W. Frank and A. Seeger; *Applied Physics* **3**(1), 61-6 (1974).

- J. Gebauer (2000). Native Leerstellen in GaAs - der Einfluss von Stoechiometry und Dotierung. Mathematisch-naturwissenschaftlicher Bereich. Halle (Saale), Martin Luther Universitaet.
- J. Gebauer, R. Krause-Rehberg, C. Domke, P. Ebert and K. Urban; Phys. Rev. Lett. **78**, 3334-3337 (1997).
- J. Gebauer, R. Krause-Rehberg, C. Domke, P. Ebert, K. Urban and T. E. M. Staab; Physical Review B **63**, 63-72 (2001).
- J. Gebauer, R. Krause-Rehberg, S. Eichler and F. Börner; Appl. Surf. Sci. **149**, 110-115 (1999).
- J. Gebauer, R. Krause-Rehberg, M. Lausmann and G. Lippold; Mater. Sci. Forum **258-263**, 905 (1997).
- J. Gebauer, R. Krause-Rehberg and T. E. M. Staab; Physica Status Solidi B **220**(1), 1-3 (2000).
- J. Gebauer, M. Lausmann, F. Redmann, R. Krause-Rehberg, H. Leipner, E. Weber and P. Ebert; Phys. Rev. B **67**, 235207 (2003).
- J. Gebauer, M. Lausmann, T. E. M. Staab, R. Krause-Rehberg, H. Hakala and M. J. Puska; Phys. Rev. B **60**, 1464-1467 (1999).
- N. A. Gokcen; Bulletin of Alloy Phase Diagrams **10**(1), 11 (1989).
- A. A. Gutkin, N. S. Averkiev, M. A. Reshchikov and V. E. Sedov; Materials Science Forum **196-201**(1), 231-6 (1995).
- R. N. Hall and J. H. Racette; J. Appl. Phys. **35**(2), 379-397 (1964).
- C. Hannig, G. Schwichtenberg, E. Buhrig and G. Gaertner; Material Science and Engineering **B66**, 97-101 (1999).
- P. Hautojärvi (1979). Positrons in solids. Berlin. Springer.
- H. G. B. Hicks and P. D. Greene; Inst. Phys. Conf. Ser. **9**, 92 (1960).
- L. Hoering (2001). REM-KL in-situ Untersuchungen zu Generation, Migration und elektronischer Wirksamkeit von Gleitversetzungen in ausgewählten III/V- und II/VI-Verbindungshalbleitern. Mathematisch-naturwissenschaftlicher Bereich. Halle (Saale), Martin-Luther University.
- D. T. J. Hurle. Impurity-point defect complexes in GaAs. Proceedings of the 6th International Symposium on Gallium Arsenide and Related Compounds. I Editor(s): Hilsum, C. London, UK: Inst. Phys, Edinburgh, UK, 20-22 Sept 1976 Price: Pounds 20.00 ISBN: 0-85498-123-3.(1977)
- D. T. J. Hurle; J. Appl. Phys. **85**(10), 6957 (1999).
- R. W. Jansen and O. F. Sankey; Phys. Rev. B **39**(5), 3192-3206 (1989).
- M. Jurisch and H. Wenzl. Thermochemische Modellierung der Abhängigkeit des spezifischen elektrischen Widerstandes von GaAs vom Kohlenstoff-Gehalt. DGKK Arbeitskreis "Angewandte Simulation in der Kristallzüchtung"- 2. Workshop, Memmelsdorf, Germany (2002).
- F. Kiessling (2003). Private communication.

- F. M. Kiessling, M. Neubert, P. Rudolph and W. Ulrici; *Mater. Sci. in Sem. Proc.* (accepted for publication).
- J. Korb, T. Flade, M. Jurisch, A. Koehler, T. Reinholdt and B. Weinert; *J. Cryst. Growth* **198/199**, 343-348 (1999).
- K. Krambrock, C. L. Berre, C. Corbel, K. Saarinen and P. Hautojärvi; *Mater. Sci. Forum* **196**(201), 195-200 (1995).
- R. Krause-Rehberg, G. Dlubek and A. Polity; *Mater. Sci. Forum* **196**(201), 1649-1654 (1995).
- R. Krause-Rehberg and H. S. Leipner; *Appl. Phys. A* **64**, 457-466 (1997).
- R. Krause-Rehberg and H. S. Leipner (1999). Positron annihilation in semiconductors. Berlin, Springer-Verlag.
- R. Krause-Rehberg, K. Petters and J. Gebauer; *Physica B* **273-274**, 714-17 (1999).
- R. Krause-Rehberg, A. Polity, T. Drost, G. Roos, G. Pensl, D. Volm and B. K. Meyer; *Mater. Sci. Forum* **143**(147), 1099-103 (1994).
- F.A. Kröger (1964). The chemistry of imperfect crystals. Amsterdam. North Holland Publishing Company.
- S. Kuisma, K. Saarinen, P. Hautojärvi, C. Corbel and C. LeBerre; *Phys. Rev. B* **53**(15), 9814-30 (1996).
- K. Kuriyama, K. Tomizawa, S. Uematsu and H. Takahashi; *Appl. Phys. Lett.* **65** (6), 746-748 (1994).
- T. Laine, K. Saarinen, J. Mäkinen, P. Hautojärvi, C. Corbel, L. N. Pfeiffer and P. H. Citrin; *Phys. Rev. B* **54**(16), R11050-11053 (1996).
- J. I. Landman, C. G. Morgan, J. T. Schick, P. Papoulias and A. Kumar; *Physical Review B* **55**(23), 15581-6 (1997).
- C. Le Berre, C. Corbel, K. Saarinen, S. Kuisma, P. Hautojärvi and R. Fornari; *Phys. Rev. B* **52**(11), 8112-20 (1995).
- H. Lei, H. S. Leipner, V. Bondarenko and J. Schreiber; *J. Phys.: Condens. Matter* **15**, 1-7 (2003).
- R. Leon, P. Werner, K. M. Yu, M. Kaminska and E. R. Weber; *Applied Physics A* **D61**(1), 7-16 (1995).
- K. G. Lynn, J. R. MacDonald, R. A. Boie, L. C. Feldman, J. D. Gabbe, M. F. Robbins, E. Bonderup and J. Golovchenko; *Phys. Rev. Lett.* **38**, 241-244 (1977).
- J. R. MacDonald, K. G. Lynn, R. A. Boie and M. F. Robbins; *Nucl. Instrum. Meth.* **153**, 189-194 (1978).
- J. Maguire, R. Murray, R. C. Newman, R. B. Beall and J. J. Harris; *Appl. Phys. Lett.* **50**(9), 516-518 (1987).
- S. A. McQuaid, R. C. Newman, M. Missous and S. O'Hagan; *Appl. Phys. Lett.* **61**(25), 3008-3010 (1992).
- N. F. Mott and H. S. N. Massey, Eds. Theory of atomic collisions. Oxford, University Press (1965).
- S. Muto, S. Takeda, M. Hirata, K. Fujii and K. Ibe; *Phil. Mag. A* **66**(2), 257-268 (1992).

- U. Myler, R. D. Goldberg, A. P. Knights, D. W. Lawther and P. J. Simpson; *Appl. Phys. Lett.* **69**(22), 3333-5 (1996).
- U. Myler and P. J. Simpson; *Phys. Rev. B* **56**(22), 14303-14309 (1997).
- M. Neubert and P. Rudolph; *Progress of Crystal Growth and Characterization* **43**, 119-185 (2001).
- R. C. Newman; *Semiconductor Science and Technology* **9**(10), 1749-62 (1994).
- J. E. Northrup and S. B. Zhang; *Phys. Rev. B* **47**(11), 6791-6794 (1993).
- J. P. Peng, K. G. Lynn, M. T. Umlor, D. J. Keeble and D. R. Harshman; *Phys. Rev. B* **50**(15), 11247-50 (1994).
- A. Polity, F. Rudolf, C. Nagel, S. Eichler and R. Krause-Rehberg; *Phys. Rev. B* **55**(16), 10467 (1997).
- M. Puska (1978). Elinaikaspektrin sovitushjelman LIFSPECFIT kehittäminen. Otaniemi, Teknillinen Korkeakoulu.
- M. J. Puska; *J. Phys.: Cond. Mat.* **1**, 7347-7366 (1989).
- M. J. Puska, C. Corbel and R. M. Nieminen; *Phys. Rev. B* **41**(14), 9980-93 (1990).
- M. J. Puska and R. M. Nieminen; *J. Phys. F.* **13**, 333-346 (1983).
- M. J. Puska and R. M. Nieminen; *Rev. Mod. Phys.* **66**(3), 841-897 (1994).
- M. J. Puska and R. M. Nieminen; *Reviews of Modern Physics* **66**(3), 841-97 (1994).
- M. A. Reshchikov, A. A. Gutkin and V. E. Sedov; *Mater. Sci. Forum* **196-201**, 237-242 (1995).
- P. Rudolph and M. Jurisch; *Journal of Crystal Growth* **198/199**, 325-35 (1999).
- P. Rudolph, M. Neubert, A. S. and M. Seifert; *Crystal Res. Technol.* **32**, 35-50 (1997).
- K. Saarinen, P. Hautojärvi, P. Lanki and C. Corbel; *Phys. Rev. B* **44**(19), 10585-600 (1991).
- K. Saarinen, P. Hautojärvi, A. Vehanen, R. Krause and G. Dlubek; *Phys. Rev. B* **39**(8), 5287-96 (1989).
- K. Saarinen, S. Kuisma, P. Hautojärvi, C. Corbel and C. LeBerre; *Phys. Rev. Lett.* **70**(18), 2794-7 (1993).
- K. Saarinen, A. P. Seitsonen, P. Hautojärvi and C. Corbel; *Phys. Rev. B* **52**(15), 10932-46 (1995).
- T. Saucy, C. P. Palsule, M. Holtz, S. Gangopadhyay and S. Massie; *Phys. Rev. B* **53**(4), 1900-1906 (1996).
- S. Schuppler, D. L. Adler, L. N. Pfeiffer, K. W. West, E. E. Chaban and P. H. Citrin; *Appl. Phys. Lett.* **63**(17), 2357-2359 (1993).
- S. Schuppler, D. L. Adler, L. N. Pfeiffer, K. W. West, E. E. Chaban and P. H. Citrin; *Phys. Rev. B* **51**(16), 10527-10538 (1995).
- H. Seong and L. J. Lewis; *Phys. Rev. B* **52**(8), 5675-84 (1995).
- Y. Y. Shan, K. G. Lynn, P. Asoka-Kumar, S. Fung and C. D. Beling; *Phys. Rev. B* **55**, 9897-9903 (1997).
- S. Shionoya (1966). Luminescence in inorganic Solids. New York, Academic.
- Y. Shirai and J. Takamura; *J. Phys.: Cond. Mat.* **1**, SA125-129 (1989).

- E. Soininen, J. Mäkinen, P. Hautojärvi, C. Corbel, A. Freundlich and J. C. Grenet; *Phys. Rev. B* **46**(19), 12394-12401 (1992).
- B. Somieski, T. E. M. Staab and R. Krause-Rehberg; *Nucl. Instr. Meth. Phys. Res. A* **381**, 128-140 (1996).
- M. J. Stott and R. N. West; *J. Phys. F* **8**, 635-350 (1978).
- M. Suezawa, A. Kasuya, Y. Nishina and K. Sumino; *J. Appl. Phys.* **76**(2), 1164-1168 (1994).
- M. Suezawa, A. Kasuya, Y. Nushina and K. Sumino; *J. Appl. Phys.* **69**, 1618-1624 (1991).
- S. Szpala, P. Asoka-Kumar, B. Nielsen, J. P. Peng, S. Hayakawa, K. G. Lynn and H.-J. Gossmann; *Phys. Rev. B* **54**(7), 4722-31 (1996).
- M. Tajima, R. Toba, N. Ishida and M. Warashina. 1st Int. Conf. Materials for Microelectronics, Barcelona.(1994)
- T. Y. Tan; *J. Phys. Chem. Solids* **55**(10), 917-929 (1994).
- T. Y. Tan, U. Gösele and S. Yu; *Crit. Rev. Sol. State Mater. Sci.* **17**(1), 47-106 (1991).
- T. Y. Tan, H. M. You and U. M. Gösele; *Appl. Phys. A* **56**, 249-258 (1993).
- M. Tatsumi, T. Kawase, Y. Iguchi, K. Fujita and M. Yamada (1994). Characterization of semi-insulating III-IV materials grown by vapor pressure controlled Czochralski method. Singapore, World Scientific.
- C. C. Tin, C. K. Teh and C. K. Weichman; *J. Appl. Phys.* **62** (6), 2329-2335 (1987).
- R. Toba, M. Warashina and M. Tajima; *Mat. Sci. Forum* **196-201**, 1785 (1995).
- K. Tomizawa, K. Sassa, Y. Shimanuki and J. Nishizawa; *Inst. Phys. Conf. Ser.* **91**, 435-438 (1987).
- T. Troev, V. Dimova, R. Zolov and B. Levay; *Radiochem. Radioanalyt. Lett.* **37**, 61-66 (1979).
- J. A. van Vechten; *J. Electrochem. Soc.* **122**, 423 (1975).
- H. Wenzl, A. Dahlen, A. Fattah, S. Petersen, K. Mika and D. Henkel; *J. Cryst. Growth* **109**(1-4), 191-204 (1991).
- H. Wenzl, W. A. Oates and K. Mika. Handbook of Crystal Growth. D. T. J. Hurle. Amsterdam, North Holland.(1994)
- R. N. West. Positron studies of lattice defects in metals. Positrons in solids. P. Hautojärvi. Berlin, Springer: 89.(1979)
- J. L. Weyher, P. Gall, L. S. Dang, J. P. Fillard, J. Bonnafe, H. Rufer, M. Baumgartner and K. Lohnert; *Semicond. Sci, Technol.* **7**, A45 (1992).
- C. Weyrizli. Zahlenwerte und Funktionen aus Naturwissenschaften und Technik. K.-H. Hellwege and O. Madelung. Heidelberg, Springer. **22**.(1989)
- J. M. Whelan, J. D. Struthers and D. J.A.; *Proceedings of the International Conference on Semiconductor Physics, Prague*, (1960).
- E. W. Williams; *Phys. Rev.* **168**(3), 922 (1968).
- R. W. Williams and A. R. Mackintosh; *Phys. Rev.* **168**(3), 679 (1968).
- H. Xu; *J. Appl. Phys.* **68**(8), 4077-86 (1990).

- B. G. Yacobi and D. B. Holt (1990). Cathodoluminescence Microscopy of Inorganic Solids. New York and London, Plenum.
- H. M. You, U. Goesele and T. Y. Tan; J. Apl. Phys. **73 (11)**, 7207-7216 (1993).
- S. B. Zhang and J. E. Northrup; Phys. Rev. Lett. **67(17)**, 2339 (1991).

Eidesstattliche Erklärung

Hiermit erkläre ich an Eides Statt, dass ich die vorliegende Arbeit selbständig und ohne fremde Hilfe verfasst und nur die angegebenen Quellen und Hilfsmittel verwendet habe. Ergebnisse anderer wissenschaftlicher Arbeiten wurden als solche gekennzeichnet. Diese Arbeit wurde bisher weder im In- noch im Ausland in gleicher oder ähnlicher Form in einem Prüfungsverfahren vorgelegt. Ich erkläre hiermit, dass ich mich bis zu dem jetzigen Zeitpunkt noch nie um einen Doktorgrad beworben habe.

Halle(Saale), November 2003

Vladimir Bondarenko

Curriculum vitae

Family name: Bondarenko
Given name: Vladimir (ukr. Volodymyr)
Nationality: Ukrainian
Date of birth: 15.02.1978
Birth-place: Sumy, Ukraine
Marital status: single
Address: Heinrich und Thomas Mann Str. 28, 06108 Halle/Saale

1985-1993 Elementary school
1993-1995 Secondary school
1995-2000 Study at Sumy State University
May 1999 Bachelor's degree in "Electronics"
June 2000 Degree of Master of physical electronics

July 2000- February 2001 Junior researcher at Sumy Institute for Surface Modification

From February 2001- PhD student at Martin-Luther-Universität Halle-Wittenberg in the framework of Graduate School 415 (DFG)

Acknowledgments

First of all I would like to thank my supervisor Prof. R. Krause-Rehberg, owing to whom I got the possibility to conduct the research described in this thesis. His constant support in the organization of my scientific work, many fruitful discussions and nice ideas are greatly appreciated.

I am grateful to my first colleagues in the positron laboratory Dr. F. Redmann, K. Petters and A. Massoud, from whom I had learned my first practical knowledge on the field of positron annihilation.

I owe many thanks Dr. H.S. Leipner and Dr. H. Lei, whose help with cathodoluminescence measurements and many useful discussions contributed a lot to the investigation of Si-doped GaAs.

The work on the VCz-GaAs benefited significantly from the intensive collaboration with Dr. F. Kiessling (IKZ, Berlin), who had personally grown all the VCz crystals and organized their systematic characterization, and to whom my especial thanks are addressed.

The help of Dr. J. Schreiber, Dipl. Ing. H. Mähl and Dipl. Phys. S. Vasnyov in the performing of CL-measurement on VCz GaAs are deeply appreciated.

I am indebted to Dipl. Phys. B. Gründig-Wendrock (TU Akademie Freiberg) for her willing help with the Hall Effect measurements and for interesting discussions concerning the interpretation of experimental results.

I am very grateful to Dr. M. Bäumlner (FIAF, Freiburg), who shared with me the results of her photoluminescence investigation on GaAs:Si wafers and put them at my disposal for further positron annihilation study.

I owe to thank A. Müller (electronic workshop), T. Shurig (Glassblower) and the team of the mechanical workshop for their help with any technical aspects of my work.

I would like to express my especial gratefulness to Freiburger Compound Materials in the person of Dr. S. Eichler and Dr. F. Börner. Most of GaAs wafers investigated in this work originated from the crystals grown at FCM. I appreciate highly all the seldom but always extremely useful discussions I had the pleasure to have with S. Echler and F. Börner.

I owe my thanks to Prof. H. R. Höche, chief of the Graduate School 415 of the Deutsche Forschungsgemeinschaft (DFG), where I have been fortunate to be a scholar during the last three years. The financial support obtained from DFG for the work described in Chapter 4 is also deeply appreciated.

I would like to use this opportunity to thank the supervisor of my master thesis and my first employer, Prof. A. Pogrebnjak, with the help of whom I did my first steps into the scientific world.